

STRUCTURAL AND AEROELASTIC FLUTTER ANALYSIS OF
WING STORE SYSTEMS AND STRUCTURAL MODIFICATION APPROACH
IN AEROELASTICITY

A THESIS SUBMITTED TO
THE GRADUATE SCHOOL OF NATURAL AND APPLIED SCIENCES
OF
MIDDLE EAST TECHNICAL UNIVERSITY

BY

AYTAÇ AKPINAR

IN PARTIAL FULFILLMENT OF THE REQUIREMENTS
FOR
THE DEGREE OF MASTER OF SCIENCE
IN
MECHANICAL ENGINEERING

SEPTEMBER 2021

Approval of the thesis:

**STRUCTURAL AND AEROELASTIC FLUTTER ANALYSIS OF
WING STORE SYSTEMS AND STRUCTURAL MODIFICATION
APPROACH IN AEROELASTICITY**

submitted by **AYTAÇ AKPINAR** in partial fulfillment of the requirements for the degree of **Master of Science in Mechanical Engineering, Middle East Technical University** by,

Prof. Dr. Halil Kalıpçılar
Dean, Graduate School of **Natural and Applied Sciences** _____

Prof. Dr. M. A. Sahir Arıkan
Head of the Department, **Mechanical Engineering** _____

Asst. Prof. Dr. Orkun Özşahin
Supervisor, **Mechanical Engineering, METU** _____

Examining Committee Members:

Assoc. Prof. Dr. Yiğit Yazıcıoğlu
Mechanical Engineering, METU _____

Asst. Prof. Dr. Orkun Özşahin
Mechanical Engineering, METU _____

Prof. Dr. Yavuz Yaman
Aerospace Engineering, METU _____

Assoc. Prof. Dr. M. Bülent Özer
Mechanical Engineering, METU _____

Asst. Prof. Dr. Bekir Bediz
Mechatronics Engineering, Sabancı University _____

Date: 08.09.2021

I hereby declare that all information in this document has been obtained and presented in accordance with academic rules and ethical conduct. I also declare that, as required by these rules and conduct, I have fully cited and referenced all material and results that are not original to this work.

Name, Last name: Aytac Akpınar

Signature:

ABSTRACT

STRUCTURAL AND AEROELASTIC FLUTTER ANALYSIS OF WING STORE SYSTEMS AND STRUCTURAL MODIFICATION APPROACH IN AEROELASTICITY

Akpınar, Aytaç
Master of Science, Mechanical Engineering
Supervisor: Asst. Prof. Dr. Orkun Özşahin

September 2021, 133 pages

The preliminary aeroelastic design process of the wings with stores is one of the most significant design activities to be considered in the aerospace industry. The focus of this thesis is mainly based on the dynamic aeroelasticity of the wing store systems including the discipline of mechanical vibrations. In the present study, the Finite Element Method (FEM) and structural modification approach are primarily implemented in the wing store aeroelastic systems. Aero-structural modeling and aeroelastic flutter analysis of the wing store systems are performed for 1-D beam-like and 2-D delta wings. A lumped mass store model is introduced to beam-like wings while a 1-DOF pitching elastic store model is introduced for delta wings. The structural model for the wing store systems is defined through the Finite Element Method (FEM) and store attachment is considered as local structural modifications. The structural and aeroelastic flutter characteristics of beam-like wings and delta wings with stores are investigated including different types of flutter solution methods, namely, K-Method, P-K Method, and Non-Iterative P-K Method. The traditional redesign process of the aeroelastic model is redefined by introducing the Dual Modal Structural Modification (DMSM) method as aeroelastic systems are concerned. The design optimization study for the store parameters is carried out

considering the worst-case flutter criteria. This thesis includes different types of solution methods that are developed in-house and by utilizing commercial software.

Keywords: Wing Store Flutter, Structural Modification, Store Design Optimization

ÖZ

KANAT YÜK SİSTEMLERİNİN YAPISAL VE AEROELASTİK ÇIRPINTI ANALİZİ VE AEROELASTİSİTEDE YAPISAL DEĞİŞİKLİK YAKLAŞIMI

Akpınar, Aytaç
Yüksek Lisans, Makina Mühendisliği
Tez Yöneticisi: Dr.Öğr.Üyesi Orkun Özşahin

Eylül 2021, 133 sayfa

Kanat yük sistemleri için yapılan ön aeroelastik tasarım çalışmaları havacılık endüstrisinde icra edilen en önemli tasarım çalışmalarından biridir. Bu tez temelde mekanik titreşim disiplinin dahil olduğu dinamik aeroelastisite ile ilgilidir. Çalışmada geliştirilen kanat yük aeroelastik sistemlerinde ağırlıklı olarak Sonlu Elemanlar Yöntemi ve yapısal modifikasyon yaklaşımı uygulanmıştır. Kanat yük sistemlerinin yapısal ve aerodinamik modellenmesi tek boyutlu kiriş benzeri ve iki boyutlu delta kanat yapıları kullanılarak icra edilmiştir. Kiriş benzeri kanat yapıları için yük modeli olarak toplu kütle kullanılırken, yunuslama salınımı bir serbestlik dereceli elastik yük ise delta kanat modeli için tanımlanmıştır. Sonlu Elemanlar Yöntemi kullanılarak yapısal model geliştirilmiş ve yükün kanada bağlantısı bölgesel yapısal modifikasyon olarak tanımlanmıştır. Kiriş benzeri ve delta kanat altında yük ile yapısal ve aeroelastik çarpıntı karakteristiği, K-Metodu, P-K Metodu ve Yinelemesiz P-K Metodu çarpıntı çözüm yöntemleri uygulanarak incelenmiştir. Aeroelastik sistemler düşünülerek, yapının geleneksel tasarım süreci İkili Modal Yapısal Modifikasyon yönteminin sürece dahil edilmesi ile süreç yeniden tanımlanmıştır. Yük tasarım parametreleri için en kötü çarpıntı ölçütü düşünülerek

tasarım eniyileme alıřması icra edilmiřtir. Bu tez zgn olarak geliřtirilmiř ve ticari yazılım kullanılarak geliřtirilmiř farklı zm yntemlerini iermektedir.

Anahtar Kelimeler: Kanat Yk ırpıntısı, Yapısal Modifikasyon, Yk Tasarımı Eniyilemesi

To my mom,

ACKNOWLEDGMENTS

I would like to express my gratitude to Asst. Prof. Dr. Orkun Özşahin for his guidance, advice, encouragement, constructive criticism, and professional understanding throughout the research.

I am also grateful to İbrahim Murat Karbancıođlu, Kemal Uçan, and Emre Dede for their encouragement and support throughout the study.

I would like to express my deepest gratitude to my dear wife, Büşra Akpınar for her constant love and endless support through my life.

Last and foremost, I would like to give my thanks to my lovely sister, Bahar Akpınar, and my father Atilla Akpınar for all their lifelong support, encouragement and always being there for me. I am so blessed to have you in my life.

TABLE OF CONTENTS

| | |
|---|-----|
| ABSTRACT..... | v |
| ÖZ | vii |
| ACKNOWLEDGMENTS | x |
| TABLE OF CONTENTS..... | xi |
| LIST OF TABLES | xiv |
| LIST OF FIGURES | xvi |
| LIST OF ABBREVIATIONS | xix |
| LIST OF SYMBOLS | xx |
| CHAPTERS | |
| 1 INTRODUCTION | 1 |
| 1.1 Theoretical Background | 1 |
| 1.2 Literature Review | 4 |
| 1.3 Research Objectives | 7 |
| 1.4 Scope and Contents of the Study..... | 8 |
| 2 STRUCTURAL AND AERODYNAMIC MODELING FOR AEROELASTIC ANALYSIS | 11 |
| 2.1 Aeroelastic Systems | 11 |
| 2.2 Evaluation of the Aeroelastic Equation of Motion..... | 14 |
| 2.3 Structural Models | 17 |
| 2.3.1 Modeling of Continuous Systems | 17 |
| 2.3.1.1 Rayleigh-Ritz “Assumed Shapes” Method..... | 18 |
| 2.3.1.2 Finite Element Method (FEM) | 21 |

| | | |
|-------|--|----|
| 2.4 | Aerodynamic Models..... | 25 |
| 2.4.1 | Evaluation of GAFs by Theodorsen Aerodynamics..... | 25 |
| 2.4.2 | Evaluation of GAFs by Doublet Lattice Method (DLM)..... | 30 |
| 2.5 | Flutter Calculation Procedures..... | 33 |
| 2.5.1 | The K-Method | 34 |
| 2.5.2 | The P-K Method | 35 |
| 2.5.3 | Non-Iterative P-K (NIPK) Method..... | 36 |
| 3 | CLEAN WING CASE STUDIES | 41 |
| 3.1 | High Altitude Long Endurance (HALE) Wing..... | 42 |
| 3.1.1 | Structural Analysis | 46 |
| 3.1.2 | Aeroelastic Analysis..... | 47 |
| 3.2 | Goland Wing..... | 51 |
| 3.2.1 | Structural Analysis | 54 |
| 3.2.2 | Aeroelastic Analysis..... | 57 |
| 3.3 | AGARD 445.6 Wing | 62 |
| 3.3.1 | Structural Analysis | 64 |
| 3.3.2 | Aeroelastic Analysis..... | 66 |
| 4 | AEROELASTICITY OF THE WINGS WITH EXTERNAL STORES..... | 73 |
| 4.1 | Beam-Like Wing with Concentrated Mass Model | 73 |
| 4.1.1 | Rigid Body Motion of the Concentrated Mass..... | 74 |
| 4.1.2 | Evaluation of Concentrated Mass Matrix for Wing Store Systems .. | 76 |
| 4.1.3 | Structural Equations of Motion | 77 |
| 4.2 | Flat-Plate Delta Wing with Flexible External Store Model..... | 78 |
| 4.2.1 | Finite Element Model | 81 |

| | | |
|---------|--|-----|
| 4.3 | Wing Store Flutter Case Studies | 83 |
| 4.3.1 | Beam-Like Wing with Concentrated Mass Case Study..... | 83 |
| 4.3.1.1 | Structural Analysis..... | 84 |
| 4.3.1.2 | Aeroelastic Analysis | 86 |
| 4.4 | Flat-Plate Delta Wing with Flexible External Store Case Study | 88 |
| 4.4.1.1 | Structural Analysis..... | 89 |
| 4.4.1.2 | Aeroelastic Analysis | 92 |
| 5 | STRUCTURAL MODIFICATIONS IN AEROELASTICITY..... | 97 |
| 5.1 | Dual Modal Space Modification | 101 |
| 5.2 | Evaluation of Generalized Aerodynamic Force (GAF) Matrix by Structural Modification | 103 |
| 5.3 | Case Study – Local Mass Modification on Cantilevered Plate Wing | 103 |
| 5.3.1 | Aeroelastic Analysis of Clean Wing | 105 |
| 5.3.2 | Aeroelastic Analysis of Clean Wing with Lumped Mass | 107 |
| 5.3.3 | Comparison of Computational Time | 109 |
| 6 | DESIGN OPTIMIZATION OF WING-STORE SYSTEMS BASED ON THE FLUTTER CRITERIA..... | 113 |
| 6.1 | Wing Store Aeroelastic Model Definition | 113 |
| 6.2 | Flutter Critical Multi-Store Design Parameters | 115 |
| 6.3 | Multi-Store Attachment Locations at Worst-Case Flutter Condition | 120 |
| 7 | CONCLUSION..... | 123 |
| 7.1 | General Conclusions | 123 |
| 7.2 | Recommendations for Future Work | 126 |
| | REFERENCES | 127 |

LIST OF TABLES

TABLES

| | |
|--|-----|
| Table 2.1 – Cantilever Beam Boundary Condition Parameters | 20 |
| Table 2.2 Flutter Solution Algorithm for Non-Iterative P-K (NIPK) Method in Pseudo Code Form | 38 |
| Table 3.1 Case Studies Analysis Summary | 42 |
| Table 3.2 HALE Wing Properties[34]..... | 43 |
| Table 3.3 HALE Wing Equivalent Beam Structural Properties | 45 |
| Table 3.4 Comparison of HALE Wing Natural Frequency Results | 46 |
| Table 3.5 Analysis Conditions | 48 |
| Table 3.6 Comparison of HALE Wing Flutter Results | 49 |
| Table 3.7 Goland Wing Properties[39] | 52 |
| Table 3.8 Goland Wing Equivalent Model Structural Properties..... | 54 |
| Table 3.9 Comparison of Goland Wing Natural Frequency Results | 55 |
| Table 3.10 Analysis Conditions | 57 |
| Table 3.11 Goland Wing Flutter Non-Iterative P-K Method Analysis Domain | 59 |
| Table 3.12 Comparison of Goland Wing Flutter Results | 60 |
| Table 3.13 Material Properties for Weakened AGARD 445.6 Wing..... | 63 |
| Table 3.14 Comparison of Natural Frequencies | 66 |
| Table 3.15 Aeroelastic Analysis Conditions for AGARD 445.6 Wing | 67 |
| Table 3.16 AGARD 445.6 Wing Flutter Speed Index Results..... | 71 |
| Table 4.1 Beam-Like Wing with Concentrated Mass Properties [5] | 83 |
| Table 4.2 Comparison of Wing/store Flutter Speeds and Frequencies by Present FEM Methodology | 87 |
| Table 4.3 Comparison of Clean Wing Natural Frequencies..... | 89 |
| Table 5.1 Comparison of First Five Natural Frequencies of the Clean Wing | 104 |
| Table 5.2 Comparison of Flutter Speed of the Clean Wing | 106 |
| Table 5.3 Comparison of Mass Attached Wing Flutter Results | 108 |
| Table 5.4 Comparison of Computational Time | 110 |

| | |
|--|-----|
| Table 6.1 Store Design Constraints | 116 |
| Table 6.2 Optimization Case-1 Results | 118 |
| Table 6.3 Optimization Case-2 Results | 118 |
| Table 6.4 Optimization Case-3 Results | 118 |
| Table 6.5 Set of Stores Selected in Virtual Inventory..... | 120 |

LIST OF FIGURES

FIGURES

| | |
|--|----|
| Figure 1.1 Collar's Triangle | 1 |
| Figure 1.2 Typical Flutter Analysis Flow Chart..... | 3 |
| Figure 1.3 Aerodynamic Models in Aeroelasticity[2]..... | 4 |
| Figure 1.4 Structural Models in Aeroelasticity[2]..... | 4 |
| Figure 2.1 Typical Cantilevered Wing Model [17] | 12 |
| Figure 2.2 Geometry of the Wing Section[18]..... | 13 |
| Figure 2.3 Coupled Bending-Torsion Element | 21 |
| Figure 2.4 Real and Imaginary Parts of $C(k)$ | 28 |
| Figure 2.5 Panels on Wing | 31 |
| Figure 2.6 The Classical V-g and V-f Curves | 34 |
| Figure 3.1 Sample HALE UAV [32]..... | 42 |
| Figure 3.2 HALE Wing Analysis Workflow..... | 44 |
| Figure 3.3 HALE Wing Equivalent Beam Geometry | 45 |
| Figure 3.4 HALE Wing Natural Frequencies and Mode Shapes | 47 |
| Figure 3.5 Analysis Case-3 V-f and V-g Graphs | 50 |
| Figure 3.6 Analysis Case-5 V-f and V-g Graphs | 50 |
| Figure 3.7 Analysis Case-7 V-f and V-g Graphs | 51 |
| Figure 3.8 Goland Wing Analysis Workflow..... | 53 |
| Figure 3.9 Goland Wing Equivalent Beam Geometry | 54 |
| Figure 3.10 Mode-1 (7.626 Hz)..... | 56 |
| Figure 3.11 Mode-2 (15.231 Hz)..... | 56 |
| Figure 3.12 Mode-3 (38.449 Hz)..... | 56 |
| Figure 3.13 Mode-4 (54.188 Hz)..... | 57 |
| Figure 3.14 Mode-5 (69.142 Hz)..... | 57 |
| Figure 3.15 Analysis Case-2 V-f and V-g Graphs | 61 |
| Figure 3.16 Analysis Case-6 V-f and V-g Graphs | 61 |
| Figure 3.17 Analysis Case-8 V-f and V-g Graphs | 61 |

| | |
|--|----|
| Figure 3.18 AGARD 445.6 Wing Planform | 62 |
| Figure 3.19 AGARD 445.6 Wing Analysis Workflow..... | 63 |
| Figure 3.20 AGARD 445.6 Wing Finite Element Model..... | 64 |
| Figure 3.21 Comparison of Mode Shapes..... | 65 |
| Figure 3.22 Comparison of GAF Entries for Mach Number, $M = 0.954$ | 69 |
| Figure 3.23 Comparison of AGARD 445.6 Wing Flutter Speed Index..... | 70 |
| Figure 3.24 Comparison of AGARD 445.6 Wing Flutter Frequency Ratio | 70 |
| Figure 4.1 Rigidly Attached Wing Store Configuration | 74 |
| Figure 4.2 A 3-D Structure on the Supports[48]..... | 75 |
| Figure 4.3 Wing Store Section..... | 76 |
| Figure 4.4 Attachment Locations Between the Wing and Store [9] | 79 |
| Figure 4.5 Section of Delta Wing Model with an External Store[9] | 80 |
| Figure 4.6 Illustration of the Stiction Force [49] | 81 |
| Figure 4.7 Illustration of the Elements of the FE Model | 82 |
| Figure 4.8 Beam-Like Wing FEM with Concentrated Mass at Wingtip | 84 |
| Figure 4.9 Wing Store Natural Frequencies vs Nondimensional Spanwise Location of Concentrated Mass for the First Four Modes | 85 |
| Figure 4.10 Wing/store Flutter Speed at Different Store Attachment Locations.... | 87 |
| Figure 4.11 A Snapshot of the Wind Tunnel Model[52] | 89 |
| Figure 4.12 The First Four Natural Frequencies of Wing Store Against Different Store Span Locations | 90 |
| Figure 4.13 Mode-1 [3.78 Hz], $y/c = 0.548$ | 91 |
| Figure 4.14 Mode-2 [9.78 Hz], $y/c = 0.548$ | 91 |
| Figure 4.15 Mode-3 [16.11 Hz], $y/c = 0.548$ | 91 |
| Figure 4.16 Mode-4 [20.53 Hz], $y/c = 0.548$ | 92 |
| Figure 4.17 Aerodynamic Mesh and Aspect Ratio of the Boxes..... | 93 |
| Figure 4.18 Flutter Speed at Different Store Attachment Locations | 94 |
| Figure 4.19 Flutter Frequency at Different Store Attachment Locations | 94 |
| Figure 5.1 Modern Fighter Aircraft and Its External Store Inventory [55] | 98 |
| Figure 5.2 Traditional Redesign Process of Structural Model..... | 99 |

| | |
|---|-----|
| Figure 5.3 New Redesign Process of Structural Model | 101 |
| Figure 5.4 Wing Geometry (in meters)[60]..... | 104 |
| Figure 5.5 Mass Attachment Locations and Labels on the Structure..... | 105 |
| Figure 5.6 Nastran DMAP NIPK-Method V-g and V-f Graphs | 106 |
| Figure 5.7 V-g and V-f Plots for the MF5 Mass Attachment Case..... | 109 |
| Figure 6.1 – External Store Definitions..... | 114 |
| Figure 6.2 Optimization Cases for Store Design Parameters | 117 |
| Figure 6.3 Worst-Case Flutter Loading Configuration | 121 |

LIST OF ABBREVIATIONS

ABBREVIATIONS

| | |
|-------|---|
| AGARD | Advisory Group for Aerospace Research and Development |
| AIC | Aerodynamic Influence Coefficient |
| CFD | Computational Fluid Dynamics |
| DLM | Doublet Lattice Method |
| DMAP | Direct Matrix Abstraction Program |
| DMSM | Dual Modal Structural Modification |
| DOF | Degrees of Freedom |
| EOM | Equation of Motion |
| EVP | Eigenvalue Problem |
| FEM | Finite Element Method |
| GAF | Generalized Aerodynamic Force |
| GVT | Ground Vibration Test |
| HALE | High-Altitude Long Endurance |
| IRS | Improved Reduced System |
| LCO | Limit Cycle Oscillation |
| NIPK | Non-Iterative PK |
| ROM | Reduced Order Model |
| SEREP | System Equivalent Reduction Expansion Process |
| UAV | Unmanned Aerial Vehicle |
| VLM | Vortex Lattice Method |

LIST OF SYMBOLS

SYMBOLS

| | |
|--------------------|--|
| k_w | Spring constant for plunging motion |
| k_θ | Spring constant for pitching motion |
| q_∞ | Dynamic pressure |
| ρ | Air density |
| ℓ | Wingspan, distance from the root chord to the tip of a wing |
| ℓ_e | Uniform beam element of the span length |
| $\{\eta\}$ | Vector of modal displacements |
| $\{x\}$ | Vector of nodal displacements |
| $\{x^e\}$ | Vector of elemental nodal displacements |
| ω | Circular frequency, $2\pi f$ |
| M | Mach number |
| $[\phi]$ | Mode shape matrix |
| $[\bar{Q}_{aero}]$ | Generalized Aerodynamic Force (GAF) Matrix |
| $[M]$ | Mass matrix |
| $[M^e]$ | Elemental mass matrix |
| $[K]$ | Stiffness matrix |
| $[K_e]$ | Elemental stiffness matrix |
| $[M_o]$ | Rigid body mass matrix |
| m | Mass per unit length |
| m_e | Lumped mass |
| I_e | Lumped inertia |
| I_p | Inertia per unit length about the elastic axis |
| I_c | Inertia per unit length about the center of mass |
| x_θ | A dimensionless parameter representing the distance between the mass axis and elastic axis |
| a_x | Distance between elastic and inertia axes |

| | |
|-------------|---|
| $F(t)$ | Aerodynamic forces |
| w | Transverse deflection (bending) |
| w_y | Angle due to transverse displacement |
| θ | Pitching rotation (torsion) |
| D_w | Number of modes in bending |
| D_θ | Number of modes in torsion |
| λ_i | Generalized coordinates related to bending |
| δ_i | Generalized coordinates related to torsion |
| Ψ_i | Shape functions for bending |
| Θ_i | Shape functions for torsion |
| $[I]$ | Identity Matrix |
| $[0]$ | Matrix of Zeros |
| $\{N\}$ | Row vector of shape functions |
| γ | Transient decay rate coefficient |
| p | Eigenvalue defined in P-K Method |
| w_j | Normal velocity |
| $\{p_k\}$ | Resultant force in k-set |
| $\{u_k\}$ | Displacement in k-set |
| $[A_{jj}]$ | Aerodynamic Influence Coefficient (AIC) Matrix in j-set |
| $[D_{jk}]$ | Substantial differentiation matrix |
| $[S_{kj}]$ | Integration matrix |
| $[Q_{kk}]$ | Aerodynamic Influence Coefficient (AIC) Matrix in k-set |
| $[Q_{dd}]$ | Aerodynamic Influence Coefficient (AIC) Matrix in d-set |
| $[G_{kd}]$ | Interpolation Matrix |
| U_f | Flutter Speed |
| ω_f | Flutter Frequency |
| ρ_f | Free-stream density at flutter |
| w_b | Equivalent beam width |

| | |
|---------------------|---|
| h_b | Equivalent beam height |
| ρ_{wing} | Wing material density |
| μ | Mass ratio |
| ω_a | Angular frequency of the first torsion mode |
| m_w | Wing panel mass |
| m_c | Concentrated mass |
| V_c | Volume of the truncated cone |
| y_{span} | Concentrated mass location along the span |
| \ddot{q} | Linear acceleration |
| \ddot{q}_θ | Rotational acceleration |
| M_s | Store mass (Concentrated mass) |
| M_1 | Mass of the flexible external store |
| M_2 | Mass of the aft connection point |
| e_1 | Distance between the store tip and the fore attachment point |
| e_2 | Distance between the aft and fore attachment point |
| e_3 | Mass center location of the external store from fore attachment point |
| β | Store pitch angle |
| k_s | Store pitch stiffness |
| ω_s | Store pitch frequency |
| A_0 | Store excitation amplitude |
| ξ_s | Store modal damping rate |
| J_β | Store pitch moment |
| σ | Store pitch stiction gap angle |
| P_1, P_2 | Fore and aft attachment points |
| x_s, y_s, z_s | Distances of concentrated mass CoG about flexural axis |
| α_i, β_i | Cantilever Beam Boundary Condition Parameters |
| Z_1, Z_2 | Vertical displacements of the fore and aft attachment points |

| | |
|--------------------------|--|
| A_{ij}, B_{ii}, T_{ii} | Rayleigh-Ritz method system matrices elements |
| a | Dimensionless parameter for the elastic axis |
| b | Half-chord length |
| $C(k)$ | Theodorsen's function |
| e | Dimensionless parameter for the center of mass |
| E | Elastic modulus |
| EI | Bending rigidity |
| g | Damping term |
| G | Shear modulus |
| GJ | Torsional Rigidity |
| H | Aerodynamic transfer function |
| k | Reduced frequency |
| r | Mass radius of gyration |
| s | Laplace variable |
| T | Torsional constant |
| U | Free stream velocity |

CHAPTER 1

INTRODUCTION

1.1 Theoretical Background

Aeroelasticity considers the effects of the interacting inertia, aerodynamic and elastic forces on the aerospace structures, such as an aircraft. Collar [1] defines the aeroelasticity with a famous triangle, which is shown in Figure 1.1. The discipline of mechanical vibrations directly concerns such forces.

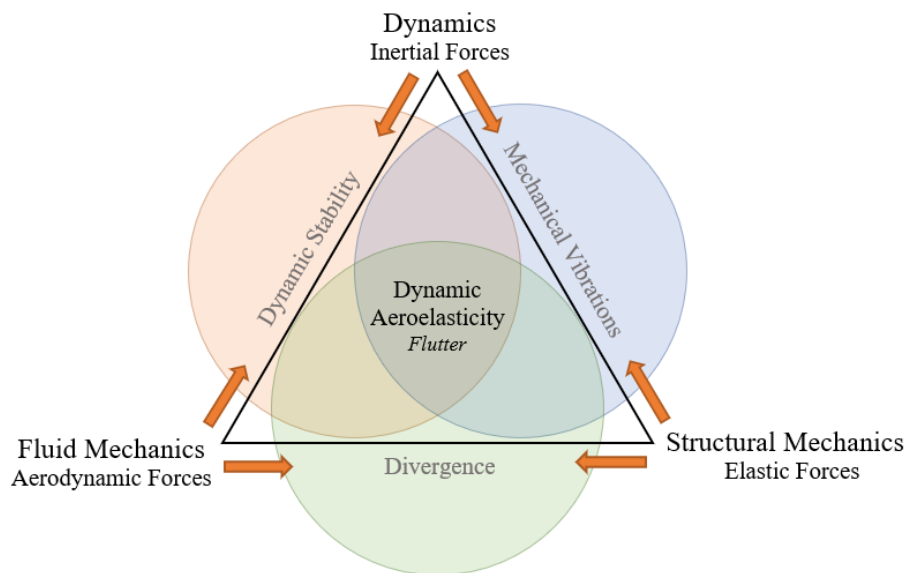


Figure 1.1 Collar's Triangle

The most critical design problems in the aerospace industry can be experienced as aeroelastic problems. They arise because of aerospace structures' flexible characteristics which means that the structure is not completely rigid. The common characteristic is generally observed whereas the aeroelastic problems are considered. Aerodynamic forces produce structural deformations and resulting deformations alter the aerodynamic forces. Respectively, the resulting aerodynamic forces

reproduce structural deformations, and this process continues successively until a state of equilibrium is reached. Generally, the equilibrium point is a failure of the structure.

Aeroelasticity can be classified into two categories, namely, static aeroelasticity and dynamic aeroelasticity. The design of an aircraft is generally formed by considering these two. Divergence is a phenomenon such that gradual change in the wing twist deflection leads to a rise of aerodynamic forces, thus, the rising of wing twist continues until structural failure takes place. Consequently, divergence is investigated in static aeroelasticity. On the other hand, the flutter phenomenon is investigated in dynamic aeroelasticity, which includes mechanical vibrations. Flutter is encountered as a consequence of elastic deflections of lifting surfaces like wings and fluid-structure interaction is observed in an oscillatory manner. Such interaction produces aerodynamic loads, and it gives rise to structural deflection with each oscillation. This situation leads to divergent oscillations, i.e., structural failure. Flutter generally occurs due to the bending-torsion coupling for the first modes of the aircraft bare wing, i.e., clean wing.

In addition, military aircraft are demanded to carry a large variety of wing-attached stores to maintain their operational requirements. External stores can be defined as any equipment such as general-purpose bombs, pods, missiles, guns, and fuel tanks that are mounted to the wing structure. When rigid mounting of the external store attachment is considered, the coupling of the above-mentioned modes of the structure occurs earlier than the clean wing case. This phenomenon is defined as a typical wing store flutter. In general, aeroelastic coupling of structural vibration modes involves non-linear stiffness and aerodynamics. This situation leads to sustained, non-divergent, non-destructive vibration of the flexible air vehicle, which is called Limit Cycle Oscillations (LCO). LCO is typically seen at high-performance aircraft with stores. The oscillation amplitude of the structure is occasionally limited through non-linear stiffness and aerodynamics. The existence of LCO may cause undesired vibration of the airframe and it may reduce the handling of aircraft and may result in a significant decrement in the cycle fatigue life of the structure.

Since air vehicles are prone to aerodynamic and structural effects due to having flexible bodies, they are designed to avoid aeroelastic flutter due to their destructive nature. The typical flutter analysis flow chart is given in Figure 1.2. Firstly, a structural model is developed, commonly through the Finite Element Method (FEM). Then, Ground Vibration Test (GVT) is performed with a physical prototype of the structure and the analytical modal model is updated as a result of GVT. Lastly, flutter analysis is conducted with an aeroelastic model, which is constructed by combining aerodynamics and a refined or updated structural model.

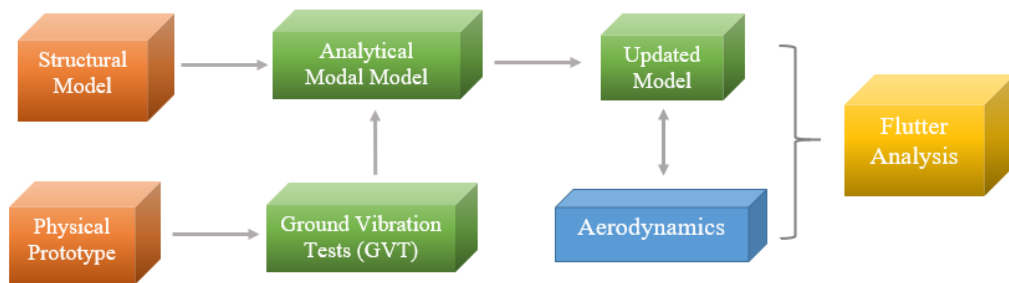


Figure 1.2 Typical Flutter Analysis Flow Chart

The accuracy of the flutter analysis depends on the fidelity levels of the aerodynamic and structural models. High-fidelity flutter calculations are mainly not preferred for multidisciplinary design optimizations due to the associated computational cost. On the contrary, Reduced Order Models (ROMs) with fewer degrees of freedom are widely used for that purpose. The aerodynamic models, which are employed in aeroelasticity, are presented in Figure 1.3, whereas structural models are shown in Figure 1.4.

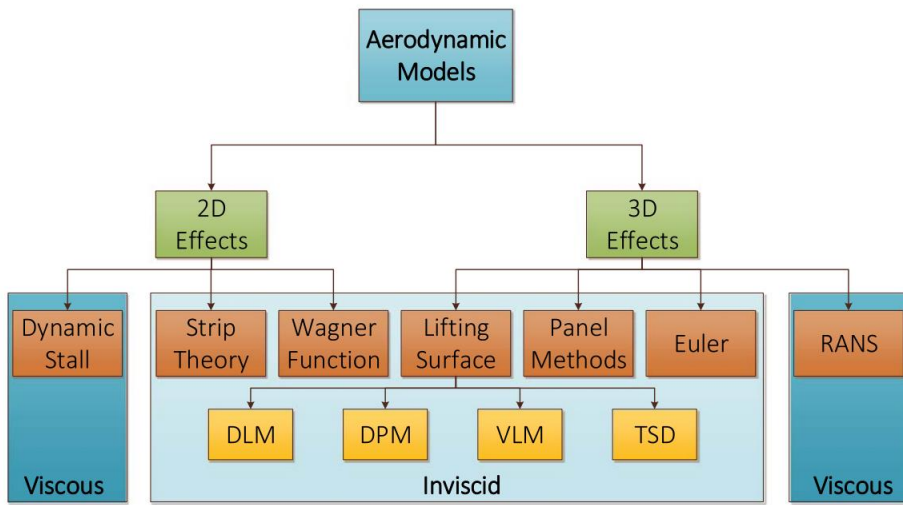


Figure 1.3 Aerodynamic Models in Aeroelasticity[2]

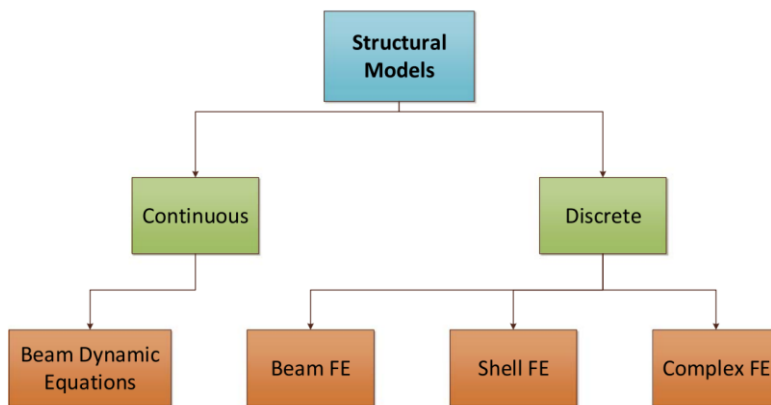


Figure 1.4 Structural Models in Aeroelasticity[2]

Structural models can be divided into two main groups, namely, continuous, and discrete models. Likewise, aerodynamic models can be grouped into two groups, which include 2-D and 3-D aerodynamic effects.

1.2 Literature Review

In the earlier work for the wing store systems, the studies were initially focused on the influence of the store mass and its spanwise location on the flutter speed. One of the first studies mentioning particularly the effects of external stores on flutter was

developed by Goland & Luke [3]. In the developed work, differential EOM of the wing through the extended Galerkin's Method was used. On the other hand, the first experimental study on the wing store flutter was conducted by Runyan & Sewall [4]. Then, these experimental results were compared with analysis of differential equations by Runyan and Watkins [5]. These studies have shown that the effect of the store mass and its spanwise location has a significant effect on the flutter.

These studies are followed by works that consider the influence of the structural characteristics of the attachment elements, i.e., pylons on flutter speed. Reed et al. [6] investigated the effects of the store attachment elements on flutter speed employing passive spring-damper elements in the wing store system. The study shows that introducing these types of elements increases the system flutter speed and reduces the dependency of the flutter on the inertia and center of gravity of the store. Yang and Zhao [7] investigated the flutter speed of the wing store system with the pylon stiffness by dividing it into three different groups, in which the wing is modeled as a 2-D airfoil. Although the linear studies are not limited to these, nonlinear aeroelasticity was attracted and studied by many researchers. Desmarais and Reed [8] analyzed the effects of the mounting characteristics with nonlinear pylon by using describing function method. Tang et al. [9] experimentally and theoretically studied the flutter and LCO characteristics of the wing store model where von Karman plate theory was used to model the wing structure. Kim and Strganac [10] studied the store-induced nonlinearities for the wing store system employing a nonlinear equation of motion. Likewise, Beran et al. [11] investigated the non-linear aeroelastic responses of a wing store structure, and transonic disturbance methodologies were adopted to model aerodynamic loads.

When the attachment of the store to the wing is considered as a structural modification, the dynamic characteristics of a modified structure such as a wing store system can be obtained by using the original system dynamic properties, for instance, a clean wing. Canbaloglu and Özgüven [12] developed an effective structural modification method when an additional degree of freedom is introduced into the modification. In the study, the modification is in the form of beams mounted under

the wing model that acts as stiffeners providing flexural rigidity. The performance of the method is analyzed by conducting an experiment with the GARTEUR SM-AG19 model. Therefore, a good correlation was observed between the analytical and experimental results. Then, the linear structural modifications were extended to systems with nonlinear modifications by Kalaycıoğlu and Özgüven [13]. Nonlinear modification with additional DOFs at attachment locations and nonlinear coupling with nonlinear elements were investigated analytically. The satisfactory results were obtained when analytical results are compared to the experiments.

In the optimization process of developing wing store systems, the change in the structural model is a necessity depending on the objective function of the problem. Modal characteristics of the structures, namely, frequencies, damping, and mode shapes, are generally determined from a normal mode analysis, i.e., by solving the eigenvalue problem. Many optimization cycles should be performed successively which mostly involves a computationally expensive process for large-scale systems. To overcome such high computational costs, Winter et al.[14] developed two novel Reduced Order Models (ROMs) that are based on CFD, and it is robust to change in the structural mode shapes owing to the additional lumped mass. Chen et al.[15] developed an efficient ROM in the existence of global structural modifications. In the developed work, the extended Kirsch combined method, which uses mainly the second-order eigenvector terms, was applied in the case of global structural modifications. In the above-mentioned studies, aeroelastic ROM was remodeled due to structural modifications. Consequently, they involve both reevaluations of the structural model and relevant reduced-order aerodynamic model. Apart from structural modifications, Karpel et al. [16] presented a new modal coupling technique for flutter analysis of the aircraft with multiple external store configurations. The study showed that flutter characteristics of numerous external store configurations for a typical fighter aircraft can be investigated efficiently without needing successive GVT and aeroelastic analysis.

1.3 Research Objectives

The main objective of this thesis is to develop a simple and effective aeroelastic model to conduct flutter analysis for the wing store systems that can be used during the preliminary design stage of an air vehicle. Numerous design candidates can be introduced for such systems to satisfy flutter requirements during this stage. This situation leads to an inevitable redesign process of the structure. If the aerodynamic configuration is fixed, the aerodynamic model can be used repeatedly while the structural model is being modified for the successive flutter analyses. The developed methodology has been mainly constructed based on this knowledge. This study aims at contributing to the following improvements for the wing store systems' structural and aeroelastic modeling and analyses:

- Although working with the ROMs (1-D framework) can reduce the computation time for the aeroelastic analyses, an additional improvement has been implemented to diminish overall modeling and analysis effort for the wing store systems. In the present approach, the attachment of the store is considered rigid, and it is defined as a local structural modification. By this approach, the structural model is defined simply to be coupled with an aerodynamic model to conduct flutter analysis.
- Further development has been introduced to form aeroelastic EOM by dealing with complex (Generalized Aerodynamic Force) GAF database of the 3-D aerodynamic model. Since GAF database is obtained through Aerodynamic Influence Coefficient (AIC) and lower order modal matrix of the structure, a structural modification method, namely, Dual Modal Space Method (DMSM) is implemented to approximate the modal matrix as keeping the AIC constant. Consequently, GAF database can be formed efficiently when successive structural modifications are present in the redesign process.
- Because classical flutter solution methods like K-Method and P-K Method have certain drawbacks due to utilizing an interpolation of aerodynamic

matrices, a novel Non-Iterative P-K Method (NIPK Method) is implemented in the flutter solution sequence. NIPK Method provides a fast and accurate flutter solution when comparing with the classical methods.

1.4 Scope and Contents of the Study

Structural and aerodynamic models are developed and analyzed for several clean wings and wing store systems. Store attachment is accomplished through a local structural modification in the present analysis. Besides, Dual Modal Structural Modification (DMSM) method is included in the traditional redesign process of the structural model as concerning aeroelastic analysis. Design optimization of the wing store system is performed based on a worst-case flutter criterion.

In Chapter 2, the structural and aerodynamic modeling of the cantilevered clean wing structure is presented. The beam-like 1-D structural model is developed including two distinct approaches, namely, Rayleigh-Ritz method and Finite Element Method (FEM), which are based on the Euler-Bernoulli beam theory. On the other hand, Theodorsen's aerodynamics is introduced to be coupled with beam-like 1-D wing structural models. Besides, 3-D lifting surface theory is introduced to use with 2-D shell wing structures. Generalized Aerodynamic Force (GAF) matrix definition and its evaluation are presented for the presented models. Lastly, an aeroelastic instability phenomenon solution, i.e., flutter solution is introduced.

Chapter 3 involves the flutter analysis of the clean wings. The validation of the analysis model is carried out through three well-known wing models, namely High-Altitude Long Endurance (HALE) wing, Goland wing, and AGARD wing 445.6 (weakened). Both structural models and aeroelastic models are investigated and analyses results are compared along with the reference studies.

In Chapter 4, wing store systems are investigated through two different models. The first model is based on the beam-like wing with the store. The store is assumed as lumped mass and rigidly attached to the wing. The equation of motion for the clean

is rewritten through FEM and structural modification approach when rigid store attachment is considered. The second model is based on the delta wing with flexible store attachment. The model is also developed by use of FEM. Two case studies are presented and investigated for the models. The present results are compared to reference studies.

Chapter 5 includes the structural modifications in the aeroelastic systems. The attachment of a lumped mass is considered as a local structural modification and a new method is presented for flutter analysis in the presence of local structural modifications. The evaluation of the Generalized Aerodynamic Force (GAF) matrix utilizing Dual Modal Structural Modification (DMSM) is presented. The current method is implemented in a case study. The present results are compared along with the reference experimental and analytical results.

In Chapter 6, a design optimization problem is defined based on the flutter criterion. For the given loading configurations, each with three external stores, the multi-store design parameters are optimized simultaneously depending on the worst-case flutter criterion. Lastly, for a given aircraft wing and a set of stores, a particular loading configuration is determined which causes the worst flutter condition.

CHAPTER 2

STRUCTURAL AND AERODYNAMIC MODELING FOR AEROELASTIC ANALYSIS

This chapter includes the structural and aerodynamic modeling of the cantilevered wing structure. The wing structure is modeled through the Finite Element Method (FEM) and Rayleigh-Ritz method based on classical 1-D Euler-Bernoulli beam formulation while aerodynamic loads are derived by Theodorsen's unsteady aerodynamic theory. An unsteady 3-D lifting surface Doublet Lattice Method (DLM) is introduced to model complex aeroelastic aircraft wings. Besides, the aeroelastic equation of motion and its solution methods for the flutter phenomena are presented in the chapter.

2.1 Aeroelastic Systems

The aeroelastic systems consist of two main aspects, namely structural and aerodynamic models. The structural models presented in this chapter are coupled with Theodorsen's unsteady aerodynamic model that is developed for a harmonically pitching-plunging airfoil. To investigate the aeroelastic behavior and to state model parameters of such a linear aeroelastic system, a 2 DOF pitching-plunging system is defined due to its physical simplicity. This model could correspond to a typical airfoil section through a wing structure. Since the aeroelastic analysis presented in this study mostly involve cantilevered beam-like wing sections, fundamental axes on the wing structure can be expressed through a sample beam-like wing model.

The wing model is based on the three axes definitions, which are namely the aerodynamic axis, elastic or flexural axis, and inertia or mass axis. While the wing moves through a fluid, the pressure distribution over the airfoil contributes to the

total force on the structure. The chordwise location of the resultant force is called the center of pressure. The spanwise line passing through the center of pressure is referred to as the aerodynamic axis. The chordwise location of the aerodynamic axis varies according to the flow regime. For instance, aerodynamic axis locations can be different at each subsonic and supersonic flow regime. The elastic axis of the wing is the longitudinal that transverse bending forces must pass through it while the bending of the wing shall not be coupled with the torsion. In other words, bending and torsion motions are uncoupled along the elastic axis. The inertia axis is defined as the longitudinal line passing through the average locations of the weight of the wing model. Figure 2.1 represents a typical aircraft, its cantilevered wing, and relevant axis locations.

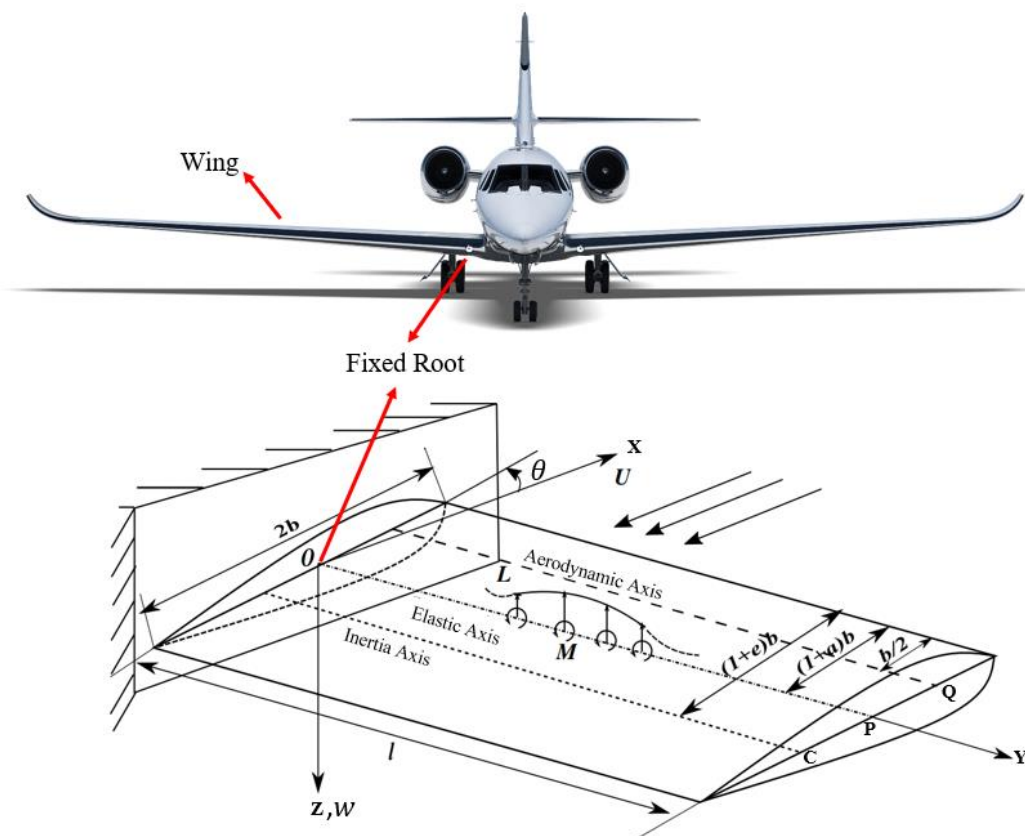


Figure 2.1 Typical Cantilevered Wing Model [17]

It is challenging that to deal with the aeroelastic behavior of the coupled bending torsion motion of the wing and its combined interactions with the aerodynamic loads. The distance between the inertia and elastic axes has a significant effect on the aeroelastic behavior of the wing. This distance is referred to as the static unbalance that is a condition where the inertia and elastic axes do not coincide with each other, and it causes structural coupling of bending and torsion modes of the wing.

After stating the basic aeroelastic system characteristics, the aforementioned typical section model is defined by Hodges et al. [18], which demonstrates the sinusoidal oscillatory motion of a 2 DOF pitching and plunging airfoil. Figure 2.2 defines the section of the wing.

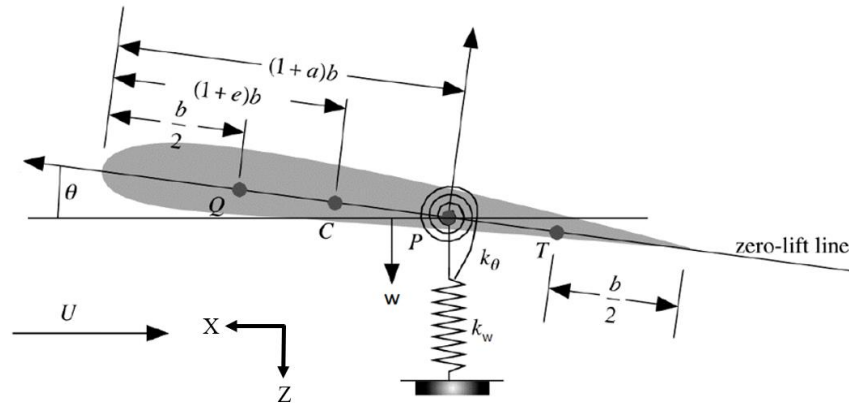


Figure 2.2 Geometry of the Wing Section[18]

The airfoil semi-chord is defined as b and airfoil is subject to a constant free stream velocity, U . The point P is defined as the reference point where plunge displacement where w is measured and it is referred to as the elastic axis. The points C , Q , and T are the center of mass that is referred to as the inertia axis, the pressure center that is referred to as the aerodynamic axis, and the three-quarter-chord, respectively. The dimensionless parameters e and a represent the locations of the points C and P . The static unbalance parameter is a dimensionless parameter representing the distance between the inertia axis and elastic axis and it is denoted by the relation $x_\theta = e - a$. Linear springs in the system are defined as spring constants, k_w for plunging and k_θ for pitching motions.

2.2 Evaluation of the Aeroelastic Equation of Motion

The collective interaction of the inertial and elastic structural forces, aerodynamic forces, and external disturbance forces leads to an aeroelastic response of the wing structure. Considering the equilibrium conditions of these forces, the equation of motion of the aeroelastic system can be given as follows:[19]

$$[M]\ddot{x}(t) + [K]x(t) = F(t) \quad (2.1)$$

where $x(t)$ is the physical deformation of the structure, $[M]$ and $[K]$ are the mass and stiffness matrices obtained by one of the convenient methods, for instance, the Finite Element Method (FEM). The structural damping term is omitted in the expression for simplicity. Besides, $F(t)$ is the aerodynamic forces that are applied to the structure, which can be divided into two sections: the aerodynamic forces arising from the structural deformation, $F_a(x)$ and the external forces, $F_e(x)$. Hence, $F(t)$ can be written as below:

$$F(t) = F_a(x) + F_e(t) \quad (2.2)$$

The external forces, $F_e(t)$ usually indicates the piston ejection forces for store separation or control surface aerodynamic forces. Since these types of forces are not considered in the present study, by taking $F_e(t) = 0$ Eq. (2.1) is expressed as in the following equation:

$$[M]\ddot{x}(t) + [K]x(t) - F_a(x) = 0 \quad (2.3)$$

Since the system given in Eq. (2.3) is self-excited, the stability condition of the system needs to be examined, which is known as flutter. The stability condition of the structure can be investigated by implementing a time marching procedure with an initial condition of $x(0)$ and $\dot{x}(0)$ specified at $t = 0$. Time-domain solutions for such systems are not computationally time efficient since it needs a nonlinear time-domain unsteady aerodynamic method, i.e., Computational Fluid Dynamics (CFD). When the infinitesimal oscillations are considered on the structure, the aerodynamic forces exhibit linear characteristics regarding the structural deformations. Thus, the

system defined in Eq. (2.3) turns into an eigenvalue problem by utilizing a amplitude linearization technique, which states a transfer function between $F_a(x)$ and $x(t)$ in the following equation:

$$F_a(x) = \int_0^t q_\infty H\left(\frac{U}{b}(t - \tau)\right) x(\tau) d\tau \quad (2.4)$$

where H is the aerodynamic transfer function, $q_\infty = 1/2\rho U^2$ is the dynamic pressure, ρ is the air density, U is the free stream velocity and b is the half chord length. The Laplace domain counterpart of Eq.(2.4) is given as follows:

$$F_a(s) = q_\infty \bar{H}\left(\frac{sb}{U}\right) x(s) \quad (2.5)$$

where \bar{H} is the Laplace domain counterpart of the aerodynamic transfer function. The matrix form of this function in the frequency domain is defined as the Aerodynamic Influence Coefficient (AIC) matrix. To obtain the general form of the aeroelastic equation of motion, Eq. (2.3) firstly transformed into the Laplace domain with the assumption of simple harmonic motion, then converted into the reduced frequency domain, k , which is defined as follows:

$$k = \frac{\omega b}{U} \quad (2.6)$$

The explanation of the reduced frequency, k is comprehensively expressed in section 2.4.1. Consequently, Eq. (2.3) can be transferred into the following equation by replacing $AIC\left(\frac{sb}{U}\right)$ with $AIC(ik)$ and s by $i\omega$, and it results in an eigenvalue problem (EVP) in terms of ω .

$$[-\omega^2[M] + [K] - q_\infty AIC(ik)]\{x\} = 0 \quad (2.7)$$

Since the FE model of the aircraft structure involves a large amount of DOF, the size of mass and stiffness matrices are excessively large, moreover, solving EVP of Eq. (2.7) needs significant computational effort. Thus, a modal technique can be introduced to the problem which can be given as below:

$$\{x\} = [\phi]\{\eta\} \quad (2.8)$$

where $[\phi]$ is the modal matrix, whose columns have a truncated set of natural modes and $\{\eta\}$ is the vector of modal displacements. Substituting Eq. (2.8) into Eq.(2.7) and pre-multiplying Eq.(2.7) with $[\phi]^T$ results in the general form of the aeroelastic equation of motion for the flutter.

$$[-\omega^2[\bar{M}] + [\bar{K}] - q_\infty GAF(ik)]\{\eta\} = 0 \quad (2.9)$$

where $[\bar{M}]$ is the generalized mass matrix, $[\bar{K}]$ is the generalized stiffness matrix, and $GAF(ik)$ is the Generalized Aerodynamic Force (GAF) matrix, which are expressed as follows:

$$[\bar{M}] = [\phi]^T [M] [\phi] \quad (2.10)$$

$$[\bar{K}] = [\phi]^T [K] [\phi] \quad (2.11)$$

$$[GAF] = [\phi]^T [AIC] [\phi] \quad (2.12)$$

where $[GAF]$ is expressed as $[\bar{Q}_{aero}]$ through the present work.

The above discussion illustrates that the existence of the aerodynamic transfer function provides to avoid solving the time-dependent EOM, whose form is usually nonlinear. On the other hand, forming an aerodynamic transfer function by use of unsteady aerodynamics results in the AIC matrix and it is a very comprehensive process. Hence, the theory of unsteady aerodynamics is implemented in the frequency domain by assuming simple harmonic motion. As a result, two distinct types of unsteady aerodynamic theory are presented for the aerodynamic modeling in this thesis, namely, Theodorsen's aerodynamics and Doublet Lattice Method (DLM).

The last discussion is based on the application of the modal approach, i.e., the use of a truncated set of structural modes. The critical flutter modes mostly occur due to the coupling of lower-order structural modes. Because of that reason, a maximum of ten numbers of the lowest natural modes are chosen for the flutter analysis of the wing structure, and fifty natural modes are adequate for the entire aircraft structure [19]. Once the lower set of modes are obtained for the analysis, the recalculation of these

modes is inevitable when structural modifications are present in the structure. Moreover, it requires a high computational cost when successive structural modifications in large DOF systems are considered. To direct approximation of the modified system's truncated set of modes can be possible by using the original structure's modal data in the aeroelastic systems. Further discussion related to this subject is stated in Chapter 5.

2.3 Structural Models

The structural modeling of the aircraft structures is comprehensive design activity in the aerospace industry. The structural models are used in both structural and aeroelastic analysis. The wing structural models can be developed by utilizing 1-D beam formulations, 2-D shells, and 3-D solid elements. Since the 1-D beam formulations require less computational effort, 1-D beam formulation will be taken into consideration within the context of this chapter.

2.3.1 Modeling of Continuous Systems

The systems encountered in aircraft aeroelasticity are mostly continuous. Therefore, an aircraft wing, fuselage, or external store can be considered as elastic continuum members which can bend and twist and have their mass and stiffness properties distributed spatially over the system. There are multiple approaches for modeling continuous systems, namely [20]

- a) the analytical method by exactly solving the governing partial differential equations
- b) an approximate approach using a series of assumed shapes to represent the deformation (i.e. Rayleigh-Ritz Method).
- c) an approximate approach using spatial discretization (i.e. Finite Element Method - FEM)

The analytical approach is satisfactory for simple systems; however, it is not useful when complicated aircraft systems are considered such as aircraft wings and external stores. The assumed mode method is still being used in the aeroelastic analysis. On the other hand, it has weaknesses when handling complex geometry. Because it works for relatively simple geometries (e.g. uniform cantilever wings). On the contrary, FEM is highly satisfactory for representing the structural vibrational characteristics of complicated aeroelastic systems such as wing store systems. Thus, the current study mostly covers the application of FEM for modeling aeroelastic systems.

2.3.1.1 Rayleigh-Ritz “Assumed Shapes” Method

The wing can be represented as a continuous cantilever 1-D beam. Rayleigh-Ritz method allows reducing the infinite number of DOF systems into a finite number. The structural dynamics of the wing structure can be modeled through the method in this manner. The energy equations refer to the classical Euler-Bernoulli beam theory for both bending and torsion including inertial coupling. Consider an unswept wing and its strain energy is defined as below:

$$U = \frac{1}{2} \int_0^\ell \left[EI \left(\frac{\partial^2 w}{\partial y^2} \right)^2 + GJ \left(\frac{\partial \theta}{\partial y} \right)^2 \right] dy \quad (2.13)$$

Similarly, kinetic energy for the beam is of the form

$$K = \frac{1}{2} \int_0^\ell \left[m \left(\frac{\partial w}{\partial t} \right)^2 - 2mbx_\theta \frac{\partial w}{\partial t} \frac{\partial \theta}{\partial t} + mb^2 r^2 \left(\frac{\partial \theta}{\partial t} \right)^2 \right] dy \quad (2.14)$$

where EI is the bending rigidity and GJ is the torsional rigidity for the uniformly distributed beam. The span of the wing and mass per unit length is denoted by ℓ and m respectively. r is the mass radius of gyration about the point P, which is the reference point where plunge displacement, w is measured in Figure 2.2. The mass radius of gyration, r is defined as below:

$$r = \sqrt{\frac{I_P}{mb^2}} \quad (2.15)$$

The relation between the moment of inertia per unit length about P, I_P and the moment of inertia per unit length about C, I_C is given as follows:

$$I_P = I_C + mb^2x_\theta^2 \quad (2.16)$$

Note that the solution is approximated by a linear combination of shape functions and the generalized coordinates in the Rayleigh-Ritz method. Hence, assumed modes are given as uncoupled free-vibration modes of the wing for bending and torsion, such that:

$$\begin{aligned} w(y, t) &= \sum_{i=1}^{D_w} \lambda_i(t) \Psi_i(y) \\ \theta(y, t) &= \sum_{i=1}^{D_\theta} \delta_i(t) \Theta_i(y) \end{aligned} \quad (2.17)$$

where D_w , D_θ , λ_i and δ_i are the number of modes representing bending, the number of modes representing torsion, generalized coordinates related with bending, and generalized coordinates related with torsion, respectively. The shape functions for the bending and torsion are given by Ψ_i and Θ_i , respectively.

These shape functions should satisfy the boundary conditions depending on the type of the problem. Since the wing is considered cantilevered, fixed-free beam boundary conditions have to be considered. The bending and torsion shape functions are given as follows [18]:

$$\Theta_i = \sqrt{2} \sin(\gamma_i y) \quad (2.18)$$

where $\gamma_i = \frac{\pi(i-\frac{1}{2})}{\ell}$

$$\Psi_i = \cosh(\alpha_i y) - \cos(\alpha_i y) - \beta_i [\sinh(\alpha_i y) - \sin(\alpha_i y)] \quad (2.19)$$

Cantilever beam boundary condition parameters $\alpha_i \ell$, $(2i - 1)\pi/2$ and β_i for $i = 1, \dots, 5$ is defined by Hodges et al. [18] in Table 2.1.

Table 2.1 – Cantilever Beam Boundary Condition Parameters

| i | $\alpha_i \ell$ | $(2i - 1)\pi/2$ | β_i |
|-----|-----------------|-----------------|-----------|
| 1 | 1.87510 | 1.57080 | 0.734096 |
| 2 | 4.69409 | 4.71239 | 1.01847 |
| 3 | 7.85476 | 7.85398 | 0.999224 |
| 4 | 10.9955 | 10.9956 | 1.00003 |
| 5 | 14.1372 | 14.1372 | 0.999999 |

The next step is to discretize the strain and kinetic energy expressions in the utilization of the Rayleigh-Ritz method. The strain and kinetic energy can be simplified due to the orthogonality of assumed modes:

$$U = \frac{1}{2} \left(\frac{EI}{\ell^3} \sum_{i=1}^{D_w} (\alpha_i \ell)^4 \lambda_i^2 + \frac{GJ}{\ell} \sum_{i=1}^{D_\theta} (\gamma_i \ell)^2 \delta_i^2 \right) \quad (2.20)$$

$$K = \frac{m\ell}{2} \left(\sum_{i=1}^{D_w} \dot{\lambda}_i^2 + b^2 r^2 \sum_{i=1}^{D_\theta} \dot{\delta}_i^2 - 2bx_\theta \sum_{i=1}^{D_\theta} \sum_{j=1}^{D_w} A_{ij} \dot{\delta}_i \dot{\lambda}_j \right) \quad (2.21)$$

where $A_{ij} = \frac{1}{\ell} \int_0^\ell \theta_i \Psi_j dy$ ($i=1, 2, \dots, D_\theta$; $j=1, 2, \dots, D_w$).

Inertial coupling between bending and torsion modes is stored by the term A_{ij} . Thus, system matrices can be written in final form as given in Eq. (2.22).

$$m\ell \begin{bmatrix} [I] & -bx_\theta [A]^T \\ -bx_\theta [A] & b^2 r^2 [I] \end{bmatrix} \begin{Bmatrix} \ddot{\lambda} \\ \ddot{\delta} \end{Bmatrix} + \begin{bmatrix} \frac{EI}{\ell^3} [B] & [0] \\ [0] & \frac{GJ}{\ell} [T] \end{bmatrix} \begin{Bmatrix} \lambda \\ \delta \end{Bmatrix} = \{0\} \quad (2.22)$$

where $[I]$ and $[0]$ are the identity matrix and matrix of zeros, respectively. The elements of $[B]$ and $[T]$ matrices are given as follows:

$$\begin{aligned} B_{ii} &= (\alpha_i \ell)^4 \\ T_{ii} &= (\gamma_i \ell)^2 \end{aligned} \quad (2.23)$$

2.3.1.2 Finite Element Method (FEM)

The structural model of a bending-torsion coupled wing and Finite Element formula derivation are defined in this section. Coupled Euler-Bernoulli beam formulation is used for necessary mathematical derivation. The uniform beam element of the span length, ℓ_e is shown in Figure 2.3.

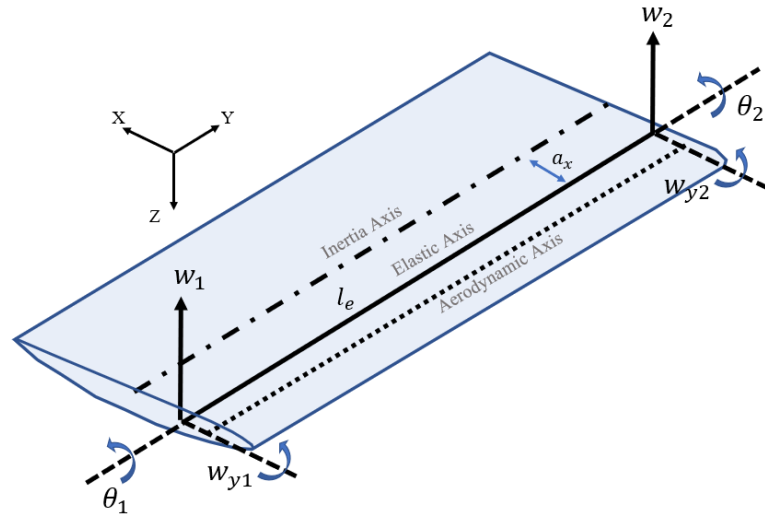


Figure 2.3 Coupled Bending-Torsion Element

2.3.1.2.1 Element Shape Functions

The cubic element accounted for the translation motion has 2 nodes at each end and 2 DOF per node element. The transverse displacement, w , and the slope, $w_y = \frac{\partial w}{\partial y}$ for bending of the beam can be expressed as follows:

$$w(y) = c_0 + c_1y + c_2y^2 + c_3y^3 ; w_y(y) = \frac{\partial w}{\partial y} = c_1 + 2c_2y + 3c_3y^2 \quad (2.24)$$

Transverse displacement and slope at both nodes are defined according to boundary conditions as follows:

$w_1 = w(0)$; $w_{y1} = w_y(0)$; $w_2 = w(\ell_e)$; $w_{y2} = w_y(\ell_e)$ where ℓ_e is the length of the beam element. The beam element for torsion has 1 DOF per node and linear function is defined below for torsion of the beam as follows:

$$\theta(y) = c_4 + c_5 y \quad (2.25)$$

The boundary conditions in the element are defined as $\theta_1 = \theta(0)$; $\theta_2 = \theta(\ell_e)$. The nodal displacements are defined for both bending and torsion at $y = 0$ and $y = \ell_e$. To obtain shape functions, displacements are defined in matrix form as given below:

$$\begin{Bmatrix} w_1 \\ w_{y1} \\ \theta_1 \\ w_2 \\ w_{y2} \\ \theta_2 \end{Bmatrix} = \begin{bmatrix} 1 & 0 & 0 & 0 & 0 & 0 \\ 0 & 1 & 0 & 0 & 0 & 0 \\ 0 & 0 & 0 & 0 & 1 & 0 \\ 1 & \ell_e & \ell_e^2 & \ell_e^3 & 0 & 0 \\ 0 & 1 & 2\ell_e & 3\ell_e^2 & 0 & 0 \\ 0 & 0 & 0 & 0 & 1 & \ell_e \end{bmatrix} \begin{Bmatrix} c_0 \\ c_1 \\ c_2 \\ c_3 \\ c_4 \\ c_5 \end{Bmatrix} \quad (2.26)$$

Displacement field, $\{x\}$ can be expressed in terms of the nodal displacements, $\{x^e\}$ as follows:

$$\{x\} = [N]\{x^e\} \quad (2.27)$$

where $\{x\} = \begin{Bmatrix} w \\ w_y \\ \theta \end{Bmatrix}$; $[N] = \begin{Bmatrix} N_w \\ N_{w_y} \\ N_\theta \end{Bmatrix}$ is a row vector of the so-called ‘‘shape functions’’

and $\{x^e\} = \{w_1 \quad w_{y1} \quad \theta_1 \quad w_2 \quad w_{y2} \quad \theta_2\}^T$.

Solve the system Eq. (2.26) to obtain coefficients and resultant shape functions are given as follows:

$$w(y) = [N_w(y)]\{x^e\} \quad (2.28)$$

where $[N_w(y)] = [N_{w1} \quad N_{w2} \quad 0 \quad N_{w3} \quad N_{w4} \quad 0]$ and the term $N_{wi}(y)$ is the Hermitian shape functions of the beam. Shape functions in explicit form can be given as follows:

$$N_{w1} = 1 - \frac{3y^2}{\ell_e^2} + \frac{2y^3}{\ell_e^3}, \quad N_{w2} = y - \frac{2y^2}{\ell_e} + \frac{y^3}{\ell_e^2}$$

$$N_{w3} = \frac{3y^2}{\ell_e^2} - \frac{2y^3}{\ell_e^3}, \quad N_{w4} = \frac{-y^2}{\ell_e} + \frac{y^3}{\ell_e^2}$$

Eq. (2.26) can be solved to obtain the torsion shape functions as follows:

$$\theta(y) = [N_\theta(y)]\{x^e\} \quad (2.29)$$

where $[N_\theta(y)] = [0 \ 0 \ N_{\theta1} \ 0 \ 0 \ N_{\theta2}]$, the term $N_{\theta i}(y)$ is the linear shape functions of torsion. The explicit form of the shape functions is given below:

$$N_{\theta1} = 1 - \frac{y}{\ell_e}, \quad N_{\theta2} = \frac{y}{\ell_e}.$$

2.3.1.2.2 Potential Energy

Potential energy terms are the same as used in Eq. (2.13), but with the revised displacement description as follows:

$$\begin{aligned} U &= \frac{1}{2} \int_0^{\ell_e} \left[EI \left(\frac{\partial^2 w}{\partial y^2} \right)^2 + GJ \left(\frac{\partial \theta}{\partial y} \right)^2 \right] dy \\ &= \frac{1}{2} \int_0^{\ell_e} \left[EI (x^T N_w'') (N_w''^T x) + GJ (x^T N_\theta') (N_\theta'^T x) \right] dy \end{aligned} \quad (2.30)$$

where the shorthand notation $' = \frac{\partial}{\partial y}$ and $'' = \frac{\partial^2}{\partial y^2}$ is used. The potential energy of the system can be written as:

$$U = \frac{1}{2} \{x\}^T [K^e] \{x\} \quad (2.31)$$

$$[K_e] = \int_0^{\ell_e} \left[[N_w'']^T (EI) [N_w''] + [N_\theta']^T (GJ) [N_\theta'] \right] dy \quad (2.32)$$

Introducing the relevant shape function polynomials into Eq. (2.32) and performing the matrix multiplications and integrations it may be shown that, for a uniform beam element $[K_e]$:

$$[K_e] = \begin{bmatrix} \frac{12EI}{\ell_e^3} & \frac{6EI}{\ell_e^2} & 0 & -\frac{12EI}{\ell_e^3} & \frac{6EI}{\ell_e^2} & 0 \\ \frac{6EI}{\ell_e^2} & \frac{4EI}{\ell_e} & 0 & -\frac{6EI}{\ell_e^2} & \frac{2EI}{\ell_e} & 0 \\ 0 & 0 & \frac{GJ}{\ell_e} & 0 & 0 & -\frac{GJ}{\ell_e} \\ -\frac{12EI}{\ell_e^3} & -\frac{6EI}{\ell_e^2} & 0 & \frac{12EI}{\ell_e^3} & -\frac{6EI}{\ell_e^2} & 0 \\ \frac{6EI}{\ell_e^2} & \frac{2EI}{\ell_e} & 0 & -\frac{6EI}{\ell_e^2} & \frac{4EI}{\ell_e} & 0 \\ 0 & 0 & -\frac{GJ}{\ell_e} & 0 & 0 & \frac{GJ}{\ell_e} \end{bmatrix} \quad (2.33)$$

2.3.1.2.3 Kinetic Energy

Kinetic energy terms are the same as used in Eq. (2.14), but with the revised displacement description as follows:

$$K = \frac{1}{2} \int_0^{\ell_e} \left[m \left(\frac{\partial w}{\partial t} \right)^2 + 2ma_x \frac{\partial w}{\partial t} \frac{\partial \theta}{\partial t} + I_P \left(\frac{\partial \theta}{\partial t} \right)^2 \right] dy \quad (2.34)$$

where inertial coupling term is given as $a_x = -bx_\theta$. The kinetic energy of the entire system can be written as:

$$K = \frac{1}{2} \{\dot{x}\}^T [M^e] \{\dot{x}\} \quad (2.35)$$

$$[M_e] = \int_0^{\ell_e} \left[[N_w]^T (m) [N_w] + [N_\theta]^T (I_P) [N_\theta] + [N_w]^T (ma_x) [N_\theta] + [N_\theta]^T (ma_x) [N_w] \right] dy \quad (2.36)$$

Introducing the relevant shape function polynomials and performing the matrix multiplications and integrations it can be shown that, for a uniform beam element

$[M_e]$:

$$[M_e] = \frac{\ell_e m}{420} \begin{bmatrix} 156 & 22\ell_e & 147a_x & 54 & -13\ell_e & 63a_x \\ 22\ell_e & 4\ell_e^2 & 21\ell_e a_x & 13\ell_e & -3\ell_e^2 & 14\ell_e a_x \\ 147a_x & 21\ell_e a_x & \frac{140I_P}{m} & 63a_x & -14\ell_e a_x & \frac{70I_P}{m} \\ 54 & 13\ell_e & 63a_x & 156 & -22\ell_e & 147a_x \\ -13\ell_e & -3\ell_e^2 & -14\ell_e a_x & -22\ell_e & 4\ell_e^2 & -21\ell_e a_x \\ 63a_x & 14\ell_e a_x & \frac{70I_P}{m} & 147a_x & -21\ell_e a_x & \frac{140I_P}{m} \end{bmatrix} \quad (2.37)$$

2.4 Aerodynamic Models

Since the solution of Eq. (2.9) requires unsteady aerodynamic theory in the frequency domain, two distinct unsteady aerodynamic models are presented to obtain GAF matrices. The first aerodynamic model is based on Theodorsen's aerodynamic formulation. Theodorsen [21] developed a procedure to obtain aerodynamic forces, which is calculated as a function of reduced frequency, k . Besides, Theodorsen applied 2-D unsteady aerodynamics involving pitching and plunging motion in incompressible for the derivation of these aerodynamic forces. The aerodynamic modeling and evaluation of GAF matrices by Theodorsen's aerodynamics are mathematically developed in the present study. Theodorsen's aerodynamics can provide an accurate mathematical analysis of flutter, nevertheless, it is not practical when complex wing structures such as flat plate delta wings are considered. For this reason, the 3-D aerodynamic modeling method namely, Doublet Lattice Method (DLM) is presented and implemented in the present study. DLM was presented by Albano and Hodden [22] considering a 3-D unsteady aerodynamic theory. The aerodynamic forces are defined as a function of Mach Number, M and reduced frequency, k . The aerodynamic modeling and evaluation of GAF matrices through DLM are carried out by use of commercial software, namely, MSC[®]FlightLoads and MSC[®]Nastran.

2.4.1 Evaluation of GAFs by Theodorsen Aerodynamics

The first-generation aircraft was suffering from structural failure and stability loss due to a lack of theory of wing oscillations. The issue was achieved by employing high Reynolds number flows and low angle of attack during the flight. An unsteady aerodynamics model for a harmonically pitching-plunging airfoil was developed by Theodore Theodorsen [21] dealing with potential flow theory. Besides, unsteady aerodynamics theory for a thin airfoil having small oscillations in incompressible flow was derived in that study. In this developed approach, structural dynamics

equations are coupled with unsteady aerodynamics to obtain flutter speeds, i.e., flutter boundaries.

The typical section of the lifting surface is presented in Figure 2.2 for fundamental definitions of the simple aeroelastic system, which is exposed to translational and rotational motions. The motion is simple harmonic; relatively w and θ are defined as follows:

$$w = \bar{w}e^{i\omega t} ; \bar{w} \text{ is the amplitude of heaving harmonic motion.}$$

$$\theta = \bar{\theta}e^{i\omega t} ; \bar{\theta} \text{ is the amplitude of pitching harmonic motion.}$$

where ω is the circular frequency of the motion. As seen from Figure 2.1, resultant lift, L , and the pitching moment, M about P can be defined based on linear aerodynamic theory. The lift involves both circulatory and non-circulatory terms, on the other hand, the pitching moment about the quarter-chord is entirely non-circulatory. The classical solution for the lift about the elastic axis, which is expressed per unit span, is defined by Fung [23] and Theodorsen [21] as follows:

$$L = \pi\rho b^2 [\ddot{w} + U\dot{\theta} - ba\ddot{\theta}] + 2\pi\rho UbC(k) \left[\dot{w} + U\theta + b\left(\frac{1}{2} - a\right)\dot{\theta} \right] \quad (2.38)$$

The moment about the point P, presented in Figure 2.2, which is referred to as the elastic axis is defined as below:

$$M = M_{\frac{1}{4}} + b\left(\frac{1}{2} + a\right)L \quad (2.39)$$

where $M_{1/4}$ is the moment about the pressure center, Q and can be obtained as follows:

$$M_{\frac{1}{4}} = -\pi\rho b^3 \left[\frac{1}{2}\ddot{w} + U\dot{\theta} + b\left(\frac{1}{8} - \frac{a}{2}\right)\ddot{\theta} \right] \quad (2.40)$$

Then, the resultant moment about the elastic axis can be defined explicitly as follows:

$$M = \pi\rho b^2 \left[ba\ddot{w} - Ub\left(\frac{1}{2} - a\right)\dot{\theta} - b^2\left(\frac{1}{8} + a^2\right)\ddot{\theta} \right] +$$

$$2\pi\rho Ub^2(a + \frac{1}{2})C(k) \left[\dot{w} + U\theta + b(\frac{1}{2} - a)\dot{\theta} \right] \quad (2.41)$$

Theodorsen's function, $C(k)$ is a complex-valued function of the reduced frequency k , given as follows:

$$C(k) = \frac{H_1^{(2)}(k)}{H_1^{(2)}(k) + iH_0^{(2)}(k)} = F(k) - iG(k) \quad (2.42)$$

where $H_n^{(2)}(k)$ are Hankel Functions of the second kind and it can be expressed in terms of Bessel functions of the first and second kind as:

$$H_n^{(2)}(k) = J_n(k) - iY_n(k) \quad (2.43)$$

Hankel Functions are not particularly significant in this study. In the equation (2.42), $F(k)$ is the real, $G(k)$ is the imaginary component of Theodorsen's function. An approximation of Theodorsen's function is given by Fung [23] in the frequency domain as follows:

$$C(k) = 1 - \frac{0.165}{1 - \frac{0.0455i}{k}} - \frac{0.335}{1 - \frac{0.3i}{k}} \quad (2.44)$$

Reduced frequency, k is the measure of unsteadiness of a flow. Greater k value means that the significance of unsteady effects becomes crucial in the flow. Figure 2.4 shows the real and imaginary parts of Theodorsen's function at different reduced frequencies. Note that for steady motion, $C(k)$ is real and equal to unity ($k = 0$). As k approaches to infinity real part of $C(k)$ approaches to 1/2.

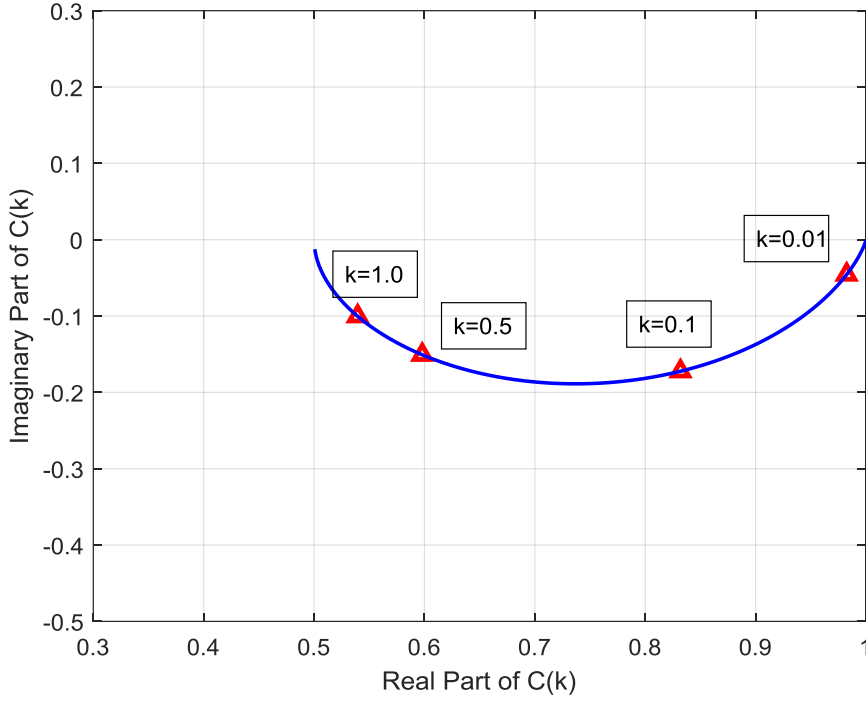


Figure 2.4 Real and Imaginary Parts of $C(k)$

The detailed derivation of Generalized Aerodynamic Force (GAF) matrices for Theodorsen's aerodynamics is based on the study of Banarjee [24]. Hence, the review of the derivation is expressed in this section. The GAF is formed by employing the principle of work. Unsteady lift and moment are defined by the aerodynamic strip theory based on Theodorsen's expressions. The displacements are transverse deflection (bending) $w(y)$ and pitching rotation (torsion) $\theta(y)$ at a spanwise distance y and they are given below:

$$\begin{aligned} w(y) &= \sum_{i=1}^n w_i(y)\eta_i(t) \\ \theta(y) &= \sum_{i=1}^n \theta_i(y)\eta_i(t) \end{aligned} \quad (2.45)$$

where $w_i(y)$ and $\theta_i(y)$ displacements components of the i^{th} mode ϕ_i , respectively, and $\eta_i(t)$ ($i = 1, 2, \dots, n$) is the generalized coordinates. Eq. (2.45) can be written in matrix form as follows:

$$\begin{bmatrix} w(y) \\ \theta(y) \end{bmatrix} = \begin{bmatrix} w_1(y) & w_2(y) & \dots & w_n(y) \\ \theta_1(y) & \theta_2(y) & \dots & \theta_n(y) \end{bmatrix} \begin{bmatrix} \eta_1 \\ \eta_2 \end{bmatrix} \quad (2.46)$$

The virtual work done (∂W) by the aerodynamic forces are given below:

$$\partial W = \sum_{i=1}^n \partial \eta_i \int_0^\ell [L(y)w_i(y) + M(y)\theta_i(y)] dy \quad (2.47)$$

where n , $M(y)$ and $L(y)$ are the number of normal modes interested, unsteady lift, and unsteady moment, respectively. Eq. (2.47) can be written in matrix form as follows:

$$\begin{bmatrix} \frac{\partial W_1}{\partial \eta_1} \\ \frac{\partial W_2}{\partial \eta_2} \\ \vdots \\ \frac{\partial W_n}{\partial \eta_n} \end{bmatrix} = \int_0^\ell \begin{bmatrix} w_1 & \theta_1 \\ w_2 & \theta_2 \\ \vdots & \vdots \\ w_n & \theta_n \end{bmatrix} \begin{bmatrix} L(y) \\ M(y) \end{bmatrix} \quad (2.48)$$

The unsteady lift $L(y)$ and unsteady moment $M(y)$ in 2-D flow are given in Eq. (2.38) and Eq.(2.41) can be written as below:

$$\begin{bmatrix} L(y) \\ M(y) \end{bmatrix} = \begin{bmatrix} QA_{11} & QA_{12} \\ QA_{21} & QA_{22} \end{bmatrix} \begin{bmatrix} w(y) \\ \theta(y) \end{bmatrix} \quad (2.49)$$

where the terms of the matrix $[QA]$ are given below:

$$QA_{11} = -\pi\rho U^2[-k^2 + 2C(k)ik]$$

$$QA_{12} = \pi\rho U^2 b [(ak^2 + ik) + 2C(k)[1 + ik(0.5 - a)]]$$

$$QA_{21} = -\pi\rho U^2 b [2C(k)ik(0.5 + a) - k^2 a]$$

$$QA_{22} = \pi\rho U^2 b^2 [2(0.5 + a)C(k)(1 + ik(0.5 - a)) + 0.125k^2 + k^2 a^2 + (a - 0.5)ik]$$

Substituting the Eq. (2.49) into Eq. (2.48), Generalized Aerodynamic Force (GAF) matrix can be obtained as follows:

$$\begin{bmatrix} \frac{\partial W_1}{\partial \eta_1} \\ \frac{\partial W_2}{\partial \eta_2} \\ \vdots \\ \frac{\partial W_n}{\partial \eta_n} \end{bmatrix} = \int_0^\ell \begin{bmatrix} w_1 & \theta_1 \\ w_2 & \theta_2 \\ \vdots & \vdots \\ w_n & \theta_n \end{bmatrix} \begin{bmatrix} QA_{11} & QA_{12} \\ QA_{21} & QA_{22} \end{bmatrix} \begin{bmatrix} w_1 & w_2 & \cdots & w_n \\ \theta_1 & \theta_2 & \cdots & \theta_n \end{bmatrix} \begin{bmatrix} \eta_1 \\ \eta_2 \\ \vdots \\ \eta_n \end{bmatrix} dy \quad (2.50)$$

$$= \begin{pmatrix} Q_{aero}^{11} & \cdots & Q_{aero}^{1n} \\ \vdots & \ddots & \vdots \\ Q_{aero}^{n1} & \cdots & Q_{aero}^{nn} \end{pmatrix} \text{ where } [\bar{Q}_{aero}] \text{ is the GAF matrix with}$$

$$[\bar{Q}_{aero}^{ij}] = \int_0^\ell [QA_{11}w_iw_j + QA_{12}w_i\theta_j + QA_{21}w_j\theta_i + QA_{22}\theta_i\theta_j] dy \quad (2.51)$$

Note that, GAF matrix, $[\bar{Q}_{aero}]$ is usually complex having real and imaginary parts.

2.4.2 Evaluation of GAFs by Doublet Lattice Method (DLM)

DLM is based on the linearized compressible aerodynamic potential theory for subsonic flow, and it is an unsteady 3-D lifting surface theory that was presented by Albano and Rodden [22]. The undisturbed flow is uniform and is either steady or varying harmonically. Moreover, the lifting surfaces are assumed as flat and lie parallel to the incoming flow.

DLM provides aerodynamic forcing harmonically for the considered lifting surface like Theodorsen's aerodynamics. The aerodynamic surface is divided into small trapezoidal lifting elements (called boxes). These boxes are aligned to the free stream direction. DLM defines an acceleration potential doublet of uniform, but unknown strength is placed at 1/4 chord of each box. A control point is placed at the 3/4 chord. The normal velocity, w_j that is induced by the inclination of the surface to the airstream is calculated at this point. The assembly of control points is referred to j-set. An aerodynamic grid point (k-set) is located at the center of the lifting element where the resultant force $\{p_k\}$ and displacement $\{u_k\}$ are calculated. The illustration of the panels on the typical 2-D wing is defined by Gülçat [25] as shown in Figure 2.5.

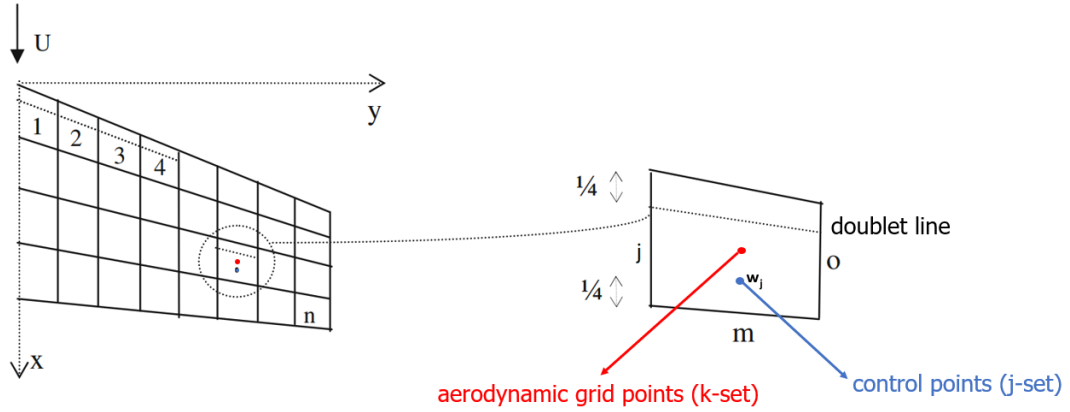


Figure 2.5 Panels on Wing

Substantial differentiation matrix (D_{jk}^1 -real part and D_{jk}^2 -imaginary part) is responsible for the relation between the downwash at the j -th point and the displacement of the k -th point. The relation is defined as follows:

$$\{w_j\} = [D_{jk}^1 + ikD_{jk}^2]\{u_k\} \quad (2.52)$$

On the other hand, the downwash can be also written as follows:

$$\{w_j\} = [A_{jj}]\left\{\frac{f_j}{q}\right\} \quad (2.53)$$

where $\left\{\frac{f_j}{q}\right\}$ is the pressure on the j -th point and $[A_{jj}]$ is the Aerodynamic Influence Coefficient (AIC) matrix is defined in j -set. The computing methodology for the aerodynamic influence coefficients is presented by Giesing, Kalman, and Rodden [26]. The forces at the k -th point are computed by integrating the pressure of each lifting element, which is given below:

$$\{p_k\} = [S_{kj}]\{f_j\} \quad (2.54)$$

where $[S_{kj}]$ is the integration matrix. The equations (2.52), (2.53) and (2.54) can be combined to give AIC matrix in k -set, $[Q_{kk}]$ as follows:

$$[Q_{kk}] = [S_{kj}][A_{jj}]^{-1}[D_{jk}^1 + ikD_{jk}^2] \quad (2.55)$$

Since the aerodynamic and structural grids are not necessarily the same, in other words, they are created independently, the transfer of displacements and forces from the structural model to the aerodynamic model must be accomplished. This transfer function can be obtained by interpolation, so-called splining. There are several methods for splining, for instance, linear and surface splines. The splining methods provide an interpolation matrix $[G_{kd}]$, which relates the structural grid points (d-set) to the aerodynamic grid points (k-set). The derivation of the interpolation matrix $[G_{kd}]$ is based on the selection of the interpolation type, which is force and displacement interpolation [27]. The force interpolation is defined mathematically as follows:

$$\{f_d\} = [G_{kd}]^T \{f_k\} \quad (2.56)$$

where $\{f_k\}$ is the force at the aerodynamic grid points and $\{f_d\}$ is the structurally equivalent value. The displacement interpolation is defined as below:

$$\{u_k\} = [G_{kd}]\{u_d\} \quad (2.57)$$

where $\{u_k\}$ is the displacement at aerodynamic grid points and $\{u_d\}$ is the displacement at structural grid points.

Evaluation of GAF matrices is performed employing MSC[®]Nastran whenever Doublet Lattice Method (DLM) is considered in the present study. All aerodynamic methods present in MSC[®]Nastran can compute the $[S_{kj}]$, $[D_{jk}^1]$ and $[D_{jk}^2]$ matrices at user-supplied Mach numbers and reduced frequencies. MSC[®]Nastran can compute the matrix $[A_{jj}]$ based on DLM theory and its computing code is based on the work of Giesing, Kalman, and Rodden [26]. To define the aerodynamic property of the model, matrix decomposition and forward and backward substitution are used in the computation of the Aerodynamic Influence Coefficient (AIC) matrix, $[Q_{kk}]$. The last step before defining in the modal domain of the AIC matrix is to transform the AIC matrix, $[Q_{kk}]$ from k-set to the d-set as follows:

$$[Q_{dd}] = [G_{kd}]^T [Q_{kk}] [G_{kd}] \quad (2.58)$$

The last step is to transform $[Q_{dd}]$ to the modal domain as follows:

$$[\bar{Q}_{aero}] = [\phi]^T [Q_{dd}] [\phi] \quad (2.59)$$

Note that the mode shape matrix of the structural model, $[\phi]$ is used for transformation and the Generalized Aerodynamic Force (GAF) matrix, $[\bar{Q}_{aero}]$ is formed accordingly.

2.5 Flutter Calculation Procedures

The aeroelastic flutter involves rapid self-feeding dynamics and is excited by aerodynamic forces. Since the flutter is potentially destructive due to these dynamic characteristics, analyzing the aeroelastic flutter is crucial for aerospace structures. The flutter equation has found a zero right-hand side and homogeneous form, and it is not possible to obtain absolute values of the modal response. Therefore, the stability of the system is required to be analyzed. The root locus approach can be implemented to calculate the stability of the system. The root locus methods based on aeroelastic stability analysis are presented by Hajela [28] and Rheinforth et al.[29].

Since the time-domain solution of nonlinear Eq. (2.3) is tedious and computationally costly, Eq. (2.3) is recasted into a set of linear systems in Eq. (2.7) which leads to an eigenvalue solution approach. However, a direct eigenvalue solution of the flutter problem is not possible since the $[\bar{Q}_{aero}]$ is a function of reduced frequency for 2-D unsteady aerodynamics. In other words, the eigensolution has to be performed at a particular flight condition i.e. airspeed, V , and altitude to determine eigenvalues. Note that the notation for the airspeed, U is replaced here by the term V to present V-g and V-g curves. The eigenvalues are obtained for each airspeed, V , and the results are given in the form of classical V-g and V-f curves as shown in Figure 2.6. The structural damping, g of each mode as a function of airspeed, V is shown by the V-g plot, while the V-f curve illustrates the frequency, f of each mode as a function of airspeed, V . The critical speed or flutter is determined by the V-g curve as the

lowest airspeed at which g curve crosses $g=0$ axis. Negative structural damping shows a stable region while positive shows an unstable region.

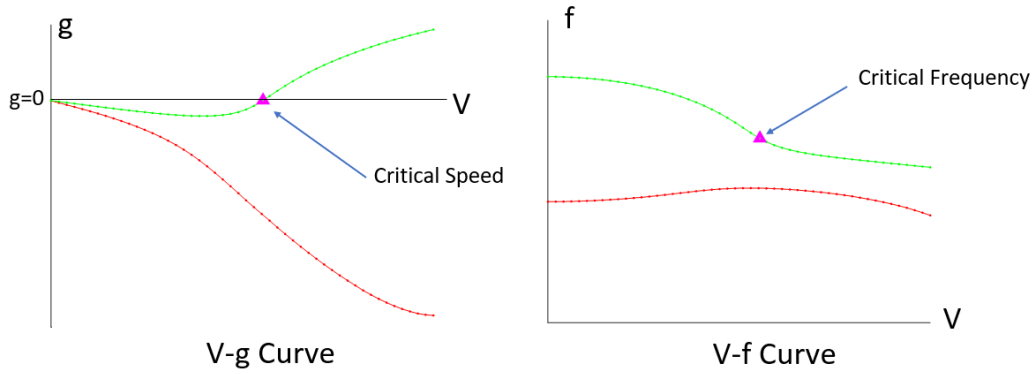


Figure 2.6 The Classical V-g and V-f Curves

The frequency-domain flutter calculation algorithms have been developed and they have been widely using in the aerospace industry. There are two commonly used algorithms, namely “K-Method” and “P-K Method” and these methods are available in MSC[®] Nastran aeroelastic solver.

Both methods involve repeated interpolations of the unsteady aerodynamic forces. A novel method performing a P-K analysis that does not require iterations, namely “Non-Iterative P-K Method” can also be employed as a flutter search algorithm. This method is not present in MSC[®] Nastran aeroelastic solver. The aforementioned K-Method, P-K Method, and NIPK-Method are mathematically developed and employed in the present flutter analysis.

2.5.1 The K-Method

The basic equation of motion for flutter analysis is employed by the K-method and it is defined as follows:

$$[-\omega^2[\bar{M}] + (1 + ig)[\bar{K}] - q_\infty[\bar{Q}_{aero}]]\{\eta\} = 0 \quad (2.60)$$

Note that general form of flutter Eq. (2.9) is modified such that artificial damping term, g is introduced to the system as a stability measure and $[\bar{Q}_{aero}]$ is a function of reduced frequency, k and Mach number, M . K-Method assumes the sinusoidal motion for the aeroelastic system, and it solves the EOM as eigenvalue problem for a series of parameters M , k and ρ . Moreover, $[\bar{Q}_{aero}]$ is interpolated for a series of k values and the eigenvalue problem is solved for each interpolated GAF matrix. Dividing each term of Eq. (2.60) by $(1 + ig)$ and substituting $q_\infty = 1/2\rho U^2$ into Eq.(2.60) gives the following equation:

$$\left[[\bar{K}] - \left\{ [\bar{M}] + \left(\frac{1}{2} \rho b^2 \right) / k^2 \right\} [\bar{Q}_{aero}] \right] \left(\frac{\omega^2}{(1+ig)} \right) \{\eta\} = 0 \quad (2.61)$$

where the complex eigenvalue is $\frac{\omega^2}{(1+ig)}$ and it can be interpreted as real values of ω and g . The airspeed, U can be obtained considering the relation $U = \frac{\omega b}{k}$.

Although the K-Method algorithm provides the solution quickly, multiple frequency and damping can be obtained at certain speed regions. Since the structural damping, g is artificially introduced to the system, in other words, g is not physical damping, the solution is valid only when $g = 0$. Frequency and damping do not accurately represent the system behavior when damping except $g = 0$. Estimating realistic damping is important in the aerospace industry. Especially, it can be vital when flight flutter tests are considered. Thus, the implementation of the K-Method for the flutter calculations can be chosen carefully by taking into consideration these drawbacks.

2.5.2 The P-K Method

The P-K Method is presented by Hassig [30] to solve the flutter equation, whose solution involves approximation such that aerodynamic forcing has constant amplitude concerning sinusoidal motion. The EOM can be written as follows:

$$\left[[\bar{M}]p^2 + (1 + ig)[\bar{K}] - q_\infty[\bar{Q}_{aero}] \right] \{\eta\} = 0 \quad (2.62)$$

where p is eigenvalue and is defined as $p = \omega(\gamma + i)$ and γ is transient decay rate coefficient, $\gamma = g/2$. The EOM for P-K Method is written slightly different than Eq. (2.60). The difference is the eigenvalue term definition and both methods generally provide the same flutter speed for $g = 0$ condition. The eigenvalue, p is expressed as sinusoidal motion, e^{pt} , and the motion is damped. On the other hand, $[\bar{Q}_{aero}]$ is expressed as, $e^{i\omega t}$ and note that motion is undamped. This produces mathematically inconsistent formulation because of the mismatch between the assumed motion of aerodynamic forces and structural forces.

An iterative approach is developed by Hassig [30] to solve the Eq. (2.62). Circular frequency and the reduced frequency are not independent since $\omega = \frac{kU}{b}$, which is obtained by the eigenvalue solution. Briefly, the eigenvalue problem is solved iteratively considering the relation mentioned above in the P-K Method. The iteration process is explained clearly by Wright J and Cooper J [20].

When an aeroelastic problem includes a significant number of structural modes and free stream velocities, the solution of the problem becomes very time-consuming owing to employing an iteration process.

P-K Method provides more realistic subcritical damping and frequency than the K-Method. Moreover, P-K Method eliminates the looping problem encountered in the K-Method. Both flutter solution methods generally yield the same flutter speed, U_f and flutter frequency, ω_f for $g = 0$.

2.5.3 Non-Iterative P-K (NIPK) Method

Pitt [31] proposed a method that solves the P-K equation (2.62) in a non-iterative manner. Determination of the free stream velocity set is the first step in the Non-Iterative P-K Method like in the classical P-K Method. $[\bar{Q}_{aero}]$ is a function of $\omega_{aero} = \frac{kU}{b}$ for each k in the determined reduced frequency set. The equation (2.62) is solved for each k value without employing interpolation of $[\bar{Q}_{aero}]$ term. The

solution results in a series of ω_{root} and γ_{root} for each ω_{aero} value of the $[\bar{Q}_{aero}]$ term. The interpolation of both ω_{root} and γ_{root} terms is employed based on the matched line at the end of each solution sequence. The interpolation procedure is repeated at each freestream velocity. The rationale of the method is interpolation process is not applied to the aerodynamic term. Hence, this process is much faster than the traditional P-K method, which requires the interpolation of large $[\bar{Q}_{aero}]$ values.

Since the solution of the eigenvalue problem results in unsorted roots or eigenvalues at each velocity, Non-Iterative P-K Method requires root tracking as a function of velocity. Root tracking is crucial when considered Non-Iterative P-K Method. The flutter solution algorithm for the method is given in Table 2.2.

Table 2.2 Flutter Solution Algorithm for Non-Iterative P-K (NIPK) Method in Pseudo Code Form

```

1:  for  $i$  in  $U$  do
2:    for  $j$  in  $k$  do
3:      Define  $\omega_{aero}^{(k)} = k^{(j)} U^{(i)} / b$ 
4:      Call  $Q_{aero}^{(j)}$ 
5:      Solve EVP for  $U^{(i)}$  and  $k^{(j)}$ 
6:      Save  $\omega_{aero}^{(k)}$ ,  $\omega_{root}^{(k)}$  and  $\gamma_{root}^{(k)}$ 
7:    end
8:    for each mode  $j$  do
9:      Interpolate  $\omega_{root}^{(k)}$  and  $\gamma_{root}^{(k)}$  satisfying the condition  $\omega_{aero} = \omega_{root}$ 
10:     Save interpolation results and track modes  $[\omega_{int}^{(j)}(U^{(i)}), \gamma_{int}^{(j)}(U^{(i)})]$ 
11:    end
12:  end
13:  for each mode  $j$  do
14:    Find mode  $j = n_{flutter}$  satisfying  $\gamma_{int}^{(j)} = 0$ 
15:    If  $n_{flutter}$  exists
16:      Interpolate frequencies and velocities for the flutter mode
17:      Save  $U_{flutter}$ ,  $\omega_{flutter}$ 
18:    end
19:  end

```

In conclusion, for the 1-D beam-like cases, structural models are developed mathematically. The first model for the beam-like wings is based on the Rayleigh-Ritz assumed shapes method where the wing is represented as a continuous cantilevered beam. The second structural model is based on the principle of FEM and Euler-Bernoulli beam theory is used for discretization of the wing structure. Besides, a 2-D aerodynamic model is defined regarding Theodorsen's aerodynamics, and it is coupled with 1-D beam-like wing structural models. The evaluation of the Generalized Aerodynamic Force (GAF) matrices by Theodorsen's aerodynamics is expressed in particular to form the aeroelastic equation of motion. The 3-D Doublet Lattice Method (DLM) is introduced, and evaluation of Generalized Aerodynamic Force (GAF) matrices is given for the 2-D wing structures through DLM. The flutter EOM is defined, and particular flutter calculation procedures are given to solve the EOM, namely, K-Method, P-K Method, and Non-Iterative P-K (NIPK) Method.

CHAPTER 3

CLEAN WING CASE STUDIES

This chapter involves the case studies to validate the aeroelastic analysis model for clean wing configurations, which means that wing pylon and external store are not present under the wing. The validation of the model is carried out through three well-known wing models, namely High-Altitude Long Endurance (HALE) wing, Goland wing, and AGARD wing 445.6 (weakened). The case studies are initially carried out for modal analysis, in general, must be completed before performing flutter analysis. Vibrational analyses are performed to determine natural frequencies and mode of vibrations (mode shapes). After that, aeroelastic analysis is performed to define dynamic aeroelastic phenomena including flutter speed and frequency.

The structural model is obtained using three different methods which are FEM with Euler Bernoulli beam formulation, Rayleigh-Ritz method by assumed mode shapes, and 1-D beam modeling in MSC[®]Patran. In the first approach, the structural model is obtained by FEM using Euler-Bernoulli beam formulation. The second approach is based on Rayleigh-Ritz method using a series of assumed shapes that involve pre-defined bending and torsion modes in the analysis. The last structural model is obtained with the help of MSC[®]Patran using FEM. Since the system matrices are required to conduct flutter analysis, both [M] and [K] matrices are exported from MSC[®]Nastran using Direct Matrix Abstraction Program (DMAP) language.

Two distinct unsteady aerodynamic models are utilized to obtain GAF matrices, namely, Theodorsen's 2-D unsteady aerodynamics and Doublet Lattice Method (DLM). The flutter solution is obtained through K-Method, P-K Method, and Non-Iterative P-K Method (NIPK-Method) flutter calculation algorithms. The classical V-g and V-f plots are presented for the specific analysis cases. Finally, results are

compared with the numerous reference studies for verification. The analysis summary table for the case studies is presented in Table 3.1.

Table 3.1 Case Studies Analysis Summary

| | Structural Model | | | | Aerodynamic Model | | Flutter Solution Method | | |
|------------------|--------------------------|----------------------|------------------|-----------|-------------------|-------------------------|-------------------------|----|------|
| | FEM-Euler-Bernoulli Beam | Rayleigh-Ritz Method | MSC® NASTRAN FEM | | DLM | Theodorsen Aerodynamics | K | PK | NIPK |
| | | | 1-D Beam | 2-D Shell | | | | | |
| HALE Wing | ✓ | ✓ | ✓ | | | ✓ | ✓ | | |
| Goland Wing | ✓ | ✓ | ✓ | | | ✓ | | ✓ | |
| AGARD Wing 445.6 | | | | ✓ | ✓ | | | ✓ | |

3.1 High Altitude Long Endurance (HALE) Wing

Since HALE Unmanned Aerial Vehicles (UAVs) are being widely employed in both the defense and civilian industry, the HALE wing is a reasonable study case for the implementation of the given linear aeroelastic model. The sample HALE UAV is presented in Figure 3.1.



Figure 3.1 Sample HALE UAV [32]

The long aspect ratio wings of HALE UAVs are exposed to large structural deflections due to interaction with the airflow and this situation results in geometric nonlinearities in the wing structure. Linear flutter analysis is ineffective when predicting flutter boundaries for such cases. Geometric nonlinearities can vanish because of minimal deflection cases and this situation can be seen at cruise conditions. Since the present study covers linear cases, current analysis can accurately predict HALE wing flutter boundary at cruise conditions [33]. HALE wing model specifications are given in Table 3.2.

Table 3.2 HALE Wing Properties[34]

| Parameter | Value | Unit |
|--------------------------------------|-----------------|------------------|
| Half span, ℓ | 16 | m |
| Chord, $2b$ | 1 | m |
| Mass per unit length, m | 0.75 | kg /m |
| Moment of inertia (50% chord), I_p | 0.1 | kg m |
| Spanwise elastic axis (from LE), a | 50% chord | - |
| Center of gravity (from LE), e | 50% chord | - |
| Spanwise bending rigidity, EI_z | 2×10^4 | N m ² |
| Torsional rigidity, GJ | 1×10^4 | N m ² |
| Chordwise bending rigidity, EI_x | 4×10^6 | N m ² |

To implement the theoretical development of the aforementioned approximate approaches, namely FEM Euler-Bernoulli beam formulation and Rayleigh-Ritz method, an in-house Matlab[®] computer code is developed. Therefore, the structural model would not be developed by relying only on external commercial software, MSC[®]Patran. It is adopted for the validation of the mathematically developed models. To define the vibrational and flutter analysis approach for the HALE wing, Figure 3.2 is given to illustrate the analysis workflow. Figure 3.2(a) shows the analysis workflow through MSC[®]Patran and MSC[®]Nastran while Figure 3.2(b) illustrates the implementation of FEM with Euler-Bernoulli beam formulation and Rayleigh-Ritz method. Both workflows utilize the same aerodynamic model which is developed through 2-D Theodorsen's aerodynamics.

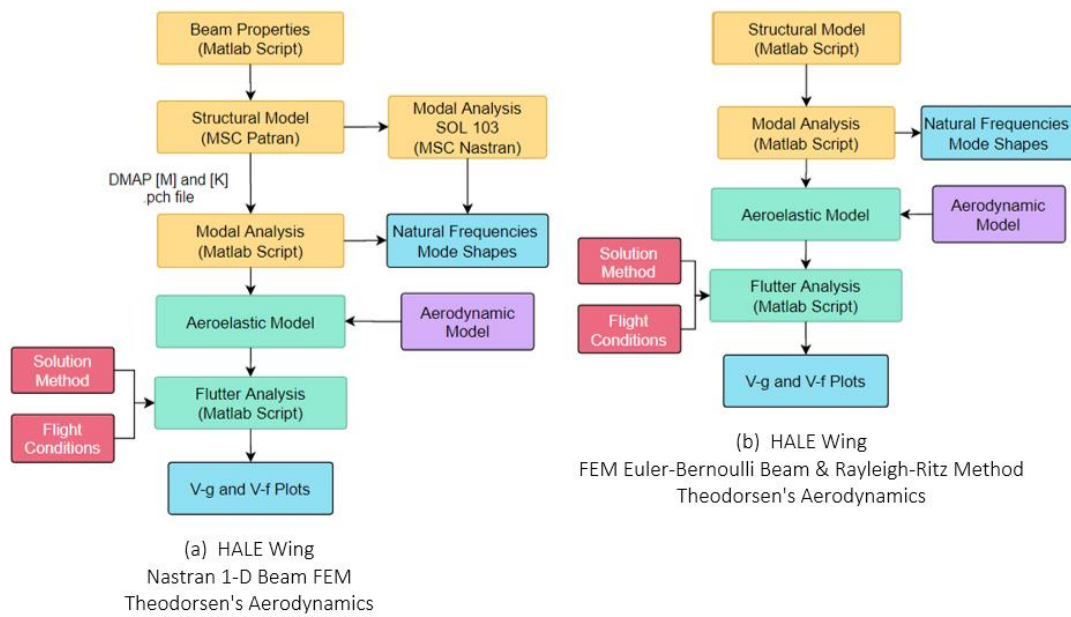


Figure 3.2 HALE Wing Analysis Workflow

In the HALE wing structural model, the equivalent beam flexural axis coincides with the wing flexural axis. It is assumed that the rigidity of the wing is concentrated throughout the entire beam. The structural nodes are strictly at the midpoints of the spanwise sections. The structural node at the wing root physically represents the intersection of the wing with the fuselage. The main assumption in the analysis is that the wing is perfectly fixed at the fuselage imposing no translational and rotational motion.

The first model is obtained by use of FEM with Euler-Bernoulli beam formulation and two distinct models are created with a total of 5 and 20 finite elements, respectively. The purpose of employing different mesh sizes is to investigate the effect of the mesh size on the flutter speed and frequency. The second model is obtained based on the Rayleigh-Ritz method as selecting 4 number of modes in bending and 4 number of modes in torsion. The evaluation of the last structural model is performed with FEM using MSC[®]Patran. In the model, 1-D CBEAM elements with 6 DOFs per node are used and the node at the wing root is fixed. Additional FEM nodes are used to visualize the deformation of the beam, and these nodes are connected to the beam nodes with the rigid elements RBE2. The structural

nodes except fixed root are constrained in translational (Y and Z axes) and rotation (X-axis) degree of freedoms. In other words, relevant deformations and rotations are omitted to obtain the Euler-Bernoulli beam model for the modal and flutter analysis. Therefore, the HALE wing equivalent beam geometry adopted in MSC[®]Patran and is presented in Figure 3.3.

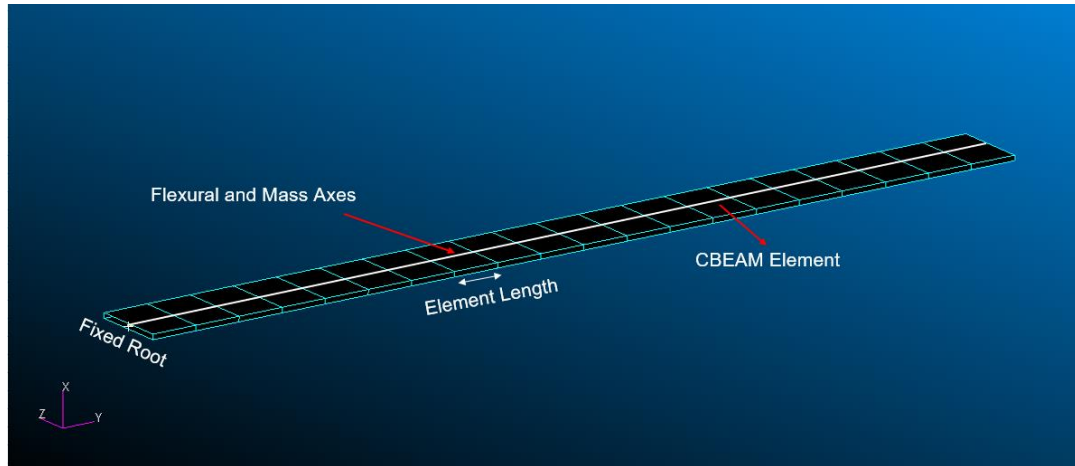


Figure 3.3 HALE Wing Equivalent Beam Geometry

In the structural model, 20 CBEAM elements with 0.8 m sectional length are used to discretize the entire wing. The beam material and geometric properties are given in Table 3.3.

Table 3.3 HALE Wing Equivalent Beam Structural Properties

| Parameter | Value | Unit |
|---------------------------------|-----------|-------------------|
| Equivalent beam width, w_b | 1.26176 | m |
| Equivalent beam height, h_b | 0.08922 | m |
| Elastic modulus, E | 267.823 | MPa |
| Shear modulus, G | 35.039 | MPa |
| Torsional constant, J | 2.854E-04 | m ⁴ |
| Material density, ρ_{wing} | 6.6623 | kg/m ³ |

3.1.1 Structural Analysis

The free vibrational analysis of the HALE wing is carried out regarding the Eq. (2.7). Thus, mode shapes and natural frequencies are obtained for all structural models. Likewise, modal analysis is carried out externally by the Lanczos algorithm [27] in MSC[®]Nastran. As a consequence of free vibration analysis, the first five natural frequencies of the HALE wing are calculated by implementing the above-mentioned methods, and obtained results are given in Table 3.4 along with the results obtained by Patil [35] for the verification purpose.

Table 3.4 Comparison of HALE Wing Natural Frequency Results

| Method | Mode-1 [Hz] | Mode-2 [Hz] | Mode-3 [Hz] | Mode-4 [Hz] | Mode-5 [Hz] |
|--|----------------|----------------|----------------|----------------|----------------|
| FEM- Euler-Bernoulli Beam (5 Elements) | 0.357 | 2.238 | 4.961 | 6.286 | 12.418 |
| FEM- Euler-Bernoulli Beam (20 Elements) | 0.357 | 2.237 | 4.942 | 6.264 | 12.275 |
| Rayleigh-Ritz Method (4 Modes in Bending & Torsion) | 0.357 | 2.237 | 4.941 | 6.264 | 12.274 |
| 1-D Beam Nastran (20 Elements) | 0.357 | 2.227 | 4.946 | 6.217 | 12.142 |
| 1-D Beam Nastran DMAP (20 Elements) | 0.357 | 2.227 | 4.946 | 6.217 | 12.142 |
| Rayleigh-Ritz Method Patil [35] | 0.357 | 2.237 | 4.941 | 6.264 | N/A |

As seen from Table 3.4, the present analysis results are very similar to each other and show a good correlation with the reference values presented by Patil [35]. In particular, direct MSC[®]Nastran results have a perfect match with the case where natural frequencies are calculated by MSC[®]Nastran exported (DMAP) mass and stiffness matrices. Besides, obtained natural frequencies and corresponding elastic modes are presented in Figure 3.4.

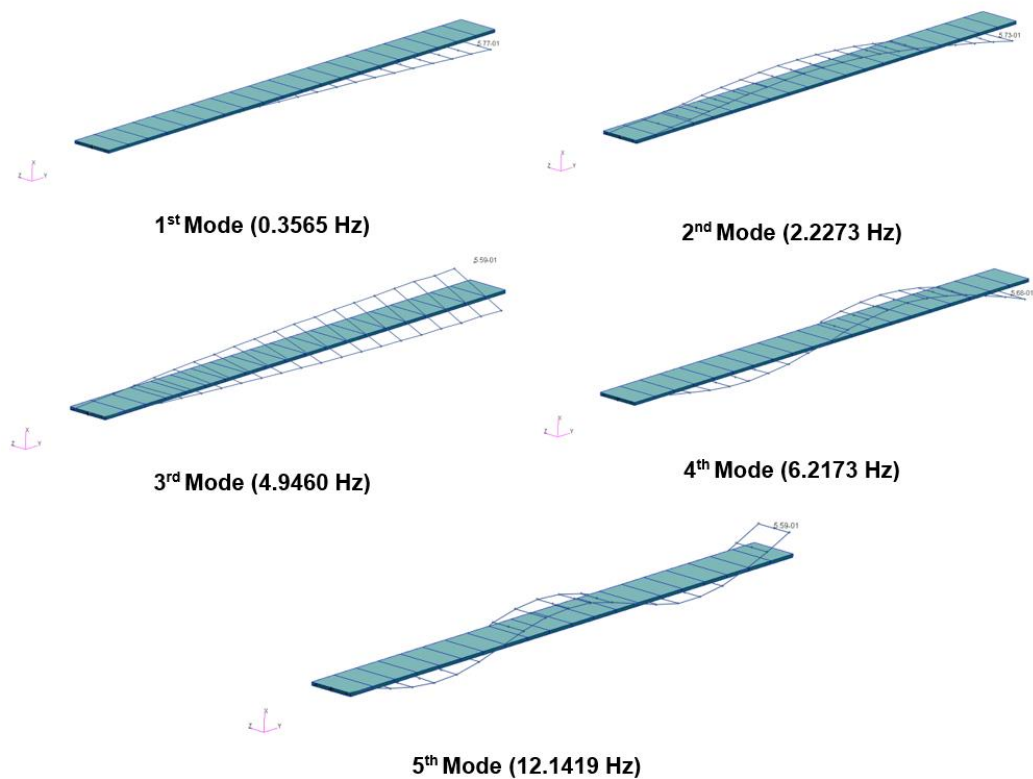


Figure 3.4 HALE Wing Natural Frequencies and Mode Shapes

3.1.2 Aeroelastic Analysis

The aeroelastic analysis combines both structural and aerodynamic analysis and the main objective of performing aeroelastic analysis is to determine the wing's flutter speed. To accomplish flutter speed, the aeroelastic equation of motion (2.9) is required to be formed. The control points (pressure center, P in Figure 2.2) on the wing must be coupled to beam structural nodes because the 1-D beam is the only deformable body on the structure. In this approach, aerodynamic and structural discretization along the spanwise direction is equivalent. Besides, each aerodynamic lifting surface corresponds to a box strip. Thus, individual control points on the box strips are uniquely connected to a structural node located on the elastic axis on the same wing strip. The connection element can be assumed as an infinite stiff beam

element. As a result, the generalized aerodynamic forces (GAFs) can be obtained by integrating lift and moment along the span. After forming an aeroelastic equation of motion, it can be solved by implementing suitable flutter calculation methods. Since flutter analysis of the HALE wing study case is aimed to compare K-Method with P-K Method, NIPK Method is not applied in the analysis.

For the HALE wing study case, the flutter speed and frequency are computed by eigenvalue analysis by implementing both K-Method and P-K Method with Theodorsen 2-D unsteady aerodynamics. Flutter boundary is searched within the pre-defined range of flight speeds. Linear flutter analysis is performed at flight conditions, which are given in Table 3.5.

Table 3.5 Analysis Conditions

| Parameter | Value | Unit |
|------------------|--------------|-------------------|
| Altitude | 20000 | m |
| Air density | 0.0889 | kg/m ³ |

The first four natural frequencies are tracked in the search of the flutter solution. Present analyses cover a total of seven different cases. The results are compared with the reference studies as presented in Table 3.6.

Table 3.6 Comparison of HALE Wing Flutter Results

| | Structural Model | Unsteady Aerodynamics | Flutter Solution Method | Flutter Speed [m/s] | Flutter Frequency [Hz] |
|------------------------|--|---|--------------------------------|----------------------------|-------------------------------|
| Analysis Case-1 | FEM - Euler Bernoulli Beam (5 Elems.) | 2-D Theodorsen Aerodynamics | K-Method | 32.52 | 3.58 |
| Analysis Case-2 | FEM - Euler Bernoulli Beam (20 Elems.) | 2-D Theodorsen Aerodynamics | K-Method | 32.40 | 3.57 |
| Analysis Case-3 | Rayleigh-Ritz Method | 2-D Theodorsen Aerodynamics | K-Method | 32.42 | 3.57 |
| Analysis Case-4 | FEM - Euler Bernoulli Beam (5 Elems.) | 2-D Theodorsen Aerodynamics | PK Method | 32.48 | 3.57 |
| Analysis Case-5 | FEM - Euler Bernoulli Beam (20 Elems.) | 2-D Theodorsen Aerodynamics | PK Method | 32.36 | 3.56 |
| Analysis Case-6 | Rayleigh-Ritz Method | 2-D Theodorsen Aerodynamics | PK -Method | 32.38 | 3.56 |
| Analysis Case-7 | 1-D Beam Nastran DMAP (20 Elems.) | 2-D Theodorsen Aerodynamics | PK Method | 32.40 | 3.57 |
| Patil [33] | Nonlinear Intrinsic Beam Theory [36] | 2-D Peters et. al [37] | K-Method | 32.21 | 3.60 |
| Patil [33] | Nonlinear Intrinsic Beam Theory [36] | 3-D Nonplanar (Doublet +Vortex) Grid: 128 x 8 | K-Method | 31.75 | 3.76 |
| Pepe [38] | Rayleigh-Ritz Method | 2-D Theodorsen Aerodynamics | Modified PK- Method [38] | 32.21 | 3.61 |

A total of seven HALE wing analysis cases have been performed and results are presented along with reference studies. Analysis cases 1 & 2 and analysis cases 4 & 5 show that applying of different size of finite elements do not produce much difference in the flutter results. Furthermore, analysis cases 3 & 6 show that K and P-K Methods yield almost the same flutter speeds, which is expected. Lastly, analysis case 7 exhibits that the development of the HALE wing aeroelastic model, which is combined through MSC[®]Nastran exported structural model and in-house 2-D aerodynamics, is performed successfully. In conclusion, the implementation of

present methods and calculation of the flutter speeds show satisfactory results with the published studies.

In addition to these numerical results, the aeroelastic stability condition of the structure can be determined by inspecting the variation in the aerodynamic damping at different flight speeds. It can be concluded from the velocity versus aerodynamic damping (V-g) graph. The corresponding vibration frequencies for the modes of interest can be seen from the velocity versus frequency (V-f) graphs. The diagrams are presented for selected cases of 3, 5, and 7 in Figure 3.5, Figure 3.6, and Figure 3.7, respectively.

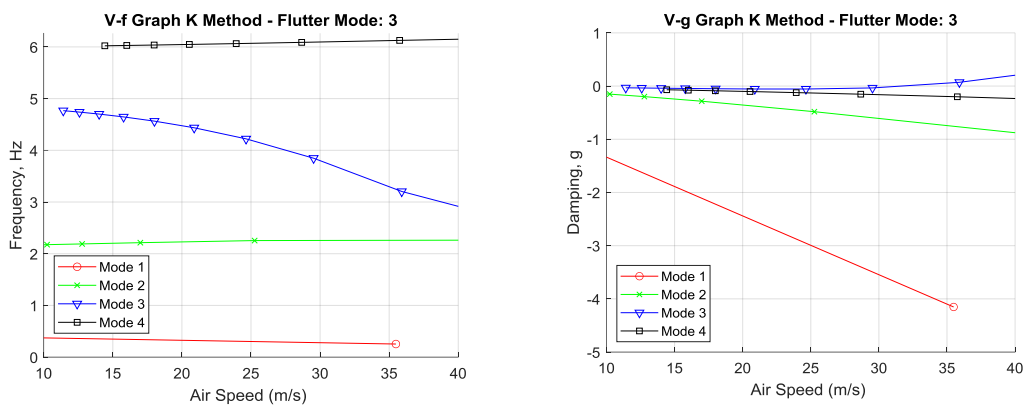


Figure 3.5 Analysis Case-3 V-f and V-g Graphs

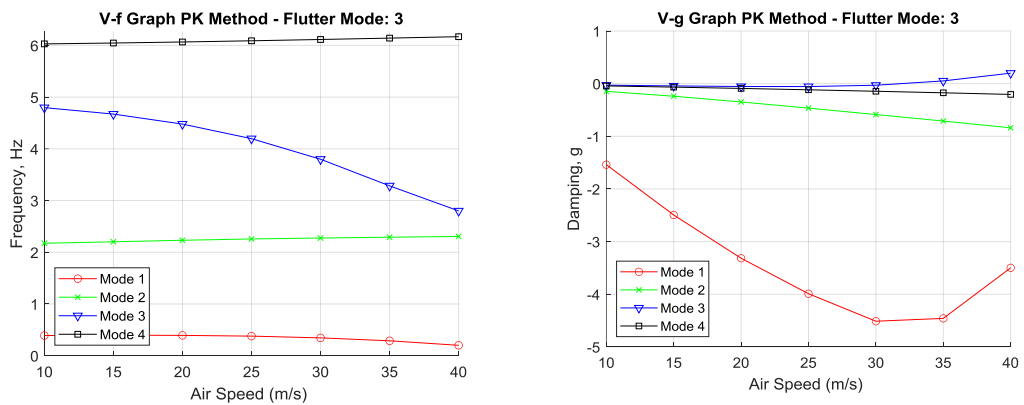


Figure 3.6 Analysis Case-5 V-f and V-g Graphs

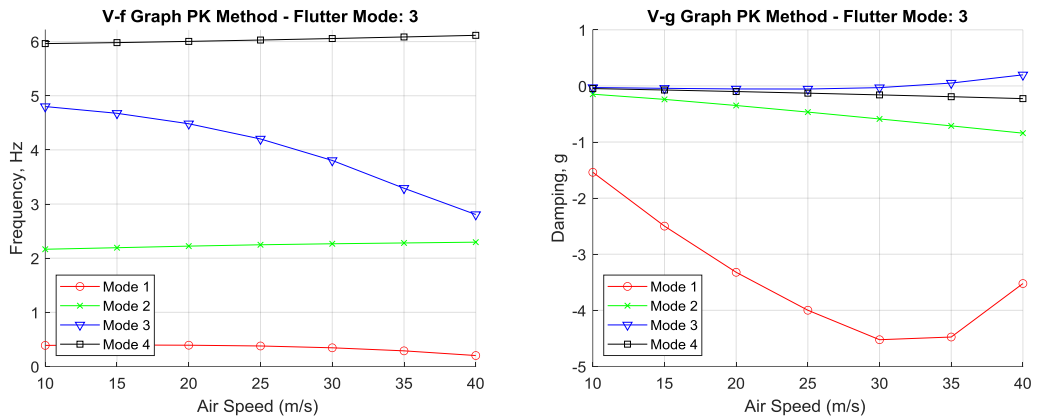


Figure 3.7 Analysis Case-7 V-f and V-g Graphs

The tendency of all four modes for the given cases is like each other. Mode-1 turns downward to stable condition up to airspeed 30 m/s. The vibration frequency of mode-3 decreases with an increase in speed and damping has gone to zero at the airspeed of 32.40 m/s, where is the onset condition for flutter. The frequency of modes-2 and mode-4 remains stable. Besides, mode-2 and mode-3 of the structure are coupled by the fluid-structure interaction. As a result, the present results for the seven different analysis cases are very similar to each other, and they show a good agreement with the reference values.

3.2 Goland Wing

The Goland wing is a stiff and low-aspect-ratio metallic wing. Because of possessing coupled bending-torsional dynamic characteristics, it has been widely used as a benchmark model by many researchers for both structural and aeroelastic validation purposes. The wing has a uniform and rectangular shape, and its geometric and structural properties are given in Table 3.7.

Table 3.7 Goland Wing Properties[39]

| Parameter | Value | Unit |
|--------------------------------------|---------------------|------------------|
| Half span, ℓ | 6.096 | m |
| Chord, $2b$ | 1.8288 | m |
| Mass per unit length, m | 35.71 | kg /m |
| Moment of inertia (50% chord), I_p | 8.64 | kg m |
| Spanwise elastic axis (from LE), a | 33% chord | - |
| Center of gravity (from LE), e | 43% chord | - |
| Spanwise bending rigidity, EI_z | 9.77×10^6 | N m ² |
| Torsional rigidity, GJ | 0.987×10^6 | N m ² |

Likewise in the HALE wing, FEM with Euler-Bernoulli beam formulation and Rayleigh-Ritz method are employed to develop the structural model in Matlab[®]. Besides, MSC[®]Patran is adopted to establish the FE model for validation of the mathematically developed models. To define the vibrational and flutter analysis approach for the Goland wing, Figure 3.8 is given to illustrate the analysis workflow. Figure 3.8(a) defines the analysis workflow through commercial software while Figure 3.8(b) illustrates the implementation of FEM with Euler-Bernoulli beam formulation and Rayleigh-Ritz method for the structural models. Both workflows utilize the same aerodynamic model which is developed through 2-D Theodorsen's aerodynamics.

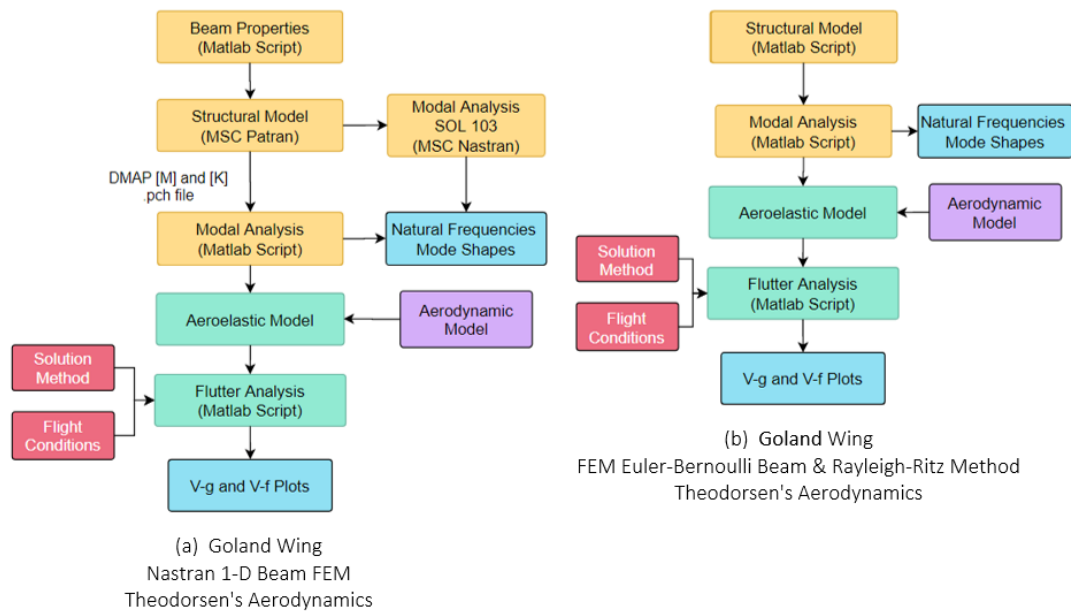


Figure 3.8 Golang Wing Analysis Workflow

There is a total of three structural models which are developed for the Golang wing. The first main model is obtained by use of FEM with Euler-Bernoulli beam formulation with different element sizes. The number of finite elements is 5 and 10 for two different cases, respectively. The second model is obtained based on the Rayleigh-Ritz method by selecting 6 modes in bending and 6 modes in torsion. The evaluation of the last structural model is carried out with FEM using MSC[®]Patran. The wing is modeled with 1-D CBEAM elements with 6 DOFs per node and lumped masses. 10 massless CBEAM elements are used to model flexible characteristics of the wing. Lumped masses with inertia are connected to the structural nodes with the rigid elements RBE2. Shear deformation is neglected to have the Euler–Bernoulli equivalent beam model. Additional nodes are used to visualize the deformation of the beam, and these nodes are connected to the beam nodes with the rigid elements RBE2. Golang wing equivalent beam geometry is presented in Figure 3.9.

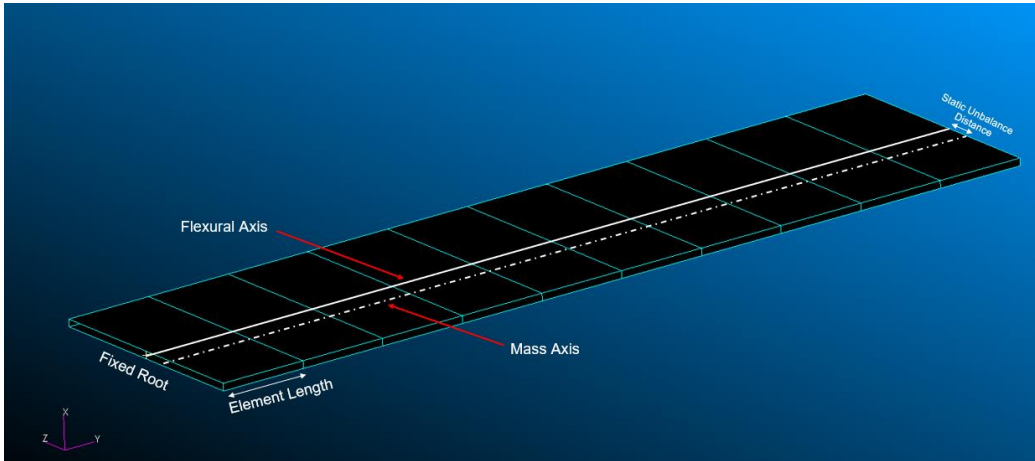


Figure 3.9 Goland Wing Equivalent Beam Geometry

10 CBEAM elements with 0.6096 m sectional length are used to discretize the entire wing in MSC[®]Patran. Relevant structural properties of the lumped element and beam are given in Table 3.8.

Table 3.8 Goland Wing Equivalent Model Structural Properties

| Parameter | Value | Unit |
|----------------------------------|-------------------------|------------------|
| Static Unbalance Distance, a_x | -0.183 | m |
| Equivalent beam width, w_b | 1.5811 | m |
| Equivalent beam height, h_b | 0.05 | m |
| Lumped Mass, m_e | 21.769 | kg |
| Lumped Inertia, I_e | 4.5395 | kgm ² |
| Elastic modulus, E | 5.9325×10^5 | MPa |
| Shear modulus, G | 1.5288×10^4 | MPa |
| Torsional constant, J | 6.4562×10^{-5} | m ⁴ |

3.2.1 Structural Analysis

The mode shapes and natural frequencies are obtained for all structural models via in-house Matlab code. Likewise, external modal analysis is also carried out by the Lanczos algorithm [27] in MSC[®]Nastran. As a result of modal analyses, the first five

natural frequencies of the Goland wing are presented with the aid of previously mentioned methods. Table 3.9 compares the natural frequencies of the Goland wing with two reference results.

Table 3.9 Comparison of Goland Wing Natural Frequency Results

| Method | Mode-1 [Hz] | Mode-2 [Hz] | Mode-3 [Hz] | Mode-4 [Hz] | Mode-5 [Hz] |
|--|-------------|-------------|-------------|-------------|-------------|
| FEM-Euler Bernoulli Beam (5 Elements) | 7.666 | 15.289 | 39.825 | 56.311 | 77.090 |
| FEM-Euler Bernoulli Beam (10 Elements) | 7.664 | 15.245 | 39.053 | 55.583 | 72.276 |
| Rayleigh-Ritz Method (6 Modes in Bending & Torsion) | 7.664 | 15.231 | 38.791 | 55.326 | 70.684 |
| 1-D Beam Nastran (10 Elements) | 7.626 | 15.231 | 38.449 | 54.188 | 69.142 |
| 1-D Beam Nastran DMAP (10 Elements) | 7.626 | 15.231 | 38.449 | 54.188 | 69.142 |
| Analytical [40] | 7.894 | 15.438 | 39.614 | 56.595 | 71.858 |
| FEM-Euler Bernoulli Beam [41] | 7.896 | 15.444 | 39.621 | 56.605 | 71.915 |

In conclusion, Euler-Bernoulli beam formulation is applied for 5 and 10 finite elements for the Goland wing. Besides, 6 modes in bending and 6 modes in torsion are used for the Rayleigh-Ritz method. The results of the present three methods show good agreement in the first 4 modes. The effect of the number of elements in Euler-Bernoulli beam formulation can be seen at mode 5, where 5 element case shows the difference compared to present results and reference studies. Here again, present results show good agreement with the reference studies for the wind-off frequencies, i.e., natural frequencies. In addition to numerical results, the first five natural frequencies and belonging elastic modes are presented from Figure 3.10 to Figure 3.14.

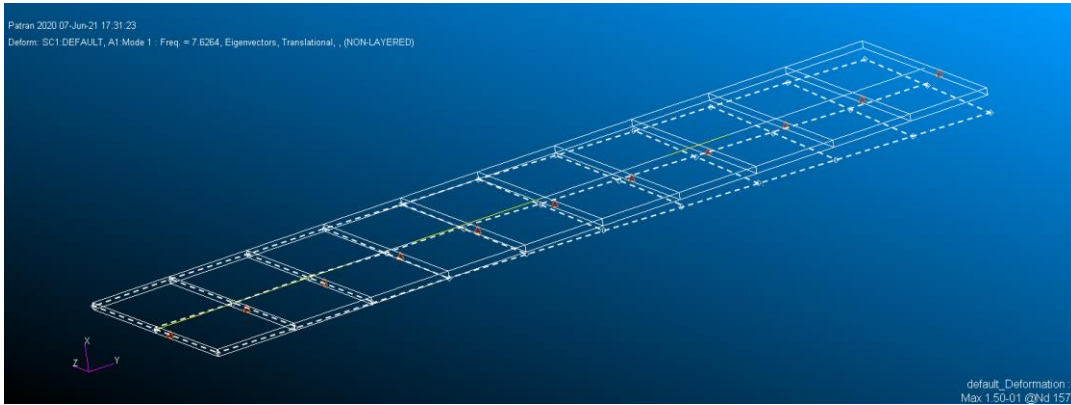


Figure 3.10 Mode-1 (7.626 Hz)

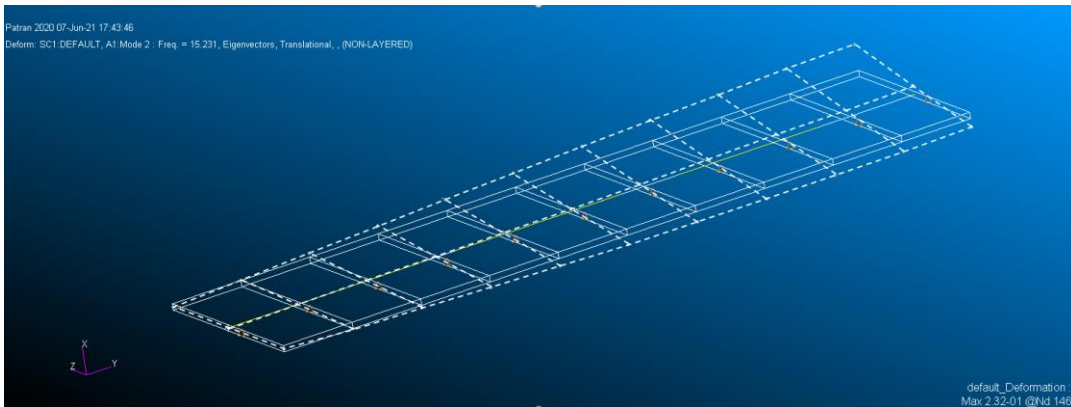


Figure 3.11 Mode-2 (15.231 Hz)

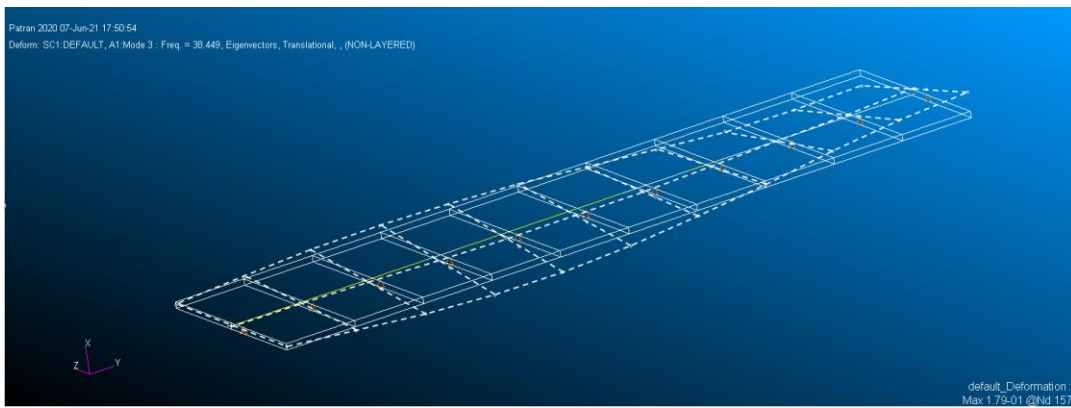


Figure 3.12 Mode-3 (38.449 Hz)

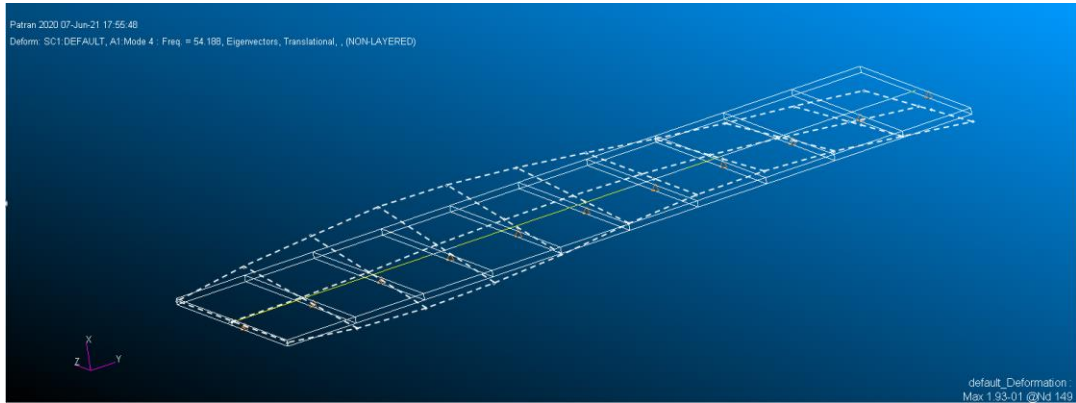


Figure 3.13 Mode-4 (54.188 Hz)

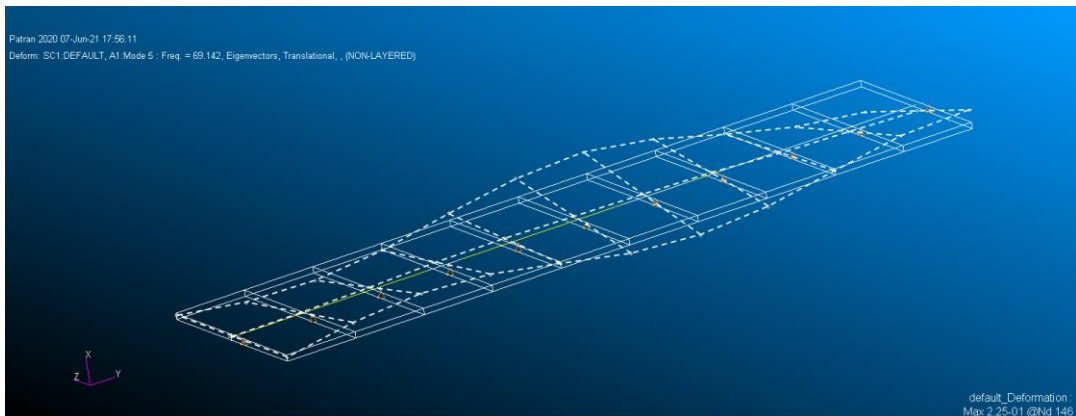


Figure 3.14 Mode-5 (69.142 Hz)

3.2.2 Aeroelastic Analysis

The flutter speed and frequency of the Golland wing are calculated with the 2-D Theodorsen's aerodynamics. Flutter boundary is searched within the pre-defined range of flight speeds and corresponding flight conditions are given in Table 3.10.

Table 3.10 Analysis Conditions

| Parameter | Value | Unit |
|-------------|-----------|-------------------|
| Altitude | Sea Level | - |
| Air density | 1.225 | kg/m ³ |

The flutter speed and frequency are predicted by eigenvalue analysis of the aerodynamic equation of motion by implementing both P-K Method and Non-Iterative P-K Method (NIPK Method). The first three natural frequencies are tracked in the analyses. The flutter results of the Goland wing are achieved by seven different analysis cases as presented in Table 3.12. 2-D Theodorsen aerodynamic formulation is applied in the aerodynamic model, which is combined with a particular structural model.

As considering the flutter analysis, the reduced frequency is calculated from the knowledge of U_{min} , U_{max} , $\omega_{min} = 2\pi f_{min}$ and $\omega_{max} = 2\pi f_{max}$. The relation is defined in the following equations:

$$k_{min} = \frac{b2\pi f_{min}}{U_{max}} \quad (3.1)$$

$$k_{max} = \frac{b2\pi f_{max}}{U_{min}} \quad (3.2)$$

where b is the semi-chord length, U_{min} is the minimum value of speed range of interest, U_{max} is the maximum value of speed range of interest, ω_{min} is the minimum value of the frequency range of interest, and ω_{max} is the maximum value of the frequency range of interest. U_{min} is generally taken as the stall speed while U_{max} is the dive speed of the wing structure. ω_{min} and ω_{max} should be determined depending on the natural frequencies of the structure. ω_{min} should be smaller than the first bending mode frequency, on the other hand, ω_{max} should be greater than the first torsion mode frequency since flutter generally occurs between these modes. For the analyses cases in which the NIPK-Method flutter solution method is employed, the parameter set in Table 3.11 is selected for GAF matrix generation. The same U_{min} and U_{max} range is used for the P-K Method solution. Since the GAF database is essentially formed by k_{min} , k_{max} and N_k , the selection of these values can affect the accuracy of the analysis results. As an example, the insufficient number of k points, or ill-selected k values can reduce the accuracy of the results.

Table 3.11 Goland Wing Flutter Non-Iterative P-K Method Analysis Domain

| Parameter | Value | Unit |
|-----------------------|--------------|-------------|
| U_{min} | 120 | m/s |
| U_{max} | 150 | m/s |
| ω_{min} | 7.6638 | Hz |
| ω_{max} | 38.8561 | Hz |
| k_{min} | 0.2935 | - |
| k_{max} | 1.8603 | - |
| Number of k , N_k | 50 | - |

Table 3.12 compares the flutter speed obtained through the exact differentiation of the equations of motion by Goland & Luke [3]. Patil and Hodges [39] and Qin and Librescu [42] have used the Goland wing to compare their results. Goland & Luke calculated the flutter parameters according to the Rayleigh method and exact differentiation of the equations of motion. Patil and Hodges implemented nonlinear intrinsic beam theory for the structural modeling and 2-D strip theory for the aerodynamics. Qin and Librescu used a thin-walled beam model for the wing structure, 2-D strip theory for the aerodynamics, and K-Method for flutter solution.

Table 3.12 Comparison of Goland Wing Flutter Results

| | Structural Model | Unsteady Aerodynamics | Flutter Solution Method | Flutter Speed, [m/s] | Flutter Frequency [Hz] |
|---|---|------------------------------------|--------------------------------|-----------------------------|-------------------------------|
| Analysis Case-1 | FEM - Euler Bernoulli Beam (5 Elems.) | 2-D Theodorsen Aerodynamics | PK-Method | 137.10 | 11.18 |
| Analysis Case-2 | FEM - Euler Bernoulli Beam (10 Elems.) | 2-D Theodorsen Aerodynamics | PK-Method | 136.83 | 11.15 |
| Analysis Case-3 | Rayleigh-Ritz Method | 2-D Theodorsen Aerodynamics | PK-Method | 136.78 | 11.14 |
| Analysis Case-4 | FEM - Euler Bernoulli Beam (5 Elements) | 2-D Theodorsen Aerodynamics | NIPK-Method | 137.24 | 11.18 |
| Analysis Case-5 | FEM - Euler Bernoulli Beam (10 Elems.) | 2-D Theodorsen Aerodynamics | NIPK-Method | 136.88 | 11.15 |
| Analysis Case-6 | Rayleigh-Ritz Method | 2-D Theodorsen Aerodynamics | NIPK-Method | 136.88 | 11.15 |
| Analysis Case-7 | 1-D Beam Nastran DMAP (10 Elems.) | 2-D Theodorsen Aerodynamics | PK - Method | 137.65 | 11.11 |
| Analysis Case-8 | 1-D Beam Nastran DMAP (10 Elems.) | 2-D Theodorsen Aerodynamics | NIPK-Method | 137.78 | 11.11 |
| Goland & Luke [3] (Exact Sol.) | Analytical | - | - | 137.5 | 11.20 |
| Patil and Hodges[39] | Intrinsic beam Patil [39] | 2-D strip theory Peters et al.[43] | - | 135.6 | 11.17 |
| Qin and Librescu[42] | Thin-walled beam model[42] | 2-D strip theory [42] | K Method | 137.0 | 11.15 |

Results presented in Table 3.12 show a reasonably good correlation with the reference flutter speed and frequency values. The results obtained here considering the eight different analysis cases validate the developed flutter computation codes. In addition to flutter speeds and frequency values, V-g and V-f graphs are presented for selected cases of 2, 6, and 8 in Figure 3.15, Figure 3.16, and Figure 3.17, respectively.

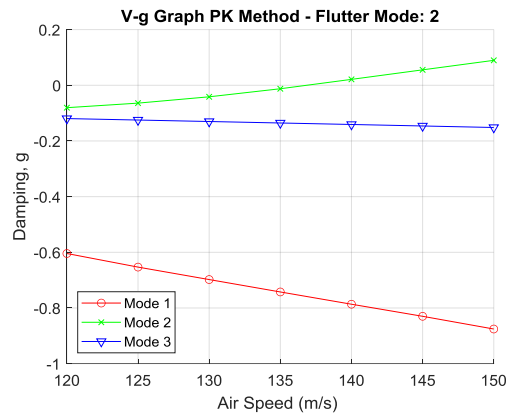
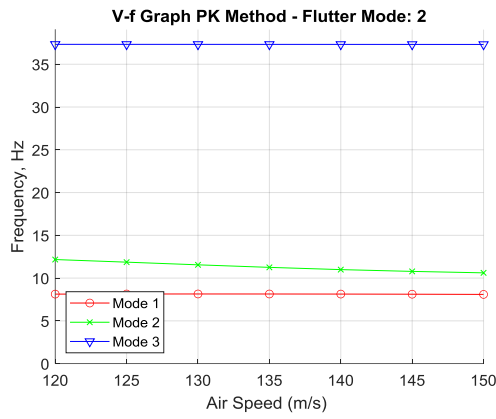


Figure 3.15 Analysis Case-2 V-f and V-g Graphs

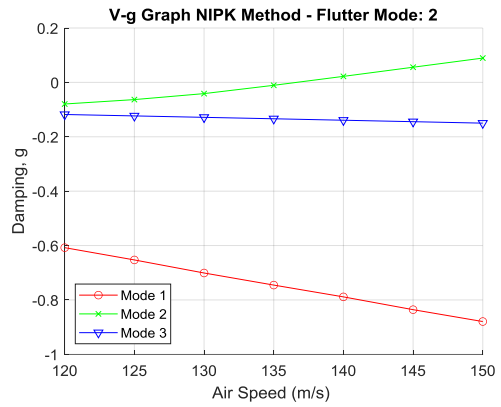
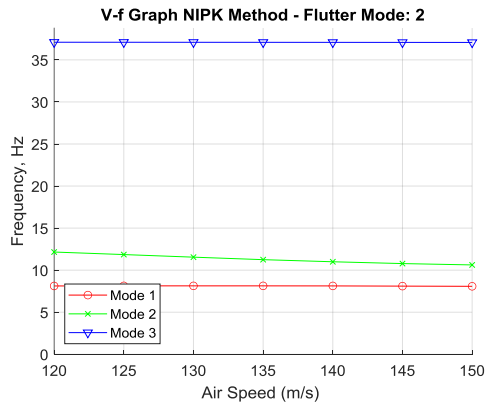


Figure 3.16 Analysis Case-6 V-f and V-g Graphs

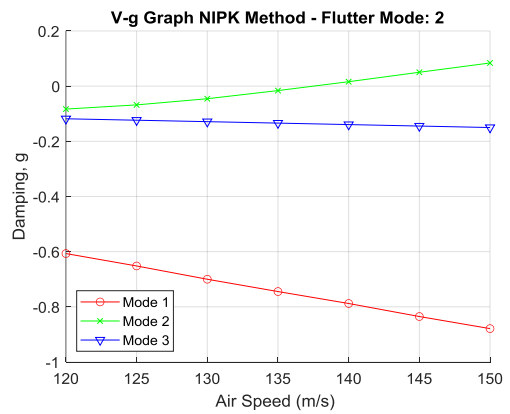
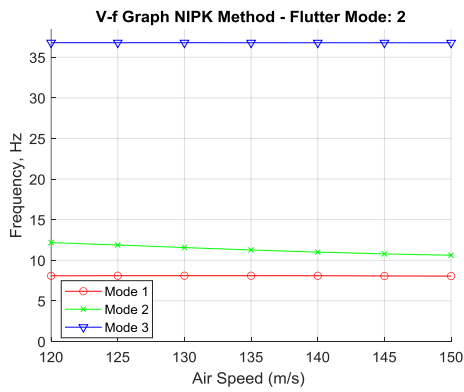


Figure 3.17 Analysis Case-8 V-f and V-g Graphs

The tendencies of all four modes for the given analysis cases are similar to each other. Mode-1 turns downward to stable condition while mode-3 remains stable in both damping and frequency. The frequency of the mode-2 slightly decreases with an increase in speed and damping has gone to zero around the airspeed approximately 137 m/s, where is the onset condition for flutter. It means that the aerodynamic instability condition is seen in the second mode. Here again, the present results for the eight different analysis cases are very similar to each other, and they show a good agreement with the reference values.

3.3 AGARD 445.6 Wing

In this case study, the well-known AGARD (Advisory Group for Aerospace Research and Development) 445.6 wing is chosen to conduct free vibrational and flutter analyses by MSC®FlightLoads and MSC®Nastran. The wing was initially tested by Yates Jr [44]. The geometrical properties of the wing are shown in Figure 3.18. The wing has a root chord of 0.559 m and tip chord of 0.368 m, a semi-span of 0.762 m, a taper ratio of 0.66, and an aspect ratio of 1.65. The wing has a quarter-chord sweep angle of 45° and NACA 65A004 profile with no twist or curvature along the length.

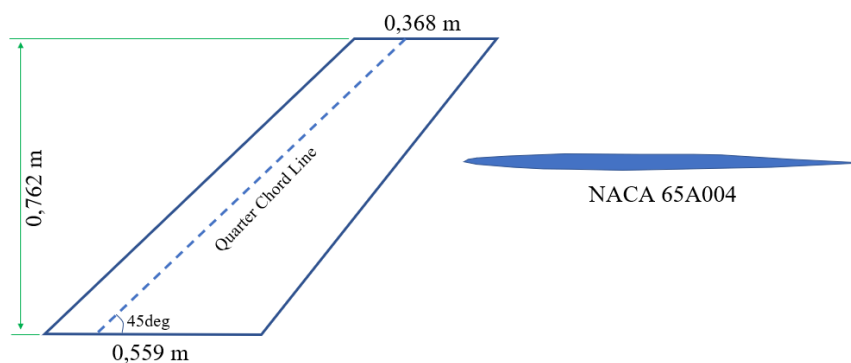


Figure 3.18 AGARD 445.6 Wing Planform

The wing material properties in each direction are presented in Table 3.13, where E is elasticity modulus, G is shear modulus, and ρ_{wing} is the density.

Table 3.13 Material Properties for Weakened AGARD 445.6 Wing

| Material Property | Value | Unit |
|-------------------|---------|-------------------|
| E_{11} | 3.1511 | GPa |
| E_{22} | 0.41621 | GPa |
| E_{33} | 0.41621 | GPa |
| ν_{12} | 0.31 | - |
| ν_{13} | 0.31 | - |
| ν_{23} | 0.31 | - |
| G_{12} | 0.4392 | GPa |
| G_{23} | 0.4392 | GPa |
| G_{13} | 0.4392 | GPa |
| ρ_{wing} | 397 | kg/m ³ |

In the analysis, MSC[®] Patran is adopted to establish the FE model. On the other hand, the aerodynamic model is created on MSC[®] FlightLoads. The wing's structural and AIC matrices are exported to Matlab[®] environment by use of MSC[®] Nastran DMAP language. Aeroelastic analyses codes are developed by utilizing Matlab[®] using the NIPK Method. To express the vibrational and flutter analyses for the AGARD 445.6 wing, Figure 3.19 is given to illustrate the analysis workflow.

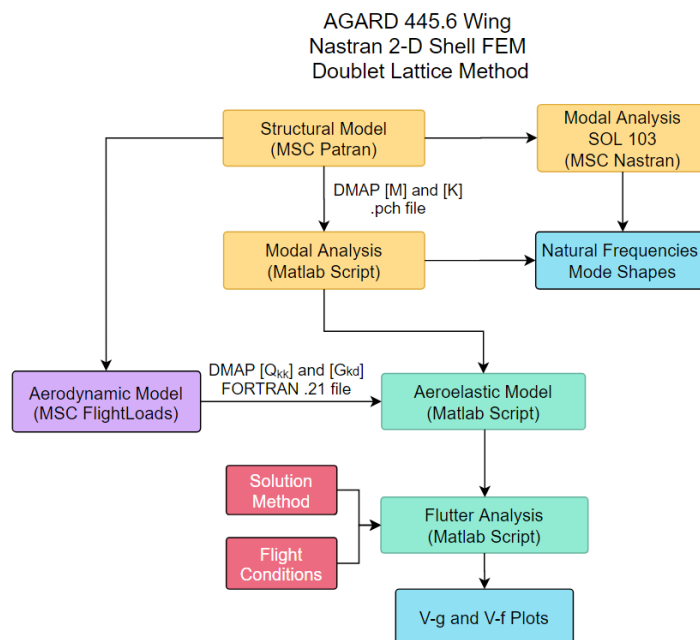


Figure 3.19 AGARD 445.6 Wing Analysis Workflow

The finite element model for the AGARD 445.6 weakened wing is created in MSC[®]Patran. The FEM has 200 quadrilateral shell elements (CQUAD4) and 231 structural nodes. The nodes at the wing root are fixed in all directions. The structural nodes except root are constrained in translational (X and Y axes) and rotation (Z-axis) degree of freedoms. The finite element model of the wing is presented in Figure 3.20.

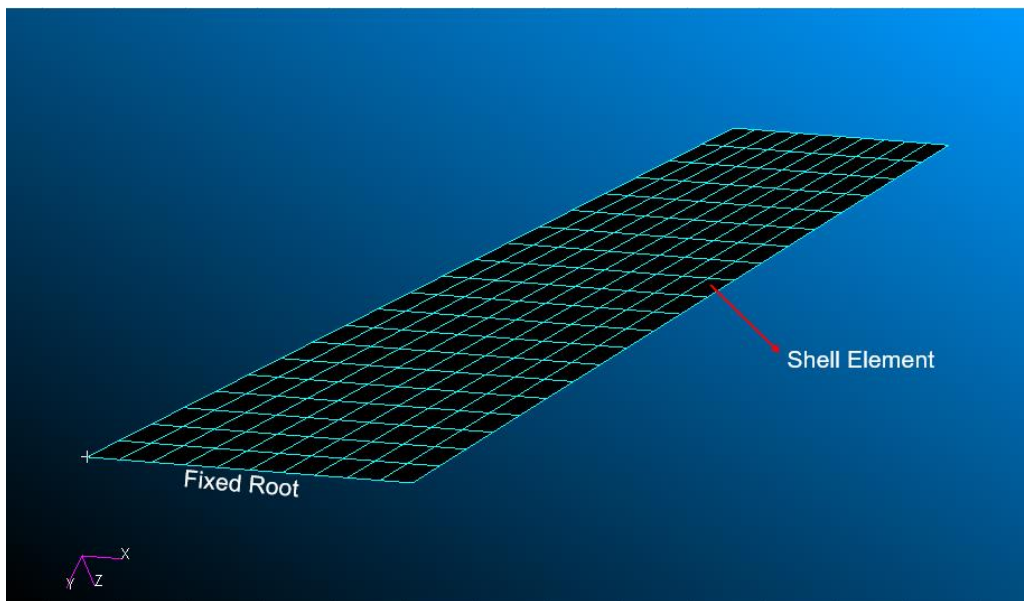


Figure 3.20 AGARD 445.6 Wing Finite Element Model

3.3.1 Structural Analysis

The free vibrational analysis of the AGARD 445.6 weakened wing is carried out with both the SOL103 normal modes sequence and Matlab[®] code. The first five elastic modes are presented and compared with experiment results by Yates [44] in Figure 3.21.

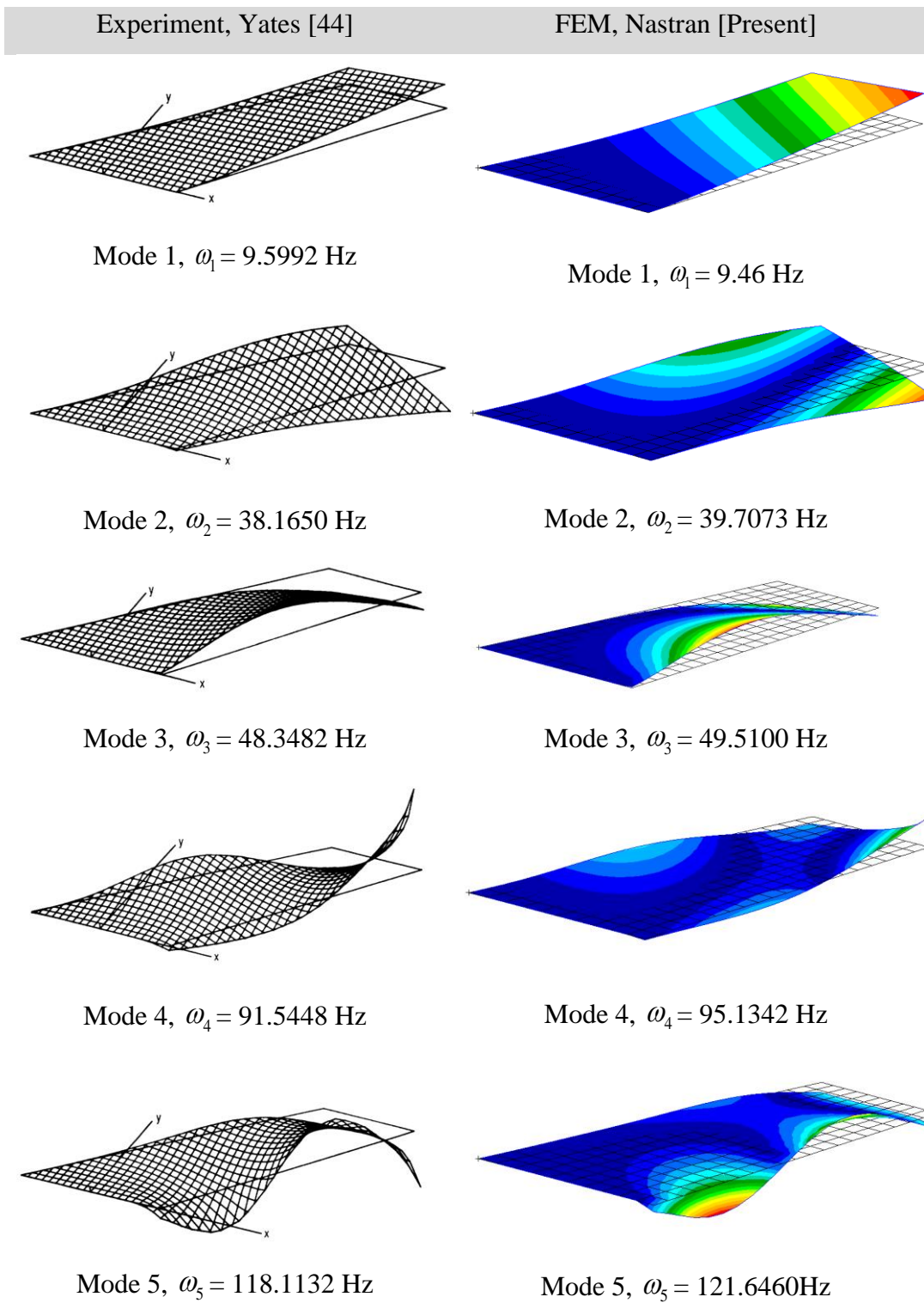


Figure 3.21 Comparison of Mode Shapes

Table 3.14 compares the first five natural frequencies of the present study with the experimental results [44], Kolonay [45], and Lee and Batina [46].

Table 3.14 Comparison of Natural Frequencies

| | Mode-1 [Hz] | Mode-2 [Hz] | Mode-3 [Hz] | Mode-4 [Hz] | Mode-5 [Hz] |
|-----------------------------------|------------------------|------------------------|------------------------|------------------------|------------------------|
| 2-D Shell Nastran | 9.46 | 39.71 | 49.51 | 95.13 | 121.65 |
| 2-D Shell Nastran DMAP | 9.46 | 39.71 | 49.51 | 95.13 | 121.65 |
| Experiment [44] | 9.60 | 38.17 | 48.35 | 91.55 | 118.11 |
| Kolonay [45] | 9.63 | 37.12 | 50.50 | 89.94 | - |
| Lee and Batina [46] | 9.60 | 38.17 | 48.35 | 91.54 | - |

The first five natural frequencies of the MSC[®]Nastran SOL103 normal modes sequence and in-house free vibration analysis with Matlab[®] using $[M]$, mass matrix and $[K]$, stiffness matrix, which are exported through MSC[®]Nastran DMAP language, are identical to each other. Present mode-4 natural frequencies slightly differ from the reference values and that difference is not critical for the flutter analysis. Consequently, the present results show a good agreement with the experimental results for natural frequencies and mode shapes. Besides, because of having a good agreement with the other reference studies, the flutter analysis can be performed by using constructed structural model.

3.3.2 Aeroelastic Analysis

Since previously investigated HALE and Goland wing structures are essentially based on 1-D beam theory, 2-D sectional lift and moment theories such as Theodorsen's aerodynamics are well suited for these structures. The reason is that unsteady approximations for the lift and moment around the elastic axis are calculated based on infinitesimal strips of the wing and integrated over the whole span of the wing, which results in overestimating the lift. Hence, the theory is suitable for surfaces with very high aspect ratios, such as the HALE wing. On the contrary, the DLM is a lifting element method based on 3-D lifting surface theory.

Since Theodorsen's aerodynamics are not preferred to use with low aspect ratio wings, such as AGARD wing, and being a 2-D shell structure, the present flutter analyses are carried out employing the DLM.

The aerodynamic model is obtained by dividing the surface into 800 aero boxes that involve spanwise 40 and chordwise 20 elements. Aero-structural coupling is achieved by using Infinite Plate Spline (IPS). The reference air density is taken as 1.225 kg/m^3 for the analyses. Mach-Reduced Frequency (M-k) sets are defined before the flutter solution. The aeroelastic analyses are performed for the following cases: Mach Numbers of 0.449, 0.678, 0.901, and 0.954. The frequencies are taken as $f_{min} = 1 \text{ Hz}$ and $f_{max} = 100 \text{ Hz}$ for the analyses.

Table 3.15 shows the flutter analysis conditions defined as Mach number, air density, density ratio, and minimum and maximum free stream airspeeds.

Table 3.15 Aeroelastic Analysis Conditions for AGARD 445.6 Wing

| Mach Number | Density[kg/m ³] | Density Ratio | U _{min} [m/s] | U _{max} [m/s] |
|-------------|-----------------------------|---------------|------------------------|------------------------|
| 0.449 | 0.42770 | 0.34886 | 100 | 200 |
| 0.678 | 0.20818 | 0.16980 | 100 | 300 |
| 0.901 | 0.09945 | 0.08112 | 150 | 350 |
| 0.954 | 0.06338 | 0.05170 | 200 | 400 |

MSC[®]Nastran is used to derive AGARD 445.6 wing's both structural and aerodynamic matrices. Flutter solution is provided by in-house Matlab[®] code implementing the Non-Iterative P-K Method (NIPK) method, which is not present in MSC[®]Nastran. To compare the flutter results against reference studies, the Flutter Speed Index (FSI) is calculated and plotted. FSI for the AGARD 445.6 wing case is defined as follows:

$$FSI = \frac{U_f}{b\omega_a\sqrt{\mu}} \quad (3.3)$$

where ω_a is the angular frequency of the first torsion mode in rad/s and μ is the mass ratio. The root semi-chord, $b_s = 0.2794 \text{ m}$ and $\omega_a = (2\pi) \times 39.7073 \text{ rad/s}$. The mass ratio, μ is defined as $FSI = m_w/(\rho_f V_c)$ where $m_w = 1.862 \text{ kg}$ is the wing

panel mass, ρ_f is the free-stream density at flutter, $V_c = 0.130 \text{ m}^3$ is the volume of the truncated cone. The second flutter parameter for comparison purposes is Flutter Frequency Ratio, ω/ω_a .

The efficient calculation of unsteady aerodynamic forces and moments results from structural deformation is challenging when especially the transonic flow regime is considered. Doublet Lattice Method (DLM) provides satisfactory results and low computational cost for the calculation of flutter boundary in subsonic flow regime. Nevertheless, transonic flows possess nonlinear characteristics and linear panel methods like DLM are not able to model combined subsonic-supersonic flows. The DLM mostly fails in predicting shock positions and intensity for such flow regimes. Therefore, an improvement of the DLM results can be particularly made in the transonic flow regime due to its nonlinear characteristics. The improvement is based on increasing the accuracy of the DLM results, which is defined as so-called corrections. For such corrections, reliable reference data such as Computational Fluid Dynamics (CFD) or wind tunnel data can be used to improve the results of the DLM.

Katzenmeier et al. [47] presented a method to correct model DLM results with small disturbance CFD results. The correction aims to improve the quality of the DLM results including limited transonic effects. Figure 3.22 compares the GAF entries for the first two elastic modes of the AGARD 445.6 wing obtained through MSC[®]Nastran DLM results along with the reference study results of Katzenmeier et al. [47] given as DLM, CFD, and corrected DLM. The GAF entries presented as real and imaginary parts for the Mach number of 0.954.

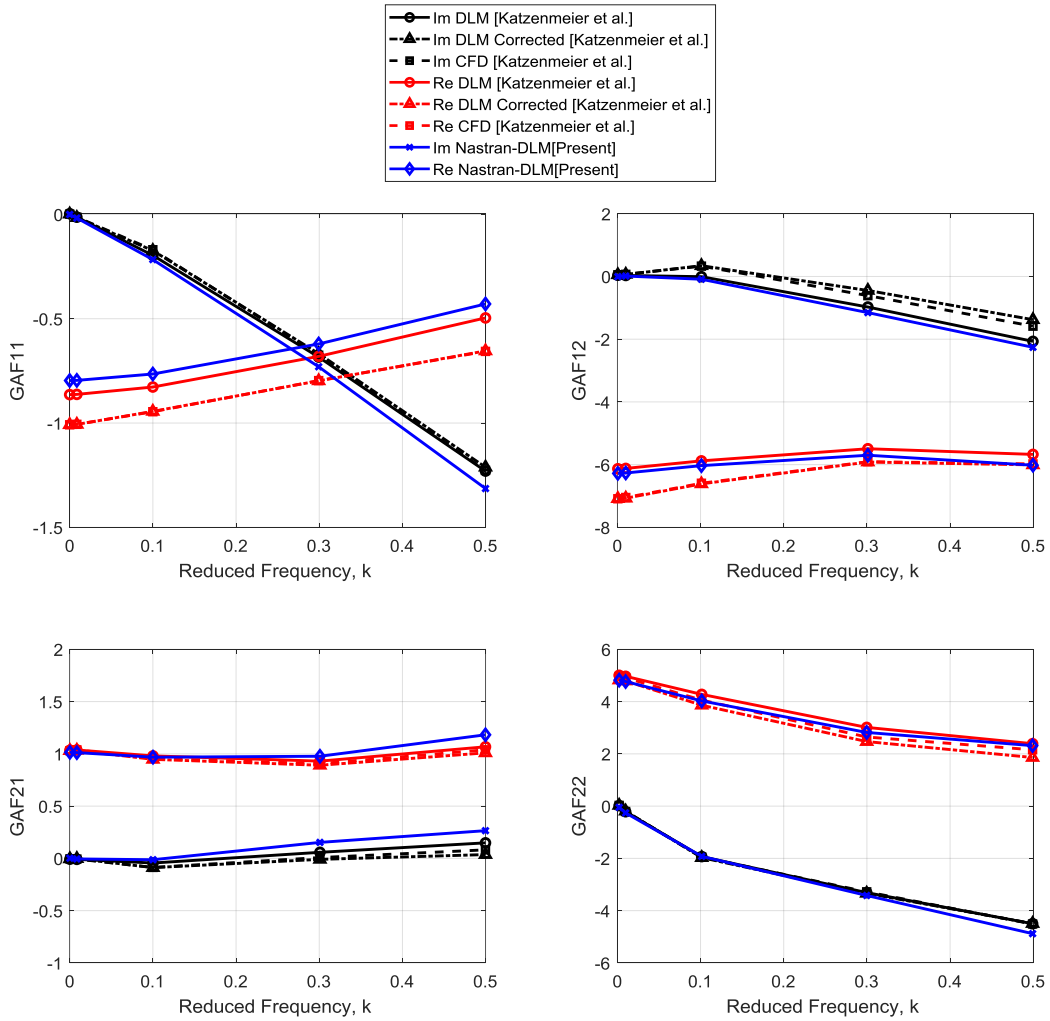


Figure 3.22 Comparison of GAF Entries for Mach Number, $M = 0.954$

A good agreement can be seen between the present MSC[®] Nastran DLM and DLM results given in the reference study. Deviations are present between CFD and DLM results because of mentioned transonic flow effects. The corrected DLM results converge the CFD results as expected.

Figure 3.23 and Figure 3.24 show a comparison of the flutter boundary and frequency of the AGARD 445.6 wing against the experimental data by Yates [44] and results calculated by CFD, DLM, and corrected DLM methods by Katzenmeier et al.[47]. The reference flutter solution is obtained by P-K Method.

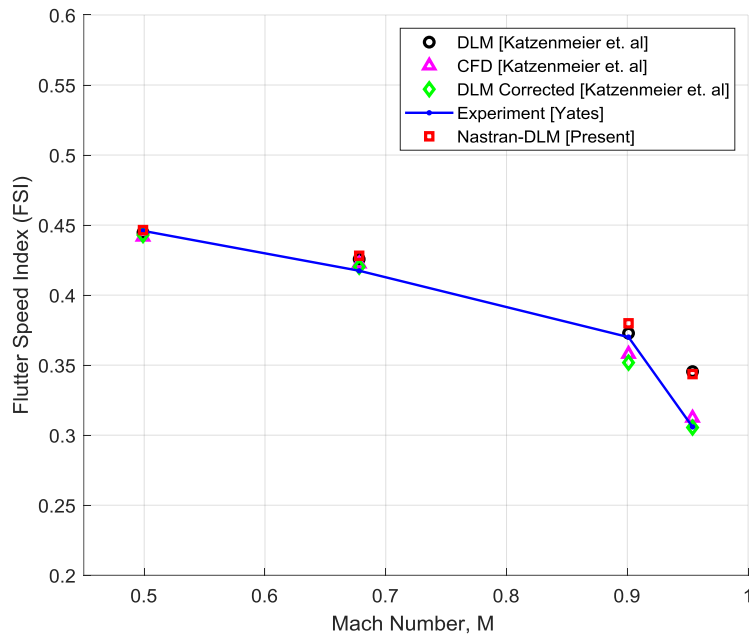


Figure 3.23 Comparison of AGARD 445.6 Wing Flutter Speed Index

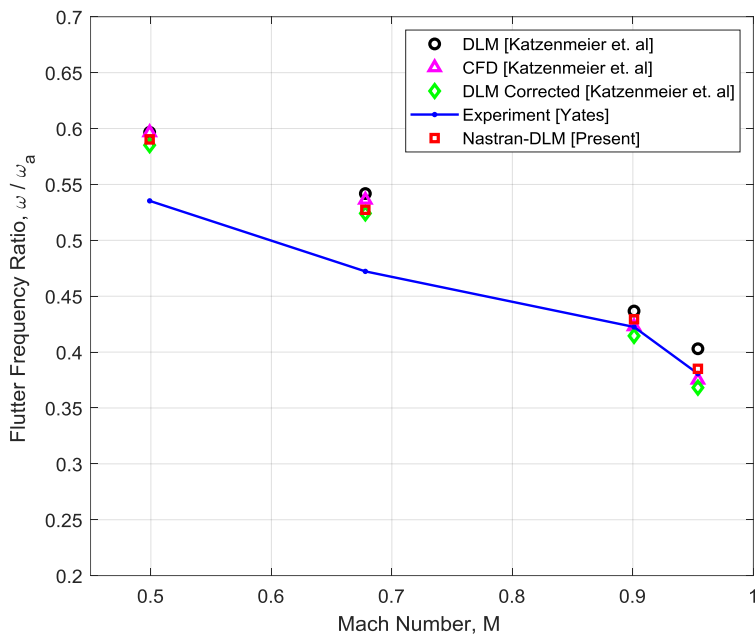


Figure 3.24 Comparison of AGARD 445.6 Wing Flutter Frequency Ratio

Table 3.16 shows FSI of the present study implementing 2-D FEM theory for the structural model and Doublet Lattice Method (DLM) for the unsteady aerodynamics.

Table 3.16 AGARD 445.6 Wing Flutter Speed Index Results

| Mach Number | FSI |
|--------------------|------------|
| 0.449 | 0.4464 |
| 0.678 | 0.4281 |
| 0.901 | 0.3799 |
| 0.954 | 0.3436 |

It can be concluded that the present analyses results are in good agreement with the experimental results and the results obtained through CFD, DLM, and corrected DLM methods by Katzenmeier et al.[47].

In conclusion, case studies for the clean wing structures are performed to validate the developed aeroelastic analysis models. The validation of the models is carried out through three well-known wing models, namely High-Altitude Long Endurance (HALE) wing, Goland wing, and AGARD wing 445.6 (weakened). In the first stage, free vibrational analyses are performed to obtain modal matrices. Following this vibrational analysis, GAF matrices are obtained and the aeroelastic equation of motion is formed. In the last step, aeroelastic analysis is performed to obtain flutter speed and frequency. For the HALE wing, natural frequencies and mode shapes are initially obtained, then 2-D Theordorsen's aerodynamics is coupled with structural models, and finally, flutter solution is achieved. A total of seven analyses cases have been investigated and validated along with the reference studies. The famous Goland wing is investigated in the second case study. The structural model is developed based on the principle of a Rayleigh-Ritz method and FEM with coupled Euler-Bernoulli beam theory. Moreover, MSC[®]Patran is utilized to develop a 1-D beam model for the wing. All structural models have been validated by comparing their first five natural frequencies along with the reference studies. The flutter solution is obtained by Theordorsen's aerodynamics, P-K, and NIPK flutter solution

algorithms. A total of eight analyses cases have been performed and results are compared along with the reference studies. The results validate the developed aeroelastic model for the Goland wing, which involves bending-torsion structural modes. The last case study is conducted through a well-known AGARD 445.6 wing (weakened). The structural model is based on the FEM by discretizing the entire wing into shell elements in MSC[®]Patran. The aerodynamic model is constructed in MSC[®]FlightLoads and Dynamics and aero-structural coupling is achieved by using Infinite Plate Spline (IPS). The first five natural frequencies of the wing are obtained and compared along with the reference studies. The aerodynamic analyses have been performed at different Mach numbers to investigate the accuracy of the DLM. The first four GAF entries are obtained utilizing the MSC[®]Nastran DMAP language and compared along with the reference study. The results show that the agreement between the obtained results and reference work is satisfactory. Lastly, Flutter Speed Index (FSI) and flutter frequency ratio are obtained for the AGARD 445.6 wing, and a comparison has been made through a work of Katzenmeier et al.[47] and an experimental study. The results of all three case studies have been shown that the developed aeroelastic models are successfully validated.

CHAPTER 4

AEROELASTICITY OF THE WINGS WITH EXTERNAL STORES

Aircraft wings are the critical aeroelastic structures concerning aeroelastic analysis, especially aeroelastic instability situation, i.e., flutter. Integrating the external stores into aircraft wings considerably affects the aeroelastic characteristics of the wing structure. It naturally changes the free vibration and dynamic responses of the aircraft wing. The large variety of wing store configurations drastically affects both the static and dynamic behavior of the aircraft wings. Moreover, the attachment element between wing and store, i.e. pylon structural characteristics significantly influence the flutter boundary. Because of being one of the most critical aeroelastic phenomena, wing store flutter shall be considered carefully in the aircraft aeroelastic design stage.

This chapter consists of two parts. The first part is the theory for the two common types of wing store systems while the second part is the case studies of them. The first model is the beam-like wing with concentrated mass. The store is attached to the wing rigidly with no additional DOFs. The structural model is developed by utilizing MSC[®]Patran and FEM with Euler-Bernoulli beam formulation. On the other hand, the aerodynamic theory is based on the 2-D Theodorsen formulation. The structural and aeroelastic analyses are conducted with in-house Matlab[®] code. The second one is the flat-plate delta wing with a flexible external store. The development of the model and pertinent analyses are conducted by utilizing MSC[®] FlightLoads and MSC[®]Nastran, respectively.

4.1 Beam-Like Wing with Concentrated Mass Model

Because of depending on large computational costs, high-fidelity methods can be reduced to numerical methods in the 1-D framework. FEM with Euler-Bernoulli

beam theory has been validated to model bending-torsion clean wing structures in the previous chapter. The clean wing FEM can be modified by rigidly attaching an external store represented by concentrated mass at the selected structural node on the wing. Figure 4.1 represents the rigidly attached wing store configuration with y_{span} denotes the concentrated mass location along the span. The attachment node is denoted by i^{th} node.

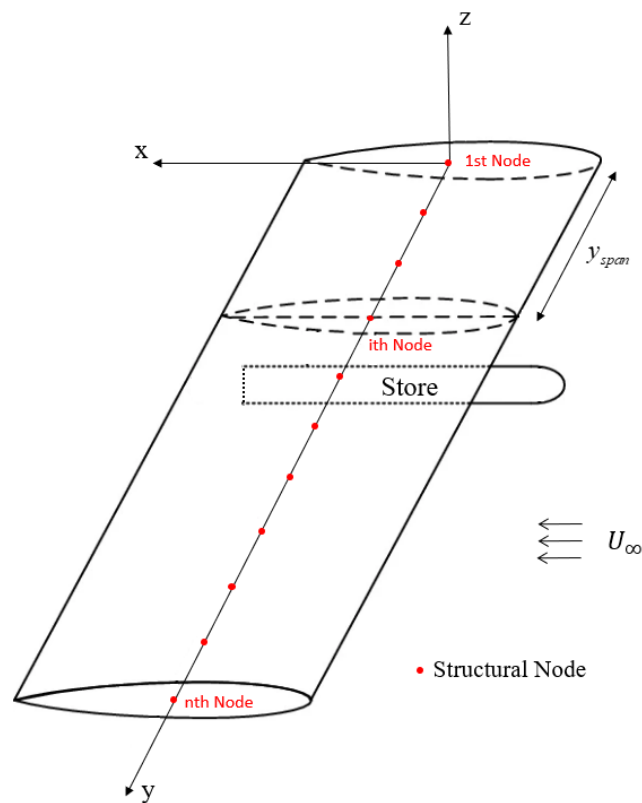


Figure 4.1 Rigidly Attached Wing Store Configuration

4.1.1 Rigid Body Motion of the Concentrated Mass

Consider the concentrated mass as a 3-D structure with a total mass of m_c and it is attached to stiff springs. Then, $O(x,y,z)$ is a general coordinate system concerning the concentrated mass center of gravity. A 3-D structure with a total mass of m_c on the supports is illustrated in Figure 4.2.

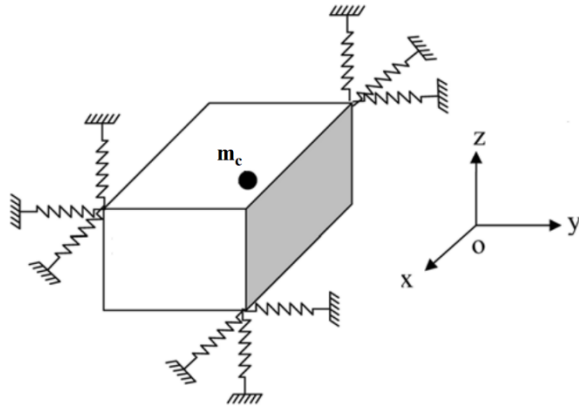


Figure 4.2 A 3-D Structure on the Supports[48]

The rigid body motion of the concentrated mass structure can be defined in 6 independent DOFs. The equations of motion of the concentrated mass under free-free condition is expressed below in the linear form [48]:

$$\begin{bmatrix} m_c & 0 & 0 & 0 & zm_c & -ym_c \\ 0 & m_c & 0 & -zm_c & 0 & xm_c \\ 0 & 0 & m_c & ym_c & -xm_c & 0 \\ 0 & -zm_c & ym_c & I_{oxx} & -I_{oxy} & -I_{oxz} \\ zm_c & 0 & -xm_c & -I_{oxy} & I_{oyy} & -I_{oyz} \\ -ym_c & xm_c & 0 & -I_{oxz} & -I_{oyz} & I_{zzo} \end{bmatrix} \begin{Bmatrix} \ddot{q}_x \\ \ddot{q}_y \\ \ddot{q}_z \\ \ddot{q}_{\theta_x} \\ \ddot{q}_{\theta_y} \\ \ddot{q}_{\theta_z} \end{Bmatrix} = \begin{Bmatrix} F_x \\ F_y \\ F_z \\ M_x \\ M_y \\ M_z \end{Bmatrix} \quad (3.4)$$

where x , y , and z are the distances of the center of mass about point $O(x,y,z)$, I is the moment of inertia, \ddot{q} is the linear acceleration, and \ddot{q}_{θ} is the rotational acceleration of the concentrated mass. In addition to these, F and M are the external forces exerted on the structure. Eq. (3.4) can be defined in a simple form as follows:

$$[M_o]_{6 \times 6} \{\ddot{q}\}_{6 \times 1} = \{F\}_{6 \times 1} \quad (3.5)$$

where $[M_o]$ is the rigid body mass matrix whose elements are the mass properties of the structure about the point $O(x,y,z)$. Note that the rigid body mass matrix, $[M_o]$ includes inertia properties of the structure.

4.1.2 Evaluation of Concentrated Mass Matrix for Wing Store Systems

Since the store is considered as concentrated mass and it is attached to the wing rigidly, the rigid body mass matrix, $[M_o]$ can be reconsidered, but this time for the wing store systems. The typical wing store section is given in Figure 4.3 with a_x is the chordwise distance between the wing flexural axis and center of gravity. The chordwise distance between the wing flexural axis and store center of gravity is denoted by x_s . The vertical distance from the wing chord line and store center of gravity is denoted by z_s . The aerodynamic loads cause the deformation such that the flexural axis of the wing moved along the z-axis, and it rotates about the flexural axis. It is assumed that the wing chord line is always parallel to the store chord line under deformation.

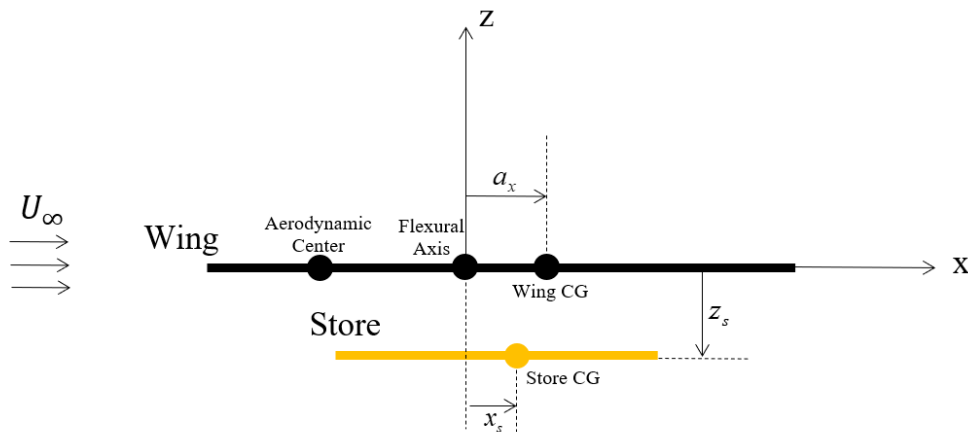


Figure 4.3 Wing Store Section

Because all the mass properties of the store are calculated about the wing flexural axis, the point $O(x,y,z)$ given in Figure 4.2 can be interpreted as the wing flexural axis for the wing store system cases. In this manner, mass properties of store can be obtained by making use of the similarity between rigid body motion of the concentrated mass and rigidly attached wing store systems. For the wing store case, M_s is the store mass, I is the store inertia term, x_s , and z_s the distances from store center of gravity to wing flexural axis. The spanwise distance between the wing structural node at a distance of y_{span} and the store center of gravity is denoted by the

term y_s . As considering the above, rigid body mass matrix, $[M_o]$ can be defined here as a mass matrix of the store, $[M_{store}]$ which can be expressed as follows:

$$[M_{store}] = \begin{bmatrix} M_s & 0 & 0 & 0 & z_s M_s & -y_s M_s \\ 0 & M_s & 0 & -z_s M_s & 0 & x_s M_s \\ 0 & 0 & M_s & y_s M_s & -x_s M_s & 0 \\ 0 & -z_s M_s & y_s M_s & I_{xx} + (y_s^2 + z_s^2) M_s & -(I_{xy} + x_s y_s M_s) & -(I_{xz} + x_s z_s M_s) \\ z_s M_s & 0 & -x_s M_s & -(I_{xy} + x_s y_s M_s) & I_{yy} + (x_s^2 + z_s^2) M_s & -(I_{yz} + y_s z_s M_s) \\ -y_s M_s & x_s M_s & 0 & -(I_{xz} + x_s z_s M_s) & -(I_{yz} + y_s z_s M_s) & I_{zz} + (x_s^2 + y_s^2) M_s \end{bmatrix} \quad (3.6)$$

Note that the store mass matrix, $[M_{store}]$ includes the inertia terms in the explicit form because the parallel axis contribution of the M_s is explicitly shown. Since the shear deformations are neglected in the Euler-Bernoulli beam model, the store mass matrix can be reduced the form as follows, where the distance, y_s is taken as $y_s = 0$.

$$[M_{store}] = \begin{bmatrix} M_s & 0 & -x_s M_s \\ 0 & I_{xx} + z_s^2 M_s & -I_{xy} \\ -x_s M_s & -I_{xy} & I_{yy} + (x_s^2 + z_s^2) M_s \end{bmatrix} \quad (3.7)$$

4.1.3 Structural Equations of Motion

The global form of system matrices provides the clean wing dynamic characteristics according to the discrete coordinates of the system. The structural part of the aeroelastic equation of motion for the clean wing can be reconsidered here. The equation can be modified for the wing store system as follows:

$$[M_{wing+store}]\{\ddot{x}\} + [K]\{\dot{x}\} = \{0\} \quad (3.8)$$

where $\{x\}$ is nodal displacements, $[M_{wing+store}]$ and $[K]$ are the global mass and stiffness matrices, respectively. Since the attachment is rigid without additional DOF, the mass matrix of the wing store structure, $[M_{wing+store}]$ can be defined as below:

$$[M_{wing+store}] = [[M_{wing}] + [\Delta M]] \quad (3.9)$$

where $[\Delta M]$ defines local structural mass modification on the wing structure and its size $n \times n$ is equal to the size of $[M_{wing}]$. Modification matrix, $[\Delta M]$ can be formed according to $[M_{store}]$ that is defined previously. The spanwise location, y_{span} of the concentrated mass and the corresponding structural node can be defined for each attachment. In the case of multiple concentrated mass attachments, this method allows modeling multiple store attachments for wing store systems. It should be noted that if a specific spanwise attachment location is defined, one is required to define a structural node at the desired attachment location. The generalized form of mass $[\bar{M}_{wing+store}]$ and stiffness $[\bar{K}]$ matrices can be obtained as below:

$$[\bar{M}_{wing+store}] = [\phi]^T \left[[M_{wing}] + [\Delta M] \right] [\phi] \quad (3.10)$$

$$[\bar{K}] = [\phi]^T [K] [\phi] \quad (3.11)$$

where $[\phi]$ is the modal matrix which is formed by the selected normal mode shapes and each column of $[\phi]$ represents a normal mode shape, ϕ_i . Furthermore, the natural frequencies ω_i and the normal mode shapes ϕ_i can be obtained by solving the eigenvalue problem of the wing store structure, where i is the order of the natural frequency or normal mode.

4.2 Flat-Plate Delta Wing with Flexible External Store Model

A delta wing is a low aspect ratio wing and is named for its similarity to a triangle. Although it is efficient in all flow regimes, it is generally used in supersonic aircraft. One of the main advantages of the delta wing is that it possesses structurally strong characteristics, which leads to carrying a large number of external stores simultaneously.

A delta wing store experimental model has been developed by Demand Tang, Peter Attar, and Earl H. Dowell [9] to investigate the flutter and Limit Cycle Oscillation (LCO) characteristics of the wing store system. The effect of the external store pitch

stiffness (attachment stiffness) and the spanwise location of the external store on the flutter speed and limit cycle oscillations (LCO) are discussed in the study.

In the present study, the wing is modeled as a simple plate with constant thickness. The external store is modeled as a slender rigid body that is attached to the wing through two support points. The vertical distance of the external store is arranged by these support points. The aft support is attached to the wing with a linear spring, on the other hand, the fore support has a joint that enables to store having pitch motion. The external store is assumed to have one degree of freedom (pitch) concerning the wing. In other words, the external store is a single degree of freedom system while considering wing store dynamics. Figure 4.4 presents the delta wing model with an external store and its two support points.

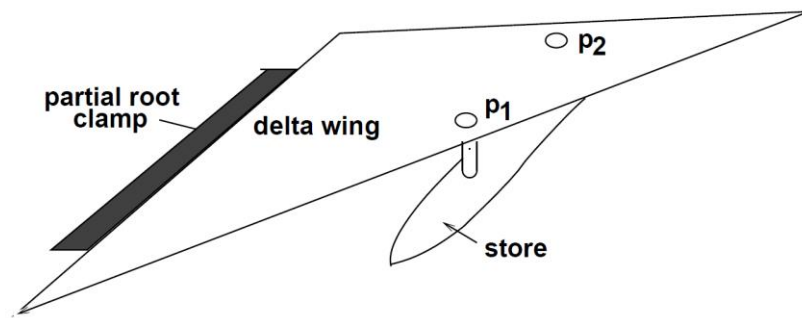


Figure 4.4 Attachment Locations Between the Wing and Store [9]

In addition, Figure 4.5 presents the section of the delta wing model with an external store. In the wing store dynamic model, M_1 is the mass of the external store and M_2 is the mass of the aft mounting point, which can be interpreted as pylon mass. P_1 and P_2 denote the fore and aft mounting points of the external store to the wing, respectively. Z_1 and Z_2 are the vertical displacements of the fore and aft mounting points of the store, respectively. e_2 is the distance between the aft and fore mounting point and e_3 is the mass center location of the external store from the fore mounting point, P_1 . The distance between the tip of the store and the fore mounting point, P_1 is denoted by the distance e_1 .

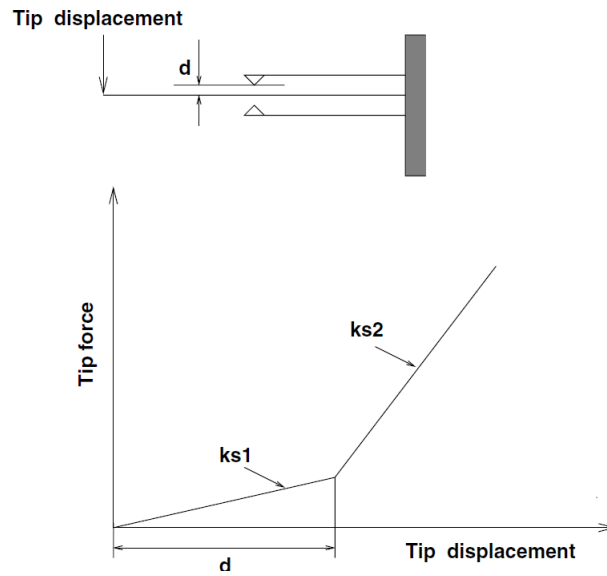


Figure 4.6 Illustration of the Stiction Force [49]

Since the present study covers the linear attachment elements between the wing and the store, nonlinear attachment parameters σ , k_{s1} and k_{s2} can be taken as $\sigma = 0^\circ$ and $k_{s1} = k_{s2}$ for the linear case.

4.2.1 Finite Element Model

Attar et al. [50] modeled the wing store structure by implementing a high-fidelity nonlinear structural model by using the commercial FE software ANSYS. In the present study, the MSC[®]Patran is used to model the wing store structure linearly and MSC[®]Nastran commercial FE code is used as the linear structural solver. The wing store system is defined through different types of finite elements. Since the flexible delta wing is assumed to have isotropic thin plate characteristics, PSHELL entry and three-node CTRIA3 elements are used to model the structure. CTRIA3 element has six degrees of freedom, three translational, and three rotations. Mass of the external store, M_1 and the mass of the aft connection point, M_2 are modeled by using the CONM2 element that includes inertia terms. The elastic part of the external store is defined by equivalent beam theory using store pitch stiffness, k_s . The flexible section of the external store is modeled by using CBAR elements.

On the other hand, the rigid section of the store is modeled by using multi-point constraint MPC elements. The type of the MPC is selected as RBE2. Figure 4.7 represents the elements used in the FE model of the delta wing store system.

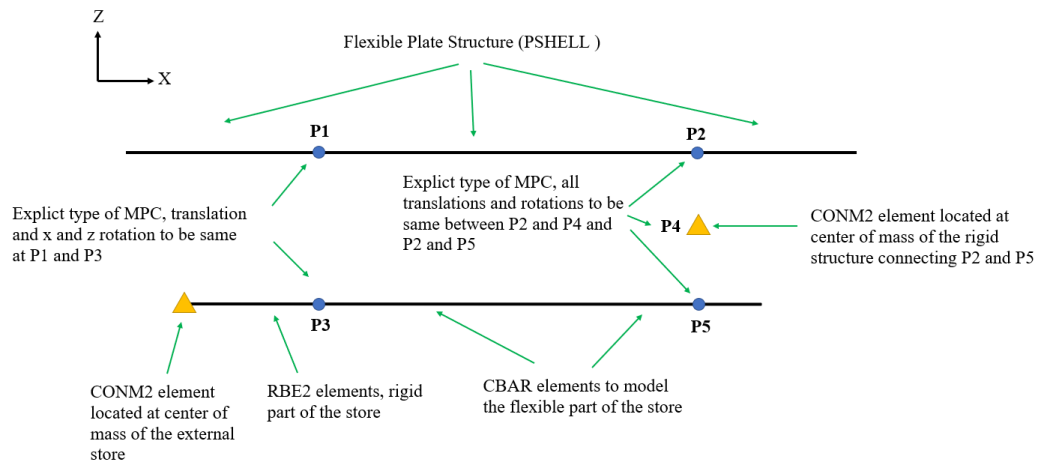


Figure 4.7 Illustration of the Elements of the FE Model

The mounting location, P1 to the joint is modeled by using the explicit type of MPC element. An explicit type of MPC allows defining one node for dependent terms and unlimited nodes for the independent terms. P3 is selected as a dependent term while P1 is selected as an independent term. The DOFs are defined as UX, UY, UZ (translational DOFs), and RX, RZ (rotational DOFs) which means the rotation about the y-axis is not constrained as the store rotates about P3. Similarly, all translations and rotations are constrained between the point P2 and P4 and P2 and P5.

4.3 Wing Store Flutter Case Studies

4.3.1 Beam-Like Wing with Concentrated Mass Case Study

The wing store system consists of a uniform cantilever wing and mass attachment as described in Runyan et al. [4]. The mass is assumed as concentrated at different spanwise locations; however, it is about 0.41 chord forward of the flexural axis of the cantilevered wing. The model specifications are described for the analyses in Table 4.1.

Table 4.1 Beam-Like Wing with Concentrated Mass Properties [5]

| Parameter | Value | Unit |
|--------------------------------------|--------------|-------------------|
| Half span, ℓ | 1.2192 | m |
| Chord, $2b$ | 0.2032 | m |
| Mass per unit length, m | 1.2942 | kg/m |
| Moment of inertia, I_p | 0.0036 | kg m |
| Spanwise elastic axis (from LE), a | 43.7 % chord | - |
| Center of gravity (from LE), e | 45.4 % chord | - |
| Spanwise bending rigidity, EI_z | 403.76 | N m ² |
| Torsional rigidity, GJ | 198.58 | N m ² |
| Store Mass, M_s | 1.443 | kg |
| Store Moment of Inertia, I_{yy} | 0.0185 | kg m ² |

Two structural models are developed for this case study. For the first model, FEM Euler-Bernoulli beam theory is initially applied to develop the clean wing structure. Then, clean wing mass matrix is modified by means of a store mass matrix to construct wing store structure. 48 beam elements are used in Euler-Bernoulli beam formulation. The necessary analytical work for developing the clean wing structural model, structural modifications, and free vibration analysis are performed by utilizing Matlab[®] code. For the second structural model, MSC[®] Patran is utilized to

model the wing store structure. Similarly, 48 CBEAM elements with 6 DOFs per node are used for the entire wing. The node at the wing root is fixed. Elemental lumped masses are connected rigidly to the nodes located on the flexural axis with rigid elements RBE2. The structural nodes except fixed root are constrained in translational (Y and Z axes) and rotation (X-axis) degree of freedoms. The store is modeled by using the CONM2 element and it is attached to the beam nodes at desired wing spanwise location by RBE2 elements. Figure 4.8 shows the FEM of the beam-like wing with the store is attached to the wingtip.

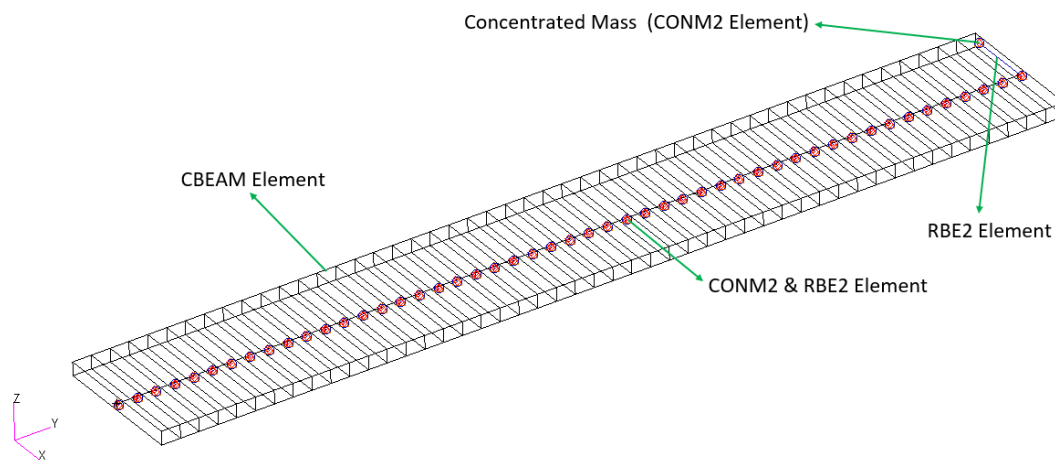


Figure 4.8 Beam-Like Wing FEM with Concentrated Mass at Wingtip

An aerodynamic model is developed by implementing 2-D Theodorsen aerodynamics. Both structural models are coupled with the same aerodynamic model to form aeroelastic models. The store aerodynamic properties are neglected in the present analysis.

4.3.1.1 Structural Analysis

The first four natural frequencies are obtained by use of both MSC[®]Nastran SOL103 sequence and in-house analysis workflow. Since MSC[®]Patran provides the $[M]$ identical to $[M_{wing+store}]$ for the entire wing store structure, modification of the

clean wing mass matrix is not performed for the MSC[®]Nastran case. On the other hand, $[M_{wing}]$ is initially obtained by utilizing FEM with Euler-Bernoulli beam theory. Then, $[M_{wing+store}]$ is formed by use of store mass modification matrix, $[\Delta M]$ and clean wing mass matrix, $[M_{wing}]$.

Calculation of the normal modes has been performed for the clean wing (store at wing root) and the wing with mass at six different spanwise positions. The mass is attached to the 0.2794 m, 0.4318 m, 0.762 m, 1.143 m, 1.1684 m, and 1.2192 m spanwise locations from the wing root, where the variation of the first four normal modes against mass nondimensional spanwise location can be seen in Figure 4.9.

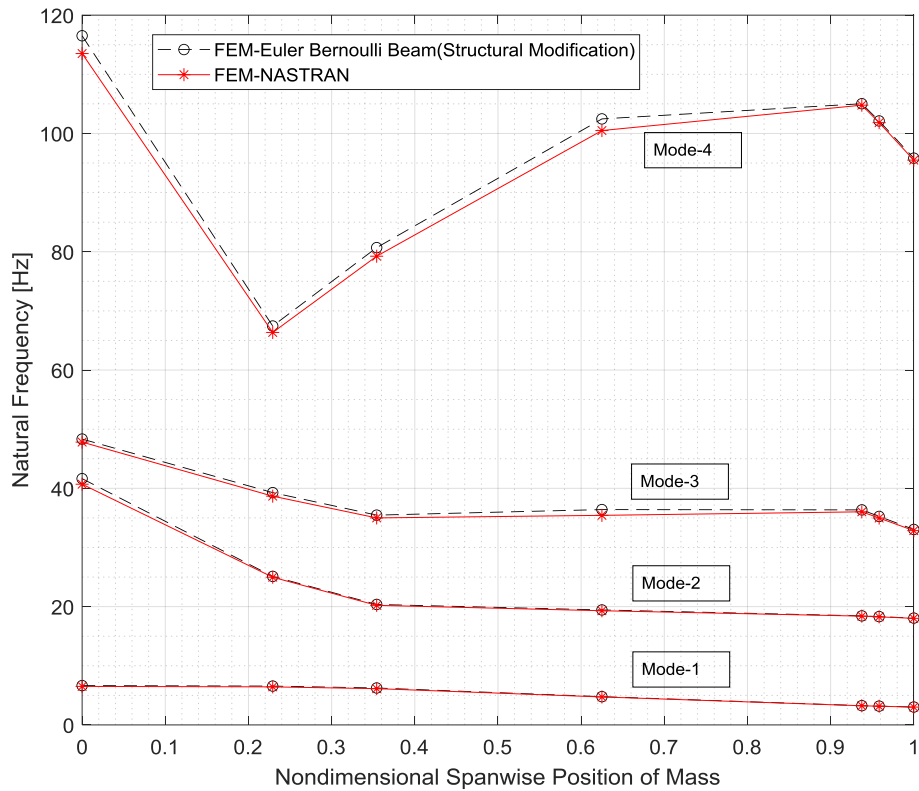


Figure 4.9 Wing Store Natural Frequencies vs Nondimensional Spanwise Location of Concentrated Mass for the First Four Modes

The first four normal modes of the wing mass structure are in good correlation when FEM with Euler-Bernoulli beam formulation and MSC[®]Nastran FEM results are considered. These results show that the development of the wing store structural model by structural modification approach has been successfully implemented for the beam-like wing with concentrated mass. Hence, the modified wing store structure is validated along with the free vibration analysis results of MSC[®]Nastran, whose solution is not included the structural modification approach.

4.3.1.2 Aeroelastic Analysis

The flutter speed and frequency of the beam-like wing store structure are calculated with the 2-D Theodorsen aerodynamics. The flutter analyses are carried out at sea level conditions taking air density as 1.225 kg/m³.

Runyan and Seawall [4] experimentally investigated a wing store system that consists of a uniform cantilever wing and concentrated mass. Then, Runyan and Watkins [5] analyzed the flutter of the same wing store system and made a comparison between the analytical and the experimental results. In this developed approach, the differential equations were used to govern the motion of a uniform wing and an exact solution was applied. Besides, the two-dimensional aerodynamic forces were derived by applying Theodorsen's aerodynamics. Since physical or mathematical simplifications are not involved in the exact solutions, Wilts [51] implemented a solution of the problem by use of finite-difference approximations to partial differential equations.

The flutter results of the FE method by use of MSC[®]Nastran and Euler-Bernoulli beam formulation and the reference studies are compared in Figure 4.10. The flutter speed ratio (U/U_0) is plotted against the span position of the concentrated mass. The spanwise position is normalized with wing half span, ℓ . U/U_0 is the ratio of the flutter speeds for the wing with a mass to the flutter speed of the clean wing. Besides, Table 4.2 shows the numerical results of the present methods.

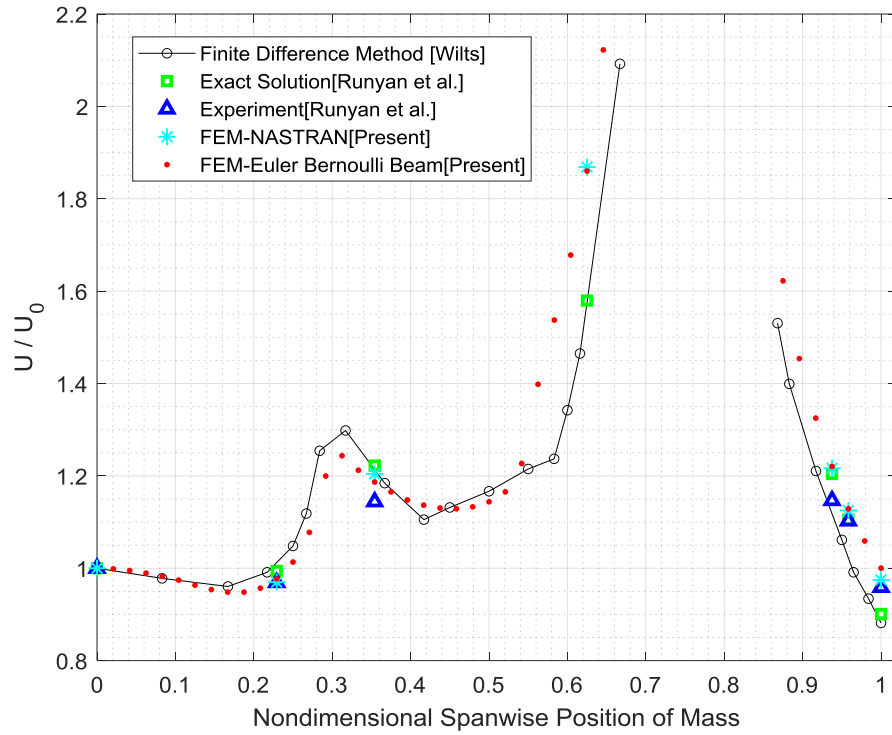


Figure 4.10 Wing/store Flutter Speed at Different Store Attachment Locations

Table 4.2 Comparison of Wing/store Flutter Speeds and Frequencies by Present FEM Methodology

| Spanwise Location of the Mass (m) | FEM-1D Beam Nastran | | FEM-Euler Bernoulli Beam Theory | |
|-----------------------------------|---------------------|-----------------|---------------------------------|-----------------|
| | U_f [m/s] | ω_f [Hz] | U_f [m/s] | ω_f [Hz] |
| 0 | 98.91 | 23.92 | 97.75 | 24.75 |
| 0.2794 | 95.94 | 19.03 | 95.54 | 19.33 |
| 0.4318 | 119.12 | 27.89 | 115.99 | 28.30 |
| 0.762 | 184.84 | 31.84 | 181.81 | 32.23 |
| 1.143 | 120.33 | 26.06 | 119.3 | 26.64 |
| 1.1684 | 111.27 | 25.38 | 110.33 | 25.52 |
| 1.2192 | 96.42 | 24.19 | 97.77 | 25.12 |

The present methods show that the shape of the reference curve follows the present curve very closely in the regions where especially nondimensional span location is below 0.6. Since the divergence was reported experimentally beyond the store

nondimensional spanwise location of 0.3542, there are no experimental results up to nondimensional spanwise store location of 0.9375. Nevertheless, it is possible to calculate the flutter speed theoretically in these regions. The slight differences can be seen between the present results and the reference studies beyond the nondimensional store span location 0.6. Consequently, it is not possible to compare the theoretical results in that region with the experiment due to a lack of experimental data. Besides the comparison of the present results with the reference studies, flutter speed and frequency of both MSC[®]Nastran and Euler-Bernoulli beam formulation with structural modification are in good correlation. Therefore, the developed structural modification method has been validated for the beam-like wing with concentrated mass.

4.4 Flat-Plate Delta Wing with Flexible External Store Case Study

The theoretical flat-plate wing store data is taken from the experimental and theoretical study of Tang et al. [9] and a photograph of the wind tunnel model can be seen in Figure 4.11. Five span locations of the store are considered in the experiment: $y/c = 0.161, 0.291, 0.419, 0.548, \text{ and } 0.677$ where y/c is the nondimensional store location, i.e. span location, y is normalized by the chord, c .

The clean wing model is a delta wing with a sweep angle of 45 deg and it is built through a thickness of 0.147 cm Lucite[®] material. The wing root is partially cantilevered. The cantilevered length is 22.86 cm and the total length of the wing chord is 38.1 cm. As presented in Figure 4.5, the wing store parameters are given as follows; $e_1 = 12.7 \text{ cm}, e_2 = 9.84 \text{ cm}, e_3 = -0.23 \text{ cm}, M_1 = 0.037 \text{ kg}, M_2 = 0.004 \text{ kg}, k_s = 36 \text{ N/m}$ and $J_\beta = 0.3686\text{E-}4 \text{ Nms}^2$. The FE model of the wing store structure is developed by utilizing MSC[®]Patran. The flexible plate structure has 3571 TRIA3 elements in the FE model. The aerodynamic model is developed in MSC[®]FlightLoads and Dynamics via the utilization of DLM. The free vibrational and flutter analyses are conducted by means of MSC[®]Nastran, which involves SOL103 and SOL145 solution sequences, respectively.

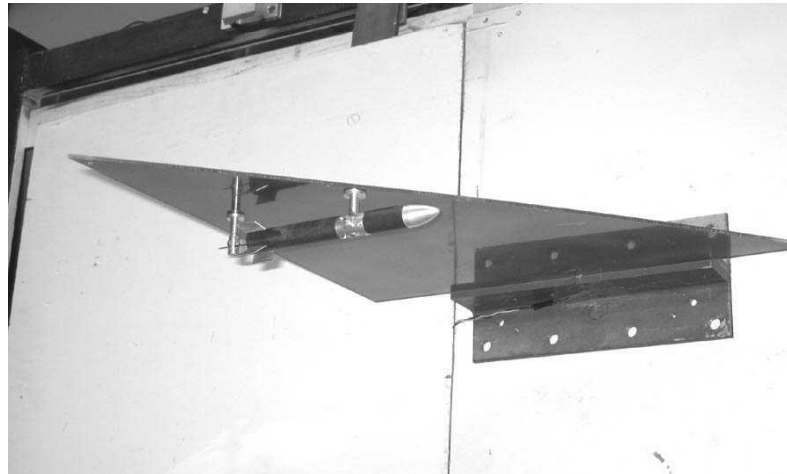


Figure 4.11 A Snapshot of the Wind Tunnel Model[52]

4.4.1.1 Structural Analysis

The wind-off frequencies of the delta wing plate without store are calculated by use of the MSC[®]Nastran Lanczos method in the SOL103 sequence. Experimental and analytical FEM reference results are presented for comparison purposes. Table 4.3 compares the first five natural frequencies of present results with the reference studies.

Table 4.3 Comparison of Clean Wing Natural Frequencies

| | FEM-ANSYS Tang et al. [9] | Experiment Tang and Dowell [53] | FEM- Nastran [Present] |
|--------------------|-------------------------------------|---|--------------------------------------|
| Mode-1 [Hz] | 4.39 | 4.5 | 4.53 |
| Mode-2 [Hz] | 17.84 | 17.2 | 17.98 |
| Mode-3 [Hz] | 20.62 | 20.54 | 20.58 |
| Mode-4 [Hz] | 42.21 | 44.4 | 42.49 |
| Mode-5 [Hz] | 51.87 | 54.4 | 51.14 |

As shown in Table 4.3, the agreement between the computational models by use of FEM and experiment is satisfactory when the wind-off frequencies of the clean wing are considered. Nevertheless, experimental results slightly differ from both reference

and present FEM results. It can be concluded that the developed flat plate FE Model is validated by computational and experimental references.

Five span attachment location of the flexible store is considered in the reference computational model and experiment. Figure 4.12 shows the comparison of the first four natural frequencies of the wing store model at different span locations of the store. The reference results are presented for von Karman plate theory, FEM by use of ANSYS and experiment. All reference data are taken from the study of Tang et al.[50].

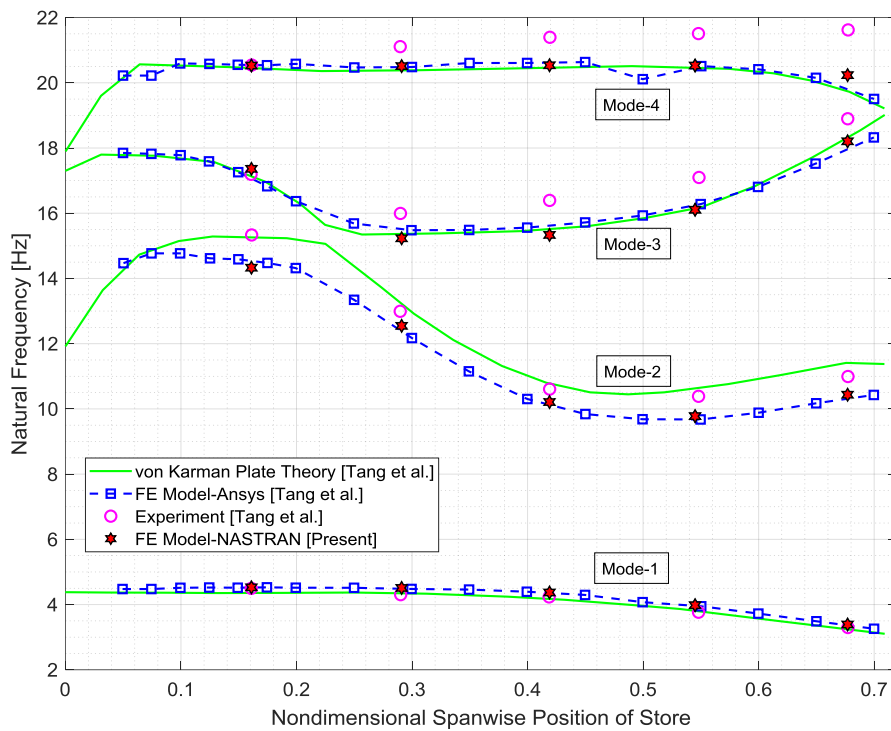


Figure 4.12 The First Four Natural Frequencies of Wing Store Against Different Store Span Locations

The present FE model has been applied to conduct free vibration analysis of the wing store at different attachment locations of the store. Experimental results slightly differ from the theoretical ones especially in mode-2, mode-3, and mode-4. The present method shows a perfect agreement with the reference FE Model for all modes

and span locations of the store. Therefore, the developed wing store FE Model is validated by computational and experimental references. Figure 4.13 - Figure 4.16 are given to show the first four natural frequencies and mode shapes of the wing store model for a store span location of $y/c = 0.548$.

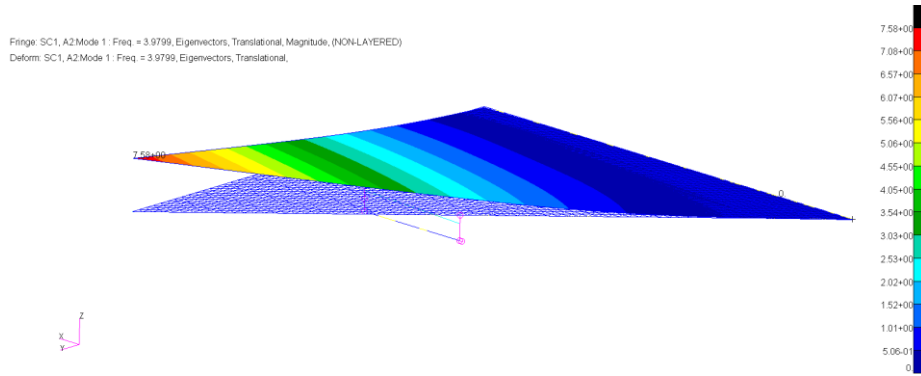


Figure 4.13 Mode-1 [3.78 Hz], $y/c = 0.548$

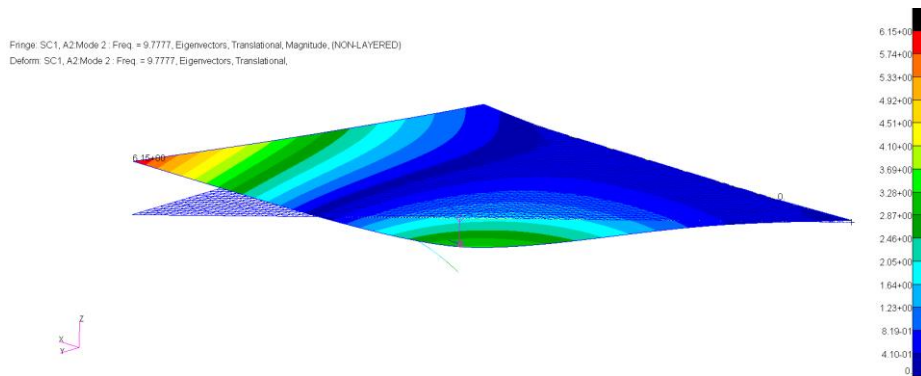


Figure 4.14 Mode-2 [9.78 Hz], $y/c = 0.548$

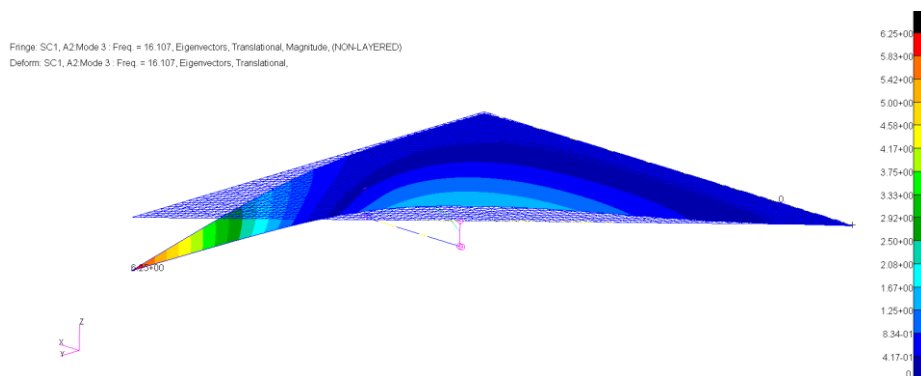


Figure 4.15 Mode-3 [16.11 Hz], $y/c = 0.548$

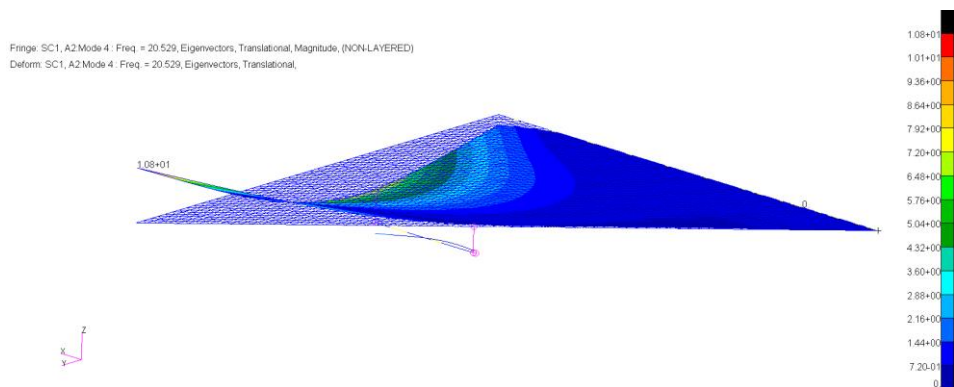


Figure 4.16 Mode-4 [20.53 Hz], $y/c = 0.548$

The mode-1 is the first wing store bending mode while the mode-2 is the first wing store torsion mode. The mode-3 is dominated by the store pitch motion. The reason is that the calculated store pitch frequency that is 15.5 Hz is in the vicinity of wing store mode-3 frequency, 16.11 Hz. Lastly, mode-4 is the second wing bending mode.

4.4.1.2 Aeroelastic Analysis

The aerodynamic model is obtained by utilizing three individual lifting surfaces and a total of 201 lifting surface boxes. The boxes should maintain a maximum aspect ratio of 3 in the Doublet-Lattice formulation [54]. Figure 4.17 shows the aerodynamic mesh and it verifies the aspect ratio of the lifting surface boxes is smaller than 3.

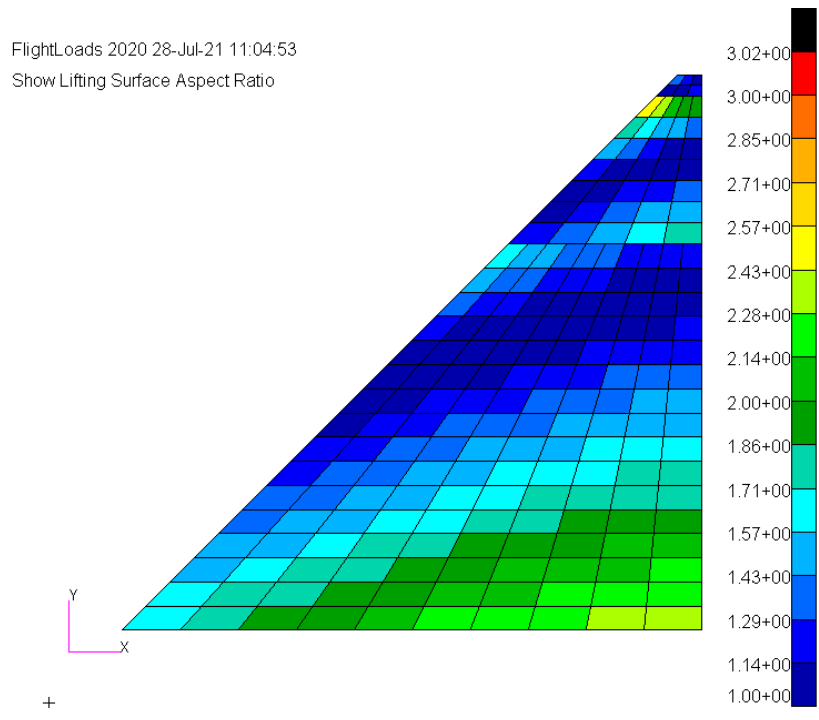


Figure 4.17 Aerodynamic Mesh and Aspect Ratio of the Boxes

Aero-structural coupling is achieved by using Infinite Plate Spline (IPS). The flutter analyses are carried out at sea level conditions with an air density of 1.225 kg/m^3 . The flutter solution is achieved by P-K Method since the MSC[®]Nastran DMAP language is not utilized in the present analysis. Besides, store aerodynamics are neglected. The reference results include von Karman plate theory with linear spring attachment [53], von Karman plate theory with nonlinear spring attachment [50], high-fidelity nonlinear structural model [50], and experiment estimated [50]. The comparison of the flutter speeds of the wing store model at different store span locations is presented in Figure 4.18. On the other hand, the flutter frequency comparison plot is presented in Figure 4.19.

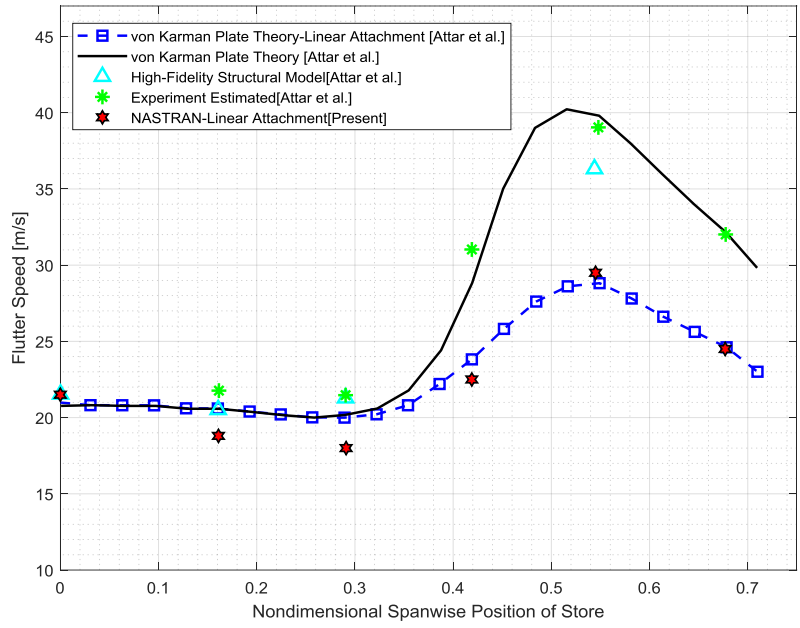


Figure 4.18 Flutter Speed at Different Store Attachment Locations

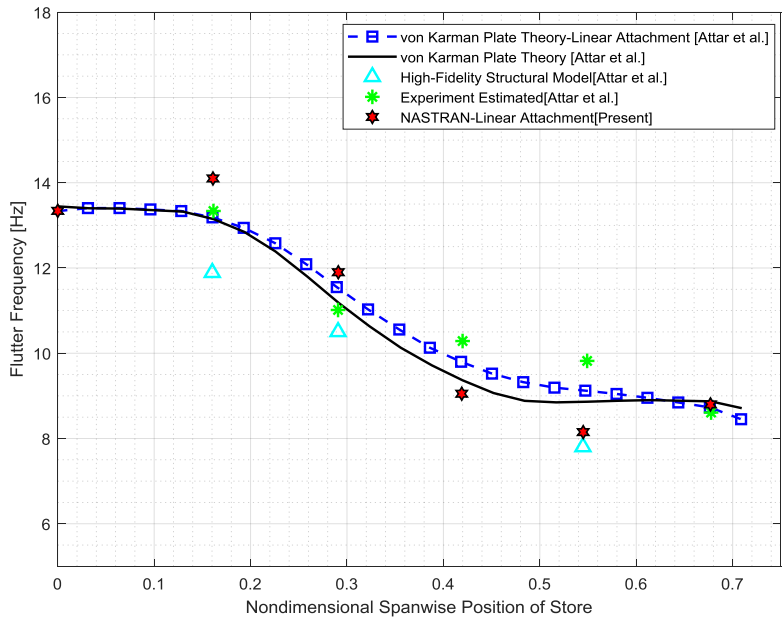


Figure 4.19 Flutter Frequency at Different Store Attachment Locations

Figure 4.18 and Figure 4.19 summarize the flutter behavior of the wing with a flexible store system at different attachment locations through implementing linear FEM. The important thing to note in analyzing the results is that the tendency of the present curves is similar to the reference curves. Figure 4.18 indicates that flutter speed diverges after the nondimensional span location $y/c=0.3$. The reason could be that the nonlinear effects become dominant after the span location $y/c=0.3$. Nevertheless, the agreement of the present results with the reference study is satisfactory when linear attachment cases are considered. Thus, both structural and aeroelastic models have been validated by comparing the results of the reference studies.

To sum up, the aeroelasticity of the wing structures with external stores has been investigated throughout the present chapter. The two different types of wing store systems are introduced. The first model depends on the beam-like wing structure with concentrated mass. The FEM is employed to develop the structural model. The wing is discretized into finite beam elements and corresponding structural nodes are used to attachment of the concentrated mass. The attachment between the wing and concentrated mass is considered rigid. The connection is introduced as a local structural modification on the wing structure. The modification matrix is formed by a mass matrix of the attached body, which is evaluated through the rigid body motion of the lumped mass element. A case study has been conducted based on the developed analytical model and FEM by MSC[®]Patran. The effect of the attachment location on both structural and aeroelastic characteristics is investigated. It is found that the flutter behavior is significantly sensitive to the attachment location of the lumped mass. The results of the present work are compared with the results in the literature. Consequently, a good correlation is observed between the present analytical model and reference experimental and analytical studies. The second wing store system is based on the flat-plate delta wing with an elastic attachment between the wing and the external store. The wing store FE model is developed in MSC[®]Patran. The FE elements used in the model are explicitly defined involving two attachment locations, attachment stiffness, store mass and inertia, and the pylon

mass. The aerodynamic model is developed in MSC[®]FlightLoads and Dynamics via the utilization of DLM. The store aerodynamics are not included in the analyses. The present results are compared to published works and a good agreement is observed between the results. Hence, a comprehensive FE model for the wing with a flexible store system has been validated. The important thing in the implementation of the FEM for wing store systems is that the store attachment is not limited to the attachment of the one store. The present method can also be utilized for multi-store attachments.

CHAPTER 5

STRUCTURAL MODIFICATIONS IN AEROELASTICITY

Flutter analyses are carried out with discrete sets of modal data, which includes natural frequencies, mode shapes, and generalized modal masses of the pertinent aerospace structure. These may be obtained directly from Ground Vibration Tests (GVT) or analytically. Since the ground vibration tests are costly and very time-consuming activities, these tests are not practical in the aerospace industry. Besides, one of the drawbacks of performing ground tests is that it requires a physical prototype of the structure, which is usually not possible to be provided at an early design stage of the structure. If a design change arises as a result of ground vibration tests, a redesign process should be considered, and tests need to be repeated.

A redesign process is inevitable if the design does not satisfy the flutter requirements, or a large number of design candidates are present. It is generally not possible to perform ground vibration tests when a redesign process is necessary. The analytical models can easily be utilized for such cases to predict flutter behavior and they are cost-effective than conducting ground tests. For instance, a fighter aircraft is equipped with a large number of external stores and these lead to many fighter store loading configurations. The modern fighter and its external store inventory can be seen in Figure 5.1.



Figure 5.1 Modern Fighter Aircraft and Its External Store Inventory [55]

The combination of possible store configurations must be examined analytically before flight tests. At this point, a redesign process is required to calculate flutter speeds for all external store configurations. The redesign process commonly involves successive structural modifications in the model and recomputing the flutter solution. Searching for the most suitable design candidate is the ultimate goal of the redesign process. This can be accomplished by implementing various optimization frameworks. In the traditional approach, the redesign or optimization process can be given in Figure 5.2.

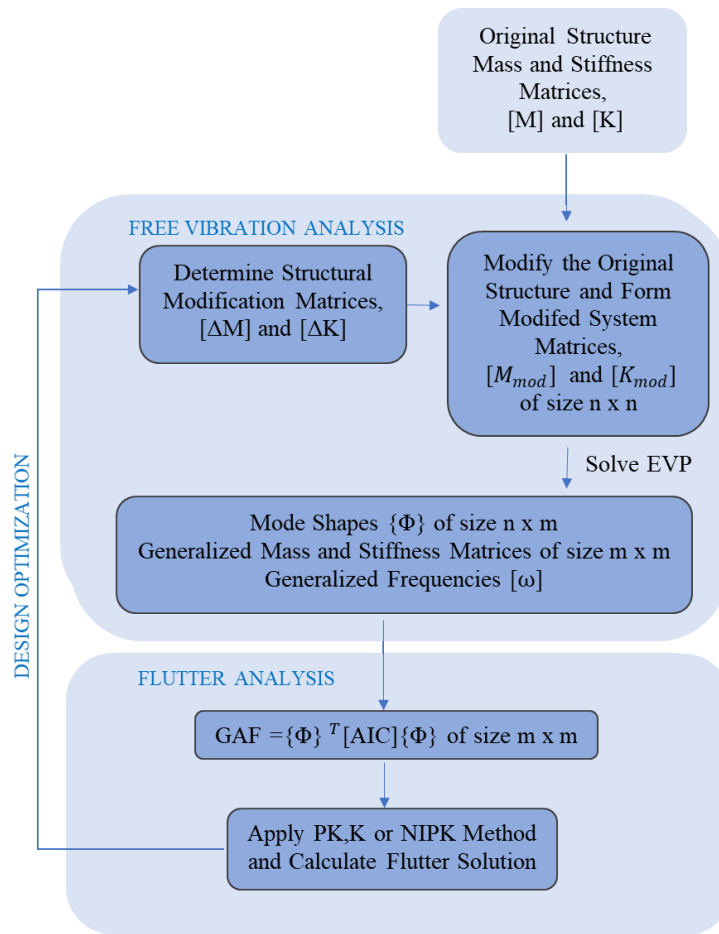


Figure 5.2 Traditional Redesign Process of Structural Model

The process given in Figure 5.2 is applied and verified by calculating the flutter speed and frequency of beam-like wings with concentrated mass in Chapter 3. The original system consists of “n number of DOFs” that can be interpreted as a very large number. The structural modification is applied to the original structure assuming no additional DOFs in the structure where the modification is local. After solving the eigenvalue problem (EVP), n number of mode shapes and natural frequencies are obtained. In the aeroelastic analysis, “m number of DOFs” is typically interested, which is a significantly smaller number when compared to full system DOF. Then, m x m size of the generalized mass and stiffness matrices and n x m size of mode shape matrix of the modified structure can be formed accordingly. Finally, Generalized Aerodynamic Force (GAF) matrix can be formed utilizing the n x m size of the mode shape matrix.

The critical issue in the traditional methodology is that repeatedly solving the EVP with full size of $n \times n$ system matrices. Execution time is very high in this process depending on the size of the original system when a large number of successive modifications are considered.

To generate reduced-order models (ROMs) that represent the dynamic characteristics of the full order aeroelastic system in a low computational cost manner, there exist several modal reduction methods in the literature. Static condensation method by Guyan [56], Improved Reduced System (IRS) method by O'Callahan [57] and System Equivalent Reduction Expansion Process (SEREP) by Kammer [58] can be given as examples. Such methods can be applied to aerospace structures when considering aeroelastic analysis. In this case, the equations of motion are much smaller, but the Aerodynamic Influence Coefficient (AIC) matrix must be recalculated since the aerodynamic model is constructed based on the reduced model. Modal reduction methods are usually applied to form original structure mass and stiffness matrices defined in Figure 5.2.

The traditional redesign process can be reconstructed by implementing Dual Modal Space Modification (DMSM) given in Figure 5.3. The method has been originally developed by Luk and Mitchell [59]. The mode shapes of the modified structure are approximated by this technique. In other words, the $n \times m$ size mode shape matrix of the modified structure can be obtained by using only the original structure and modification information. Hence, the GAF matrix in each design iteration can be computed by using these mode shapes, which can be calculated by the DMSM method. The accuracy depends on the modal information stored in the original structure. The main assumptions are that structural modification is local, the total DOF of the structure does not change and the aerodynamic configuration is fixed. Therefore, the AIC matrix of the original structure can be used repeatedly used in the successive structural modifications. Since the GAF matrices are as a function of reduced frequency, k and Mach number, M , the M - k set should be determined properly such that the aeroelastic analyses domain could cover modified structure dynamics. In other words, pre-defined k_{\min} , k_{\max} - Mach number, M sets should cover

all possible modification cases. The main advantage of the application of DMSM is to avoid solving EVP with full $n \times n$ size of system matrices successively in each design iteration. The new approach significantly reduces the computational cost.

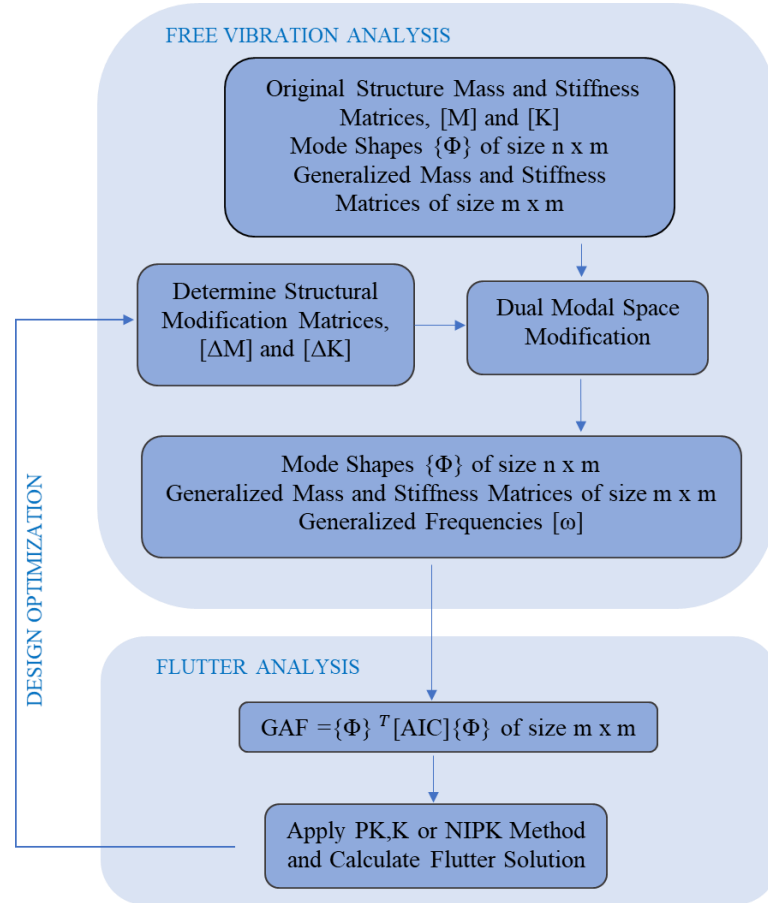


Figure 5.3 New Redesign Process of Structural Model

5.1 Dual Modal Space Modification

Since the theory is explained in detail in the work by Luk and Mitchell [59], this section covers the review of the method for free vibration analyses. The dynamic characteristics of the aeroelastic system are given in Chapter 2. The equation of motion represents the dynamics of the system in physical space. Recalling the EOM but this time transformation into modal space is defined by using the relation below:

$$\{x\}_{nx1} = [\phi_I]_{nxm} \{\eta_I\}_{mx1} \quad (4.1)$$

where $[\phi_I]_{n \times m}$ is the modal matrix of the original system and $\{\eta_I\}_{m \times 1}$ vector of principle coordinates in modal space I, results in the following relation:

$$\{\ddot{\eta}_I\} + [\omega_m]\{\dot{\eta}_I\} = \{0\} \quad (4.2)$$

where ω_m is the natural frequencies of the original system. The system of Eq. (4.2) can be considered the result of an experiment or can be obtained before aeroelastic analyses of the original structure, where “m” denotes the number of modes interested in the aeroelastic analyses. The effects of the structural modification can be included such that point mass changes, $[\Delta M]$ or stiffness changes between nodes, $[\Delta K]$. Hence, the dynamics of the system is modified such that

$$[K'] = [K] + [\Delta K] \quad (4.3)$$

$$[M'] = [M] + [\Delta M] \quad (4.4)$$

Then, the following relation can be formed by including the modifications to the original system given in Eq. (2.7)

$$[M']\{\ddot{x}\} + [K']\{\dot{x}\} = \{0\} \quad (4.5)$$

Make the same coordinate transformation in Eq.(4.5) by using the modal matrix of the original system, $[\phi_I]_{n \times m}$.The result of such an operation is written as follows:

$$[\bar{M}]\{\ddot{\eta}_I\} + [\bar{K}]\{\dot{\eta}_I\} = \{0\} \quad (4.6)$$

where

$$[\bar{M}] = [[I] + [\phi_I]^T [\Delta M] [\phi_I]] \quad (4.7)$$

$$[\bar{K}] = \left[\left[\omega_m^2 \right] + [\phi_I]^T [\Delta K] [\phi_I] \right] \quad (4.8)$$

Note that the system defined in Eq. (4.6), (4.7) and (4.8) is no longer diagonal. An eigen analysis should be carried out to find natural frequencies and mode shapes of the modified structure. The system of Eq. (4.6) can be transferred from modal space I to modal space II by the relation between principal coordinates $\{\eta_I\}$ and $\{\eta_{II}\}$, which is given as follows:

$$\{\eta_I\}_{mx1} = [\phi_{II}]_{m \times m} \{\eta_{II}\}_{mx1} \quad (4.9)$$

where $[\phi_{II}]$ is the modal matrix of the modified structure defined in modal space II. The backward transform should be applied by using the relation given below, in which Eq. (4.1) and Eq. (4.9) are combined.

$$\{x\}_{nx1} = [\phi_I]_{n \times m} [\phi_{II}]_{m \times m} \{\eta_{II}\}_{mx1} \quad (4.10)$$

As a result, the mode shape of the modified structure can be approximated by the product of the mode shape matrices of modal space I and modal space II. This technique clearly shows that the accuracy of the mode shapes of the modified system relies on the modal information that exists in the original system.

5.2 Evaluation of Generalized Aerodynamic Force (GAF) Matrix by Structural Modification

The derivation of the GAF matrix is expressed throughout Chapter 2. Recalling the Eq. (2.50) and Eq. (2.59), the general form of the GAF can be defined as follows:

$$[GAF] = [\phi]^T [AIC] [\phi] \quad (4.11)$$

where $[\phi]$ is the modal matrix of the structure size of $n \times m$, where $m \ll n$. The Eq. (4.11) can be rewritten according to the procedure defined in section 5.1.

$$[GAF] = [\phi_{II}]^T [\phi_I]^T [AIC] [\phi_I] [\phi_{II}] \quad (4.12)$$

where $[\phi_I]$ is the modal matrix of the original system in modal space I and $[\phi_{II}]$ is the modal matrix of the modified structure in modal space II. Note that $[\phi_{II}]$ is formed by using the only original structure and modification information.

5.3 Case Study – Local Mass Modification on Cantilevered Plate Wing

The experimental and computational FE wing model has been developed by Moradi, Sadeghi, and Dowell [60] to investigate the variation of the flutter speed with mass

balancing. The mass is assumed concentrated lumped mass and it is attached to the wing at 15 different attachment locations. The wing is made of a thin plate of aluminum 3105 with a thickness of 0.5 mm, 0.3 m span length, and 0.1 m reference chord. The aspect ratio of the wing is 3, the lengths are 0.12 m at the wing root and 0.08 m at the wingtip. In addition, the wing has 29 deg sweptback angle. The wing geometry is presented in Figure 5.4.

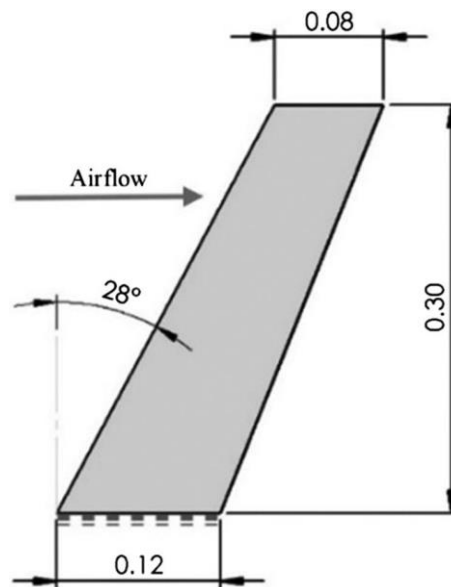


Figure 5.4 Wing Geometry (in meters)[60]

The mechanical properties of aluminum 3105 are defined as the density 2700 kg/m^3 , Poisson's ratio 0.33, and elastic modulus 75 Gpa. The wing is modeled in MSC[®] Patran using 90 QUAD4 shell elements in both reference and present study. Table 5.1 compares the first five natural frequencies of the clean wing with reference study.

Table 5.1 Comparison of First Five Natural Frequencies of the Clean Wing

| | Natural Frequency [Hz] | | | | |
|----------------------------|------------------------|--------|--------|--------|--------|
| | Mode-1 | Mode-2 | Mode-3 | Mode-4 | Mode-5 |
| FEM Nastran [60] | 4.66 | 25.67 | 35.15 | 68.93 | 97.40 |
| Experiment [60] | 4.57 | 24.80 | 33.59 | 65.62 | 94.53 |
| FEM Nastran [Present] | 4.67 | 25.70 | 35.16 | 69.02 | 97.41 |
| FEM Nastran DMAP [Present] | 4.67 | 25.70 | 35.16 | 69.02 | 97.41 |

The results show a perfect agreement between the present study and the computational results of the reference study. On the other hand, there is no significant difference between the experimental and the theoretical results.

The concentrated 10 g mass is attached to 15 different locations on the wing. The labels are denoted for chord centerline M, for trailing edge MB and for leading edge MF [60]. The mass is modeled by using the CONM2 element and there are a total of 112 nodes in the FE model of the structure. The mass attachment is defined as local structural modification in the current analyses. For instance, attachment at node 16 corresponds to the MF5 in the reference study as given in Figure 5.5.

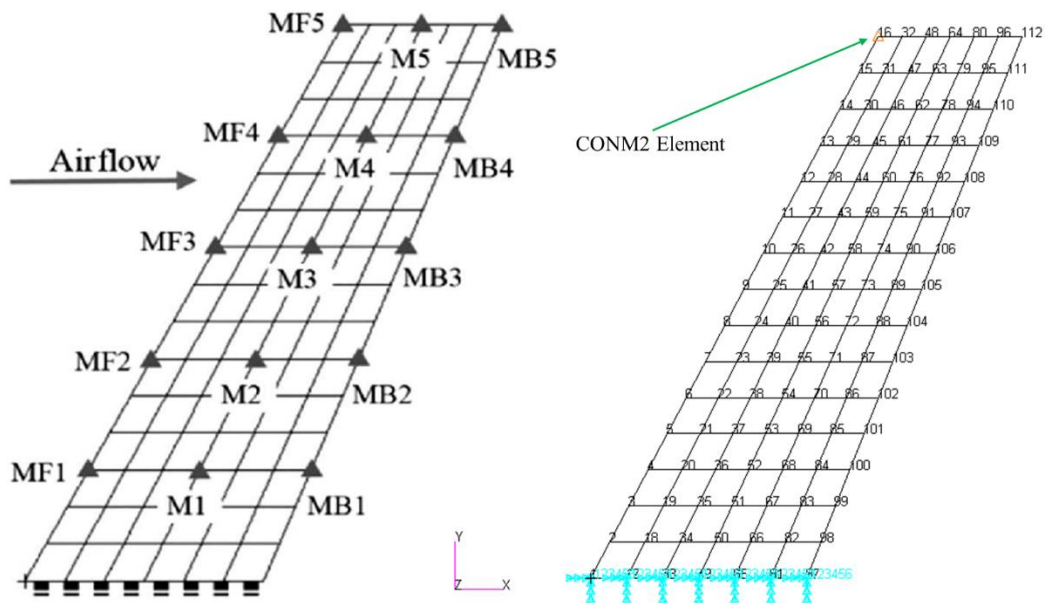


Figure 5.5 Mass Attachment Locations and Labels on the Structure

5.3.1 Aeroelastic Analysis of Clean Wing

The aerodynamic modeling of the structure is carried out by utilizing DLM in MSC[®] FlightLoads. The aerodynamic model is obtained by dividing the surface into 968 aero boxes. The analyses are carried out at sea level conditions, taking air density 1.225 kg/m³. The present results are given in three different analyses cases. The first analysis is carried out directly on MSC[®] Nastran implementing the P-K Method for

the solution. For the second and third analyses, MSC[®]Nastran DMAP is used for the clean wing to extract structural mass and stiffness matrices. Moreover, AIC matrices are exported for the defined reduced frequency and Mach numbers. The modal and flutter analyses are carried out with developed in-house Matlab[®] code. The second analysis case involves P-K Method for the flutter solution while the third analysis case has NIPK Method. Table 5.2 compares the obtained flutter speeds with the reference study for the clean wing. The V-g and V-f graphs for the MSC[®]Nastran DMAP Non-Iterative P-K Method solution can be seen in Figure 5.6.

Table 5.2 Comparison of Flutter Speed of the Clean Wing

| | Flutter Speed [m/s] | Flutter Frequency [Hz] |
|---------------------------------------|------------------------|---------------------------|
| Nastran P-K Method [60] | 22.3 | - |
| Experiment [60] | 21.5 | - |
| Nastran P-K Method [Present] | 22.04 | 18.07 |
| Nastran DMAP P-K Method [Present] | 22.05 | 18.02 |
| Nastran DMAP NIPK Method [Present] | 22.06 | 17.97 |

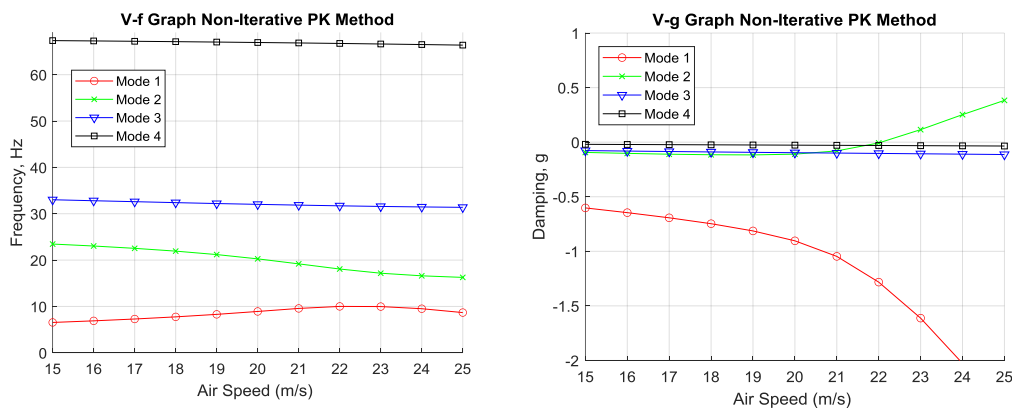


Figure 5.6 Nastran DMAP NIPK-Method V-g and V-f Graphs

As shown in Figure 5.6, the first mode is damped whereas the second mode shows positive damping as airspeed increases. The flutter occurs at the second mode in the

vicinity of airspeed 22.06 m/s. The vibration frequencies of the first mode and second mode tend to close each other around 17.97 Hz.

Since the NIPK Method provides a non-iterative solution approach, the execution time of the flutter solution by P-K Method is approximately 2.5 times slower than the NIPK Method in the current in-house flutter calculation framework. There is no significant difference in the flutter speeds among the present results. Likewise, a good agreement can be seen between the obtained results and the reference study. The results validate the FE and aerodynamic model of the structure. Besides, AIC matrix export methodology to form GAF matrices is validated with the results.

5.3.2 Aeroelastic Analysis of Clean Wing with Lumped Mass

The aerodynamic model is fixed for the clean wing in the flutter analyses. The present results are obtained by two distinct analyses cases. The first analysis case is performed such that the flutter solution is directly calculated for the wing attached mass structure. In other words, the traditional process is implemented as given in Figure 5.2 and structural modification is not implemented. The solution involves the abstraction of structural and aerodynamic matrices from MSC[®]Nastran to Matlab[®] environment by using DMAP language and NIPK Method for the in-house flutter calculation. The second analysis case is carried out such that flutter solution is obtained by implementing structural modification technique. This process has been described in Figure 5.3. The second solution involves the abstraction of structural and aerodynamic matrices of the clean wing by MSC[®]Nastran DMAP. Hence, the structure is modified for each 15 attachment cases by using the original structure information with in-house Matlab[®] codes. The clean wing AIC and mode shape matrices are used to evaluate the GAF matrices of the modified structure. The NIPK Method is applied for the flutter solution. In the reference study, analytical results belong to the direct output of the MSC[®]Nastran by providing the P-K Method. The wing with mass structure is modeled employing MSC[®]Patran for 15 attachment cases. Besides, experimental results are given in the reference study. The numerical

results of the present study and comparison with the reference study are presented in Table 5.3.

Table 5.3 Comparison of Mass Attached Wing Flutter Results

| | Flutter Speed [m/s] | | | |
|------------|------------------------|-----------------|------------------------------------|--|
| | Nastran PK-Method [60] | Experiment [60] | Nastran DMAP NIPK-Method [Present] | Nastran DMAP "Structural Modification" NIPK-Method [Present] |
| CLEAN WING | 22.30 | 21.40 | 22.00 | - |
| M1 | 22.30 | 21.50 | 22.00 | 21.97 |
| M2 | 22.30 | 21.40 | 22.00 | 22.02 |
| M3 | 23.20 | 22.20 | 22.90 | 22.91 |
| M4 | 23.60 | 22.40 | 23.60 | 23.55 |
| M5 | 23.20 | 22.40 | 23.60 | 23.69 |
| MB1 | 22.30 | 21.50 | 21.90 | 21.93 |
| MB2 | 21.00 | 21.50 | 17.90 | 17.90 |
| MB3 | 19.40 | 20.00 | 18.00 | 18.06 |
| MB4 | 18.80 | 19.50 | 18.40 | 18.39 |
| MB5 | 18.80 | 19.40 | 19.10 | 19.12 |
| MF1 | 22.10 | 21.40 | 21.70 | 21.69 |
| MF2 | 21.00 | 20.70 | 20.30 | 20.32 |
| MF3 | 23.40 | 23.10 | 22.90 | 22.89 |
| MF4 | 28.00 | 25.00 | 27.80 | 27.71 |
| MF5 | 14.00 | 16.70 | 13.85 | 13.90 |

It can be observed that both present solution cases agree with each other regarding all attachment locations. The correlation between the present results and reference results is satisfactory. The V-g and V-f plots for the MSC[®]Nastran DMAP NIPK Method (MF5 mass attachment case) are presented as an example in Figure 5.7.

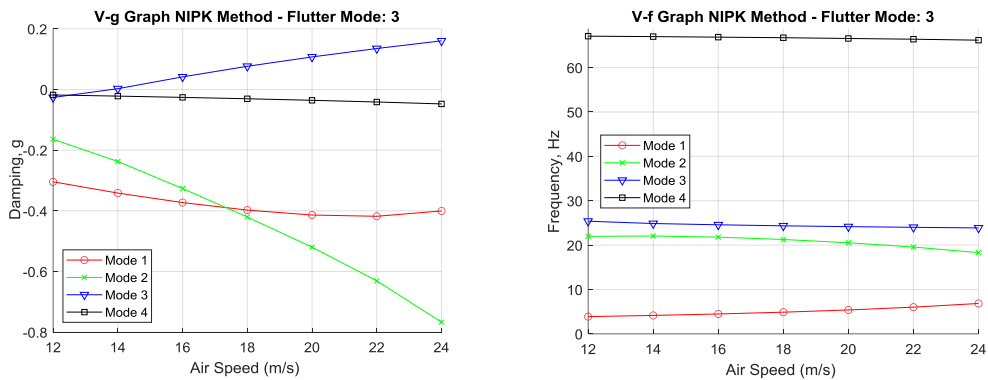


Figure 5.7 V-g and V-f Plots for the MF5 Mass Attachment Case

As can be seen in Figure 5.7, mode-2 is damped, and mode-3 shows positive damping as airspeed increases. The flutter onset can be seen in the mode-3 around 13.85 m/s airspeed. Mode-2 and mode-3 tend to close each other around vibration frequency 23 Hz.

5.3.3 Comparison of Computational Time

Flutter analysis generally begins with the calculation of the modal matrices, namely, mode shape matrix, generalized mass, and stiffness matrices. Then, GAF matrices are formed by using the mode shape matrices. Lastly, these matrices are involved in the flutter solution. To compare the computational efficiency of the structural modification approach in the flutter analysis, three different grid sizes are employed for the plate wing structure. The first model is developed by using a 6x15 grid size, which is currently utilized in the above-mentioned analysis. The second model has a 30x75 grid size while the third model has a 30x150. A total of 15 local structural modifications are introduced successively in the analysis, which has been shown in Figure 5.5. In the traditional approach, modification is directly introduced to the wing structure and eigen solution is performed with Matlab[®] built-in function “eigs”. The first ten modes are selected by “smallestabs” option to calculate eigenvalues and eigenvectors, i.e., mode shapes. On the other hand, the successive modifications are introduced to the system by implementing Dual Modal Space Method (DMSM) as shown in Figure 5.3. The comparison of the calculation time is given in Table 5.4

for the three different structural models. Note that the aerodynamic model is fixed, and the number of aero boxes is taken as 968 for all analyses. The calculations are performed with a PC that has a 3.6 GHz 6-core processor and 32 GB RAM. The results are the means of the CPU time of the total 15 successive modifications. Hence, they correspond to each modification cycle time.

Table 5.4 Comparison of Computational Time

| | Modal Matrices Calculation Time [sec] | GAF Matrices Calculation Time [sec] | Flutter Solution Time[sec] | Total Calculation Time [sec] |
|---|--|--|-----------------------------------|-------------------------------------|
| Structural Grid: 6x15 | 0.063 | 3.039 | 181.1 | 184.2 |
| Structural Grid: 6x15 (Structural Mod.) | 0.013 | 3.026 | 154.6 | 157.6 |
| Structural Grid: 30x75 | 32.26 | 3.468 | 185.6 | 221.3 |
| Structural Grid: 30x75 (Structural Mod.) | 0.274 | 3.445 | 177.8 | 181.5 |
| Structural Grid: 30x150 | 161.93 | 4.248 | 212.23 | 378.4 |
| Structural Grid: 30x150 (Structural Mod.) | 0.987 | 3.934 | 192.72 | 197.6 |

Table 5.4 indicates that as structural grid size increases the calculation of the modal matrices takes more time. For the first model, the total number of shell elements is 90, resulting in 540 DOFs in total. The computation of modal matrices takes 0.063 seconds. In the second model, 2250 elements are used with 13500 DOFs in the structure while the computation takes 32.26 seconds. The last model has 4500 elements and 27000 DOFs in the structure. The computation of the modal matrices takes 161.93 seconds, which is significantly larger than the previous models. On the other hand, the computational times of the modal matrices are 0.013, 0.274, and 0.987 seconds when the structural modification method is introduced for the three different grid sizes. A significant reduction in computation time is observed for the structural modification cases because it uses only original generalized mass and stiffness matrices and modification information. In other words, there is no need for the full system matrices to calculate the modal matrices of the modified structure.

Note that the execution times of both GAF matrices and flutter solution are close to each other because the size of the modal output matrices is the same for both approaches. Therefore, a substantial execution time reduction can be observed by implementing the structural modification method in the aeroelastic flutter analysis. The efficiency of the method appears when working with a large number of DOF systems. Even though these results belong to one modification cycle, the employment of the structural modification method considerably decreases the computation time when a large number of successive modifications is present in the analysis. Also note that NIPK Method is implemented in the solution, which provides the outputs relatively faster than P-K Method.

In summary, structural modifications are introduced to the traditional flutter solution procedure. In the traditional method, large-scale aeroelastic systems are generally converted into ROMs which reduces the computational complexity. Although ROMs are computationally efficient, it is required to recalculate the structural and aerodynamic models when structural modifications are present in the structure. This situation usually involves comprehensive effort when introducing modifications into the aeroelastic system. In particular, if there are successive modifications present in the structure, continuously constructing the aerodynamic model and related GAF matrices require tedious work. A new flutter calculation procedure is introduced when structural modifications are present in the system. In this method, the main assumptions are that modifications are local, and the aerodynamic configuration is fixed at each modification cycle. Hence, the AIC database of the original structure that is based on the M-k sets can be used for the modified structures. Since the Dual Modal Space Modification (DMSM) can approximate the modified systems' modal information based on the original structure information, DMSM is introduced to the flutter solution process. It can be implemented to both ROMs and large-scale systems, however, its significance is mostly present in large-scale systems, i.e., when working with a large number of DOFs. Furthermore, this method enables predicting the flutter speed of the modified structure by using the original modal and aerodynamic information. The validation of the new method has been carried out

through an experimental model. The reference study aimed to investigate the effect of mass balancing on flutter behavior. Consequently, a total of 15 mass attachment locations are defined on the wing structure and 10 g mass is attached to these attachment locations. For all cases, experiments were conducted, and flutter speeds were recorded. On the other hand, a computational model was developed utilizing in MSC[®]FlightLoads and Dynamics in the reference work. To validate the present aeroelastic model, the wing aero-structural model has been developed in MSC[®]FlightLoads and Dynamics. Clean wing structural and aerodynamic models are exported to Matlab[®] via utilizing DMAP language. Firstly, modifications are considered local and directly applied to the wing structure. The present results are compared to reference work and a good agreement is observed between the present and reference results. Then, a new flutter solution process has been implemented to the problem. Modifications are implemented successively by using the DMSM method and a total of 15 flutter speeds are obtained. The present results show a good correlation with the previously obtained results and reference results. In addition to that, the study is extended to analyze the new method's computational efficiency. Two additional structural models are developed which have finer mesh sizes, i.e., a large number of DOFs. The first additional model has 13500 DOFs while the second model has 27000. The new method is implemented to these structural models and modal matrices, GAF matrices, and flutter solution execution times have been recorded. The results are compared along with the results of the traditional method. It is shown that when the systems become larger, the computation time of the modal matrices drastically increases when the traditional method is considered. However, when the DMSM method is applied in the flutter solution, the modal matrices computation time is significantly decreased, especially working with a large number of DOFs systems. The computational contributions to the total flutter calculation time can be seen obviously when three distinct cases are considered.

CHAPTER 6

DESIGN OPTIMIZATION OF WING-STORE SYSTEMS BASED ON THE FLUTTER CRITERIA

The military aircraft are capable of externally carrying large varieties and combinations of external stores, such as unguided bombs, guided bombs, missiles, pods, fuel tanks, etc. The integration phase of these external stores into military aircraft involves a specific certification process. There are generally two possible situations for the certification process. In the first and most common situation, an external store is particularly designed for the aircraft whose design has already been completed. In the second situation, an aircraft is being designed but existing external store inventory would be taken into account to maintain the operational capabilities. The aeroelastic concerns, for example, flutter criteria, certainly shall be taken into consideration for the above-mentioned situations. On the other hand, determination of the worst-case flutter configuration for the existing inventory is essential because the total number of external store loading configurations is close to a million. In the present chapter, optimization of the wing store systems is investigated considering the worst-case flutter.

6.1 Wing Store Aeroelastic Model Definition

Since there is a growing demand and attraction for the tactical UAVs which are capable of carrying external stores in the defense industry, a HALE wing is adopted for the optimization case studies. When a lower bending rigidity is involved with the stores, the natural frequencies of the wing store system tend to decrease and close to each other. In this case, flutter occurs at very low airspeeds. Due to this reason, the wing is taken the same as provided in section 3.1 but this time it is stiffened by

taking spanwise bending rigidity, EI_z , $1 \times 10^6 \text{ Nm}^2$. The structural model is achieved utilizing FEM with Euler-Bernoulli beam theory. A total of 32 finite beam elements and 33 structural nodes are used to discretize the entire wing. The wing is clamped at the wing root. Each structural node (except the node at wing root) corresponds to the external store attachment location. The optimization cases involve three different types of external stores which are given in Figure 6.1. Store 1 is a representative bomb which is labeled as B-1, while Store 2 is a representative missile which is labeled as M-1. Lastly, Store 3 corresponds to another missile that is labeled as M-2.



Figure 6.1 – External Store Definitions

Stores are structurally modeled as lumped masses having store pitch inertia. The attachment of the stores into a wing is accomplished by local structural modification with store mass and inertia. The attachment between the mass and store is rigid and the chordwise location of the store center of gravity from the wing flexural axis is zero.




Theodorsen's aerodynamics is implemented for the aerodynamic modeling and store aerodynamics are neglected in the analysis. The flutter analysis condition is achieved by taking air density 0.0889 kg/m^3 that corresponds to 20000 m altitude. The flutter solution is obtained via NIPK Method. Considering the above wing store aeroelastic analysis conditions, the clean wing flutter speed is calculated as 68.03 m/s. Since the attachment of the external stores tends to decrease the flutter speed of the wing, U_{max} is taken as 80 m/s while U_{min} is taken as 5 m/s and number of k , $N_k = 15$ for all analysis cases. Since ω_{min} and ω_{max} are determined depending on the natural frequencies of the wing store structure, k_{min} and k_{max} are calculated for the particular wing store structure.

6.2 Flutter Critical Multi-Store Design Parameters

Store mechanical properties are generally determined without considering the possible effects on the vibrational characteristics of the wing store system when the store is mounted to the wing structure. In particular cases, store design authorities like to choose store mass or other properties larger to make use of its operational capability as much as possible. Since the stores are carried with air vehicles, the aeroelastic behavior of the particular wing store systems can degrade the performance or operational requirements of the air vehicles. For instance, a flight envelope of the fighter aircraft can be substantially limited when an external store is mounted to the aircraft wing. While a store design activity is being performed for a specific aircraft, the above-mentioned effects can be eliminated in advance by introducing additional design constraints during the preliminary design stage of the store if the store design authority permits. Investigating the worst-case flutter condition for the wing store system can be a good choice to introduce such design constraints for the store design activities.

Determination of the store design parameters based on worst-case flutter criteria, specifically store mass and inertia, can produce additional store design constraints. As a consequence of the mentioned necessity, three optimization cases have been defined to investigate additional store design constraints. Each optimization case involves three types of stores, and its mass and pitch moment of inertia are searched within a pre-defined analysis range. Store parameters are considered as the design variables. The design constraints are presented in Table 6.1. Upper bound of the store pitch inertias is defined by introducing a specific store pitch moment/mass ratio parameter, r . This parameter defines store pitch moment based on the store mass and it can be taken as unique to a specific store type. The ratio parameter for the B-1 is defined as r_1 , M-1 is defined as r_2 , and M-2 is defined as r_3 , which are taken as 1.69, 1.19, and 1.3, respectively.

Table 6.1 Store Design Constraints

| Store Type | Store Mass, M_s [kg] | | Store Pitch Moment of Inertia, I_s [kgm ²] | |
|---|------------------------|------|--|------------------|
| | Min. | Max. | Min. | Max. |
|  | 0 | 150 | 0 | $Max(M_s) * r_1$ |
|  | 0 | 80 | 0 | $Max(M_s) * r_2$ |
|  | 0 | 40 | 0 | $Max(M_s) * r_3$ |

The multi-store attachment locations are defined for the particular loading configurations. For the first optimization case, B-1 is attached to the 7th structural node, while M-1 is attached to the 10th structural node and M-2 is attached to the 13th node. The corresponding spanwise distances from the wing root (1st structural node) are 3 m, 4.5 m, and 6 m, respectively. For the second optimization case, B-1 is attached to the 7th structural node, while M-1 is attached 15th and M-2 is attached to the 17th structural node. The corresponding spanwise distances from the wing root are 3 m, 7 m, and 8 m, respectively. Likewise, 4th, 7th, and 17th structural nodes are defined as attachment locations for the last case, which corresponds to the 1.5 m, 3 m, and 8 m spanwise locations from the wing root. The illustration of the multi-store attachment locations for each optimization case is given in Figure 6.2.

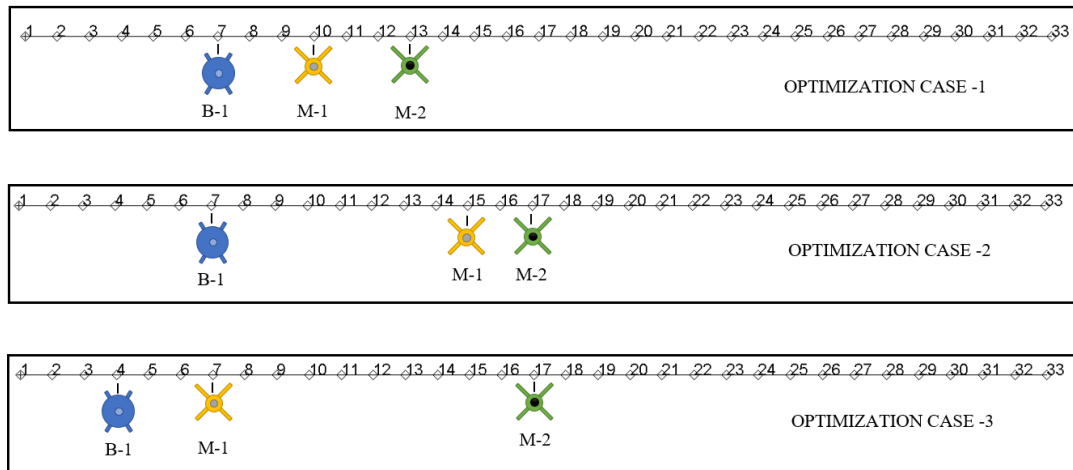


Figure 6.2 Optimization Cases for Store Design Parameters

The flutter speed is the objective or cost function used in the optimization process. Since there are six search variables and worst-case flutter is the minimum flutter speed, the “fminbnd” function in Matlab[®] is employed to find the minimum of a constrained multivariable function. Since “fminbnd” function gives local minimum solutions depending on the initial values, fminbnd is used with “GlobalSearch” function in Matlab[®]. Hence, the solver attempts to locate a solution globally which has the lowest objective function value in the defined boundary. Considering all the above, multi-store design optimization calculations have been performed with a PC that has a 3.6 GHz 6-core processor and 32 GB RAM. The parallel-run option is enabled during the executions, hence, a total of 6 cores are simultaneously utilized in the optimization process. The optimization results for Case-1, Case-2, and Case-3 are given in Table 6.2, Table 6.3 and Table 6.4, respectively.

Table 6.2 Optimization Case-1 Results




| Store Type | Store Mass, M_s [kg] | Store Pitch Moment of Inertia, I_s [kgm ²] |
|---|------------------------|--|
|  | 150.0 | 244.5 |
|  | 80.0 | 14.7 |
|  | 40.0 | 29.8 |
| Execution Time [Hours] | 18.65 | |
| Flutter Speed [m/s] | 8.40 | |

Table 6.3 Optimization Case-2 Results







| Store Type | Store Mass, M_s [kg] | Store Pitch Moment of Inertia, I_s [kgm ²] |
|---|------------------------|--|
|  | 111.73 | 251.5 |
|  | 80.0 | 15.4 |
|  | 40.0 | 37.8 |
| Execution Time [Hours] | 13.27 | |
| Flutter Speed [m/s] | 5.76 | |

Table 6.4 Optimization Case-3 Results

| Store Type | Store Mass, M_s [kg] | Store Pitch Moment of Inertia, I_s [kgm ²] |
|---|------------------------|--|
|  | 13.9 | 4.1 |
|  | 72.2 | 95.2 |
|  | 40 | 28.5 |
| Execution Time [Hours] | 10.47 | |
| Flutter Speed [m/s] | 7.62 | |

The results show that all flutter speeds are significantly lower than the flutter speed of the clean wing, which is expected. Since the mass addition tends to reduce to first bending and torsion natural frequencies resulting in the coupling of these modes in lower airspeeds.

In optimization case-1, masses of all stores are maximized at the upper bound of the mass constraint. However, it is not valid for the store pitch inertias. The B-1 store pitch inertia tends to maximize the value as considering the closest store to the wing root. On the contrary, optimization of the M-1 store inertia tends to decrease its value as locating the between the B-1 and M-2 store. Lastly, M-2's optimization results show that a moderate level of pitch store inertia is found within the pre-defined range as considering the most distant store from the wing root. Consequently, a unique combination of the store parameters results in the lowest value of flutter speed, i.e. worst-case flutter point. Similarly, in the second optimization case, M-1 and M-2 store mass close to their maximum value as seen in case-1. However, B-1's store mass is lower than case-1 despite having the same attachment location in case-1. This can be due to moving the stores M-1 and M-2 away from the B-1 leads to a change in the vibration characteristics of the wing store structure. Moreover, the store parameters of M-1 and M-2 are close to each other whereas case-1 and case-2 are compared. On the whole, the significant difference between case-1 and case-2 is seen at the B-1's store mass.

The last case differs from the first two cases as considering the B-1 and M-1 are close to the wing root and M-2 is away from the wing root. In this particular loading configuration, B-1 store parameters interestingly tend to be minimized. On the other hand, M-1's pitching inertia is close to its maximum value. No change is observed in the store mass of the M-2 as considering all three optimization cases. This is expected because heavier stores close to wingtip generally decrease the flutter speed.




All in all, three unique multi-store loading configurations have been defined and store parameters are optimized based on the worst-case flutter criteria. The optimization problem is not limited to the number of stores and accordingly

attachment locations. The optimization problem can be extended by introducing more stores and defining constant store properties at the particular attachment location. For instance, an engine or drop tank with constant parameters can be introduced at a specific span location under the wing. As a result of store parameters optimization based on the worst-case flutter criteria, an additional design constraint can be introduced in the store development phase.

6.3 Multi-Store Attachment Locations at Worst-Case Flutter Condition

Since the total number of external store loading configurations is close to a million considering the fighter aircraft, the determination of the most critical loading configuration is crucial. In this case, the total number of possible stores is generally defined in the inventory. The selected set of stores among the inventory is introduced as the candidate external stores for the attachment with their store properties. The ultimate aim is to determine store attachment locations for the given set of stores which causes the worst-case flutter condition. In the present work, the representative stores are defined in Table 6.5 to search their attachment locations. As considering the stores are representative, the store B-1, M-1 and M-2 masses are given as 150 kg, 50 kg, and 25 kg, respectively. To define store pitch moment of inertias, the pre-defined ratio parameters r_1 , r_2 and r_3 , which are again taken as 1.69, 1.19, and 1.3, respectively.

Table 6.5 Set of Stores Selected in Virtual Inventory

| Store Type | Store Mass, M_s [kg] | Store Pitch Moment of Inertia, I_s [kgm ²] |
|---|------------------------|--|
|  | 150 | 253.5 |
|  | 50 | 59.5 |
|  | 25 | 32.5 |

The all-possible conditions are considered in the determination of the attachment locations. Since a particular store can be located at 32 different attachment locations (except wing root), there is a total of 32768 possible loading configurations for the three stores. In this case, all three stores can be located at the same attachment location. A simple flutter search procedure is developed in Matlab[®] by calculating flutter speed for each case instead of utilizing a specific built-in search algorithm. Then, the lowest flutter speed case is picked among the number of 32768 cases. The worst-case flutter loading configuration is given in Figure 6.3.

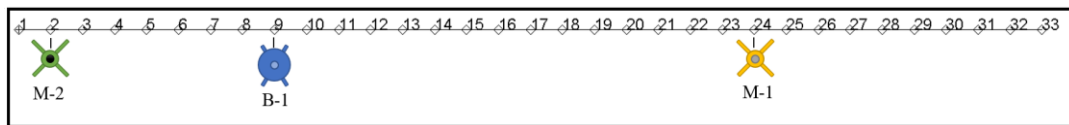


Figure 6.3 Worst-Case Flutter Loading Configuration

M-2 is found at the 2nd structural node and spanwise distance 0.5 m, B-1 is found at the 9th structural node with a spanwise distance of 4 m. Lastly, M-1 is found at the 24th structural node with a spanwise distance of 11.5 m. The flutter speed is calculated as 5.07 m/s at this multi-store loading configuration. Consequently, the calculated attachment locations cause the worst-case flutter condition considering the given number of stores and parameters.

In conclusion, two different types of study are presented in this chapter. The first study involves three optimization cases that search for the store design parameters at a given particular loading configuration. On the other hand, the second study provides the determination of the worst-case flutter loading configuration for the given set of stores. A design optimization problem for the wing store systems is introduced based on the worst-case flutter criteria. The wing is chosen as the HALE wing which is validated in chapter 3. However, the structural rigidity is increased to perform the store attachments efficiently. Accordingly, three different store types are defined in the model. Firstly, store design parameters are determined considering the three different case studies, which correspond to three different wing store loading configurations. The store mass and pitch inertias are calculated in multiple

store attachment cases considering particular loading configurations. The minimum flutter speed is searched within the pre-defined store parameters. As a result of this study, it can be concluded that additional store design constraints can be introduced in the store design activities based on the worst-case flutter condition. Additional work has been conducted considering the three designed stores with masses and inertias. The worst-case store loading configuration is searched involving all possible loading conditions. The attachment locations for the separate stores are obtained. The study of optimization can be extended by introducing a large number of stores and attachment locations since the application of FEM by structural modification easily encounters the attachment of the lumped mass elements. Besides, wing design parameters can be optimized for a given set of particular external loading configurations considering the maximum flutter speed condition. Furthermore, a full aircraft structure with external loads can be optimized by this approach.

CHAPTER 7

CONCLUSION

7.1 General Conclusions

Aeroelastic modeling and analysis of wing store systems have been investigated through the study. Since aircraft structures are mainly on the subject of aeroelasticity, the wings are utilized to investigate the aeroelastic instability problem, i.e., flutter. In the present work, it is mainly focused on the flutter analysis of wing store systems. The structural and aerodynamic models are initially developed for the clean wing structures. FE method and unsteady aerodynamics are implemented for structural and aerodynamic models, respectively. The evaluation of the aeroelastic equation of motion is performed and flutter solution methods are implemented mathematically, namely, K-Method and P-K Method. Besides, a novel approach for the flutter solution is specifically implemented, which is called the Non-Iterative P-K Method (NIPK Method). The fast and accurate solution approach of the NIPK Method is provided to solve the aeroelastic EOM during the analysis. To calculate the flutter solution, there is required to define a structural and aerodynamic model of the wing. Hence, the wing structures are modeled through the FE considering 1-D beam and 2-D shell elements. Case studies for the clean wing structure are performed to validate the developed aeroelastic analysis models. The validation of the models is carried out through three well-known wing models, namely High-Altitude Long Endurance (HALE) wing, Goland wing, and AGARD wing 445.6 (weakened).

Since the structural modeling of wing store systems are not a simple process and it mostly requires comprehensive FE modeling by utilizing commercial software, a simple and efficient analytical method is developed to model wing store systems in the 1-D framework. In the developed method, the structural modification approach is used to model wing store dynamics. The attachment of the store is defined as rigid

with no additional DOF in the system. The similarity of rigid body motion of the concentrated mass under free-free condition is taken advantage of deriving the rigid body mass matrix of the store for the wing store structures. 2-D Theodorsen aerodynamics are applied for the wing store systems in the 1-D framework whose structural model is obtained through FEM and structural modification approach. Hence, free vibration and flutter analyses of such systems are performed simply and efficiently. The developed model is used to investigate the effect of the spanwise attachment location of the store on the flutter behavior of the wing store systems. It is found that the flutter speed of the system increases as moving the store toward the wingtip. However, the flutter speed tends to decrease after a certain location of the store. Multi-store attachment cases can be easily developed by introducing this method since the structural model is developed by use of FEM and structural modification considering the 1-D framework.

Having introduced that an aeroelastic model for a 1-D cantilevered beam-like wing with lumped mass structures, a relatively comprehensive wing store system model is provided to investigate its aeroelastic behavior. For such a system, 2-D shell FEM and 3-D Doublet Lattice Method (DLM) are introduced for the structural and aerodynamic model, respectively. The commercial software is utilized to develop both structural and aerodynamic models. The store is considered flexible means that a linear spring element is used for its attachment to the wing structure. Consequently, the store has a 1-DOF pitching motion considering the one attachment location is pivoted while the other has a linear spring mounting element. In addition to this, a mass element is introduced between the store and wing structure. Hence, a realistic aeroelastic model is defined to investigate the flutter behavior for wing store systems. The varying flexible store mounting locations are considered in the analysis. A similar flutter behavior to 1-D wing store systems is observed for the flexible store case. Flutter speed tends to increase toward the wingtip but at a specific location, it decreases gradually. The main idea behind the modeling flexible store wing system by utilizing the FEM is to prove that altering the attachment location of the flexible store can be easily introduced in an aeroelastic system. Hence, the structural

characteristics of the flexible wing store system are not limited to the attachment location. For instance, the sensitivity analysis cases considering the variation on linear spring attachment element, point mass at the attachment, store mass properties, etc. can be performed efficiently by introducing this approach.

When a large number of design candidates are present during the aeroelastic analysis of the wing store systems, a significant computational effort is required to conduct such analyses. Moreover, working with high-fidelity aeroelastic models can substantially contribute to these computational efforts since it requires encountering a large number of DOFs for the wing store structures. That kind of analysis addresses the redesign or optimization activities. If the aerodynamic configuration is fixed in the successive aeroelastic analysis, the same aerodynamic model can be used repeatedly. This knowledge leads to the implementation of a structural modification approach in case of having different structural design candidates while performing aeroelastic analysis. In the present developed approach, the GAF database for the modified wing structure is obtained by implementing Dual Modal Space Modification (DMSM) method by using the original wing's AIC database. Modal matrices of the modified system are approximated by this approach to form the modified system's generalized mass, stiffness, and aerodynamic matrices. DMSM method does not require solving full system EOM by eigenvalue analysis to obtain modified system modal matrices. In other words, the DMSM method requires only original structure and structural modification information to obtain modal matrices of the modified structure. DMSM method is typically implemented to obtain modal matrices for the lower set of modes of the structure likewise flutter analysis. Hence, flutter analysis of the structurally modified structure is calculated based on the original structure and structural modification information. Moreover, it is found that it significantly reduces the calculation of the modal matrices of the modified structure, especially the large DOF systems are considered. Note that the accuracy of this method depends on the modal information that exists in the original system.

The store mass properties have been investigated considering the worst-case flutter condition for the wing store systems. The flutter speed is minimized while

optimizing the store mass and pitch moment of inertia parameters. It is found that additional store design constraints can be introduced to the store design activities. If such design constraints are considered during the preliminary design stage of the store, the operational capability of the aircraft can be maintained before conducting ground vibration and flutter flight tests. On the contrary, a ballast weight is desired to be added to the wing structure to increase the flutter speed. That kind of optimization problem can be easily obtained by implementing the same optimization approach to search for the optimal solution for the ballast weight and its location on the wing.

7.2 Recommendations for Future Work

This thesis involves the application of FEM into wing store structures to analyze its vibrational and dynamic aeroelasticity characteristics. FEM approach enables structural modifications when both forming and solving the aeroelastic equation of motion of the structure. The present approach is not limited to obtain a flutter solution but can be applied to any static aeroelastic problems like divergence. Moreover, the study can be extended to obtain the dynamic and elastic response of the aerospace structures in gust loads. Since the present study includes only linear systems considering linear attachment elements to wing structures, the non-linear attachment elements can be utilized in the present methodology. On the other hand, modifications can be extended to aerodynamics. Store aerodynamics can be included in the analyses. The study is not limited to wing store systems but can be implemented in full-scale aerospace structures. The related design optimization activities can be performed efficiently concerning FE modeling and structural modification approach.

REFERENCES

- [1] R. L. Bisplinghoff, H. Ashley, and R. L. Halfman, *Aeroelasticity*. 1983.
- [2] F. Afonso, J. Vale, É. Oliveira, F. Lau, and A. Suleman, “A review on non-linear aeroelasticity of high aspect-ratio wings,” *Progress in Aerospace Sciences*, vol. 89. 2017. doi: 10.1016/j.paerosci.2016.12.004.
- [3] M. Goland and Y. L. Luke, “The Flutter of a Uniform Wing With Tip Weights,” *Journal of Applied Mechanics*, vol. 15, no. 1, 1948, doi: 10.1115/1.4009753.
- [4] H. L. Runyan and J. L. Sewall, “Experimental Investigation of the Effects of Concentrated Weights on Flutter Characteristics of a Straight Cantilever Wing,” *NASA Technical Report, NACA-TN-1594*, 1948.
- [5] H. L. Runyan and C. E. Watkins, “Flutter of a Uniform Wing with an Arbitrarily Placed Mass According to a Differential-Equation Analysis and a Comparison with Experiment,” *NACA Technical Reports, NACA-TR-966*, 1950.
- [6] W. H. Reed, J. T. Foughner, and H. L. Runyan, “DECOUPLER PYLON: A SIMPLE, EFFECTIVE WING/STORE FLUTTER SUPPRESSOR.,” 1979.
- [7] Z. C. Yang and L. C. Zhao, “Wing-store flutter analysis of an airfoil in incompressible flow,” *Journal of Aircraft*, vol. 26, no. 6, 1989, doi: 10.2514/3.45806.
- [8] R. N. Desmarais and W. H. Reed, “Whg/Store flutter with nonlinear pylon stiffness,” *Journal of Aircraft*, vol. 18, no. 11, 1981, doi: 10.2514/3.57590.

- [9] D. Tang, P. Attar, and E. H. Dowell, "Flutter/limit cycle oscillation analysis and experiment for wing-store model," *AIAA Journal*, vol. 44, no. 7, 2006, doi: 10.2514/1.12634.
- [10] K. U. Kim and T. W. Strganac, "Nonlinear responses of a cantilever wing with an external store," in *Collection of Technical Papers - AIAA/ASME/ASCE/AHS/ASC Structures, Structural Dynamics and Materials Conference*, 2003, vol. 4.
- [11] P. S. Beran, T. W. Strganac, K. Kim, and C. Nichkawde, "Studies of store-induced limit-cycle oscillations using a model with full system nonlinearities," *Nonlinear Dynamics*, vol. 37, no. 4, 2004, doi: 10.1023/B:NODY.0000045544.96418.bf.
- [12] G. Canbaloglu and H. N. Özgüven, "Structural modifications with additional DOF - Applications to real structures," 2009.
- [13] T. Kalaycioğlu and H. N. Özgüven, "Nonlinear structural modification and nonlinear coupling," *Mechanical Systems and Signal Processing*, vol. 46, no. 2, 2014, doi: 10.1016/j.ymssp.2014.01.016.
- [14] M. Winter, F. M. Heckmeier, and C. Breitsamter, "CFD-based aeroelastic reduced-order modeling robust to structural parameter variations," *Aerospace Science and Technology*, vol. 67, 2017, doi: 10.1016/j.ast.2017.03.030.
- [15] G. Chen, D. Li, Q. Zhou, A. da Ronch, and Y. Li, "Efficient aeroelastic reduced order model with global structural modifications," *Aerospace Science and Technology*, vol. 76, 2018, doi: 10.1016/j.ast.2018.01.023.
- [16] M. Karpel, B. Moulin, L. Anguita, C. Maderuelo, and H. Climent, "Flutter analysis of aircraft with external stores using modal coupling," *Journal of Aircraft*, vol. 41, no. 4, 2004, doi: 10.2514/1.11483.

- [17] S. Kumar, A. K. Onkar, and M. Manjuprasad, “Stochastic Modeling and Reliability Analysis of Wing Flutter,” *Journal of Aerospace Engineering*, vol. 33, no. 5, 2020, doi: 10.1061/(asce)as.1943-5525.0001153.
- [18] D. H. Hodges and G. A. Pierce, *Introduction to Structural Dynamics and Aeroelasticity*. Cambridge University Press, 2002. doi: 10.1017/CBO9780511809170.
- [19] ZONA TECHNOLOGY INC, “ZAERO Theoretical Manual.” Jan. 2017.
- [20] J. R. Wright and J. E. Cooper, *Introduction to Aircraft Aeroelasticity and Loads: Second Edition*. 2015. doi: 10.1002/9781118700440.
- [21] T. Theodorsen, “General Theory of Aerodynamic Instability and the Mechanism of Flutter, NACA Report 496, 1935,” *NASA Reference Publication*. 1935.
- [22] E. Albano and W. P. Hodden, “A doublet-lattice method for calculating lift distributions on oscillating surfaces in subsonic flows,” *AIAA Journal*, vol. 7, no. 2, 1969, doi: 10.2514/3.5086.
- [23] Y. C. Fung, *An Introduction to The Theory Of Aeroelasticity*. New York: Dover Publications.
- [24] R. Banerjee, “Flutter Sensitivity Studies Of High Aspect Ratio Aircraft Wings,” in *Computer aided optimum design of structures III: optimization of structural systems and applications*, “S. Hernández” and B. C. A., Eds. Northampton Square, London, UK: Elsevier Science Publishers Ltd. Crown House Linton Road Barking, Essex IG11 8JU, 1993, pp. 373–387.
- [25] Ü. Gülçat, *Fundamentals of modern unsteady aerodynamics*. 2011. doi: 10.1007/978-3-642-14761-6.
- [26] J. GIESING and T. KALMAN, “Subsonic unsteady aerodynamics for general configurations,” 1972. doi: 10.2514/6.1972-26.

- [27] MSC, "Release Guide." MSC/Software Corporation, Newport Beach, CA, United States, 2019.
- [28] P. Hajela, "A root locus-based flutter synthesis procedure," *Journal of Aircraft*, vol. 20, no. 12, 1983, doi: 10.2514/3.48206.
- [29] M. RHEINFURTH and F. SWIFT, "A NEW APPROACH TO THE EXPLANATION OF THE FLUTTER MECHANISM," 1965. doi: 10.2514/6.1965-1101.
- [30] H. J. Hassig, "An approximate true damping solution of the flutter equation by determinant iteration," *Journal of Aircraft*, vol. 8, no. 11, 1971, doi: 10.2514/3.44311.
- [31] D. Pitt, "A new non-iterative P-K match point flutter solution," 1999. doi: 10.2514/6.1999-1353.
- [32] E. Mermer, "Conceptual design of a hybrid (turbofan/solar) powered HALE UAV ," 2016.
- [33] M. J. Patil and D. H. Hodges, "On the importance of aerodynamic and structural geometrical nonlinearities in aeroelastic behavior of high-aspect-ratio wings," *Journal of Fluids and Structures*, vol. 19, no. 7, 2004, doi: 10.1016/j.jfluidstructs.2004.04.012.
- [34] M. J. Patil, D. H. Hodges, and C. E. S. Cesnik, "Nonlinear aeroelasticity and flight dynamics of high-altitude long-endurance aircraft," *Journal of Aircraft*, vol. 38, no. 1, 2001, doi: 10.2514/2.2738.
- [35] M. J. Patil, "Aeroelastic tailoring of composite box beams," 1997. doi: 10.2514/6.1997-15.
- [36] D. H. Hodges, "A mixed variational formulation based on exact intrinsic equations for dynamics of moving beams," *International Journal of Solids and Structures*, vol. 26, no. 11, 1990, doi: 10.1016/0020-7683(90)90060-9.

- [37] D. A. Peters, S. Karunamoorthy, and W. M. Cao, "Finite state induced flow models. Part I: Two-dimensional thin airfoil," *Journal of Aircraft*, vol. 32, no. 2, 1995, doi: 10.2514/3.46718.
- [38] E. M. P. G. Pepe, "Numerical Implementation of a Frequency-Domain Panel Method for Flutter Prediction of a 3D Wing," 2015.
- [39] M. J. Patil, D. H. Hodges, and C. E. S. Cesnik, "Nonlinear aeroelastic analysis of complete aircraft in subsonic flow," *Journal of Aircraft*, vol. 37, no. 5, 2000, doi: 10.2514/2.2685.
- [40] S. H. R. Eslimy-Isfahany, J. R. Banerjee, and A. J. Sobey, "Response of a bending-torsion coupled beam to deterministic and random loads," *Journal of Sound and Vibration*, vol. 195, no. 2, 1996, doi: 10.1006/jsvi.1996.0421.
- [41] Ö. ÖZDEMİR, S. EKEN, and M. O. KAYA, "Flutter Analysis of Goland Wing via Finite Element Method," 2011.
- [42] Z. Qin and L. Librescu, "Aeroelastic instability of aircraft wings modelled as anisotropic composite thin-walled beams in incompressible flow," *Journal of Fluids and Structures*, vol. 18, no. 1, 2003, doi: 10.1016/S0889-9746(03)00082-3.
- [43] D. A. Peters and M. J. Johnson, "Finite-state airloads for deformable airfoils on fixed and rotating wings," in *American Society of Mechanical Engineers, Aerospace Division (Publication) AD*, 1994, vol. 44.
- [44] E. C. Yates, "AGARD standard aeroelastic configurations for dynamic response. Candidate configuration I.-wing 445.6," *Nasa Technical Memorandum*, 1987.
- [45] R. M. Kolonay and H. T. Y. Yang, "Unsteady aeroelastic optimization in the transonic regime," *Journal of Aircraft*, vol. 35, no. 1, 1998, doi: 10.2514/2.2260.

- [46] E. LEE-RAUSCH and J. BATINA, “Calculation of AGARD Wing 445.6 flutter using Navier-Stokes aerodynamics,” 1993. doi: 10.2514/6.1993-3476.
- [47] L. Katzenmeier, C. Vidy, and C. Breitsamter, “Correction Technique for Quality Improvement of Doublet Lattice Unsteady Loads by Introducing CFD Small Disturbance Aerodynamics,” *Journal of Aeroelasticity and Structural Dynamics*, vol. 5, no. 1, 2018.
- [48] A. Malekjafarian, M. R. Ashory, M. M. Khatibi, and M. Saberlatibari, “Rigid body stiffness matrix for identification of inertia properties from output-only data,” *European Journal of Mechanics, A/Solids*, vol. 59, 2016, doi: 10.1016/j.euromechsol.2016.03.009.
- [49] D. Tang and E. H. Dowell, “Aeroelastic analysis and experiment for wing/store model with stiction nonlinearity,” *Journal of Aircraft*, vol. 48, no. 5, pp. 1512–1530, 2011, doi: 10.2514/1.C031151.
- [50] P. J. Attar, E. H. Dowell, and D. Tang, “Delta wing with store limit-cycle-oscillation modeling using a high-fidelity structural model,” in *Journal of Aircraft*, 2008, vol. 45, no. 3. doi: 10.2514/1.32217.
- [51] C. H. Wilts, “Incompressible Flutter Characteristics of Representative Aircraft Wings,” *NASA Technical Report, NACA-TR-1390*, pp. 1385–1422, Jun. 1955.
- [52] D. Tang, P. Attar, and E. H. Dowell, “Extended Summary for Nonlinear Dynamics of A Very High Dimensional System: A Wing with Stores,” Durham, North Carolina.
- [53] D. Tang and E. H. Dowell, “Experimental and theoretical study of gust response for a wing-store model with freeplay,” *Journal of Sound and Vibration*, vol. 295, no. 3–5, 2006, doi: 10.1016/j.jsv.2006.01.024.
- [54] W. P. Rodden and E. H. Johnson, “MSC/NASTRAN Aeroelastic Analysis – USERS’S GUIDE.” The Nacneal-Schwendler Corporation.

- [55] D. M. Pitt and D. P. Haudrich, "Determination of the flutter critical stores configuration utilizing an optimized artificial neural network," in *Collection of Technical Papers - AIAA/ASME/ASCE/AHS/ASC Structures, Structural Dynamics and Materials Conference*, 2007, vol. 8. doi: 10.2514/6.2007-2365.
- [56] R. J. Guyan, "Reduction of stiffness and mass matrices," *AIAA Journal*, vol. 3, no. 2, 1965, doi: 10.2514/3.2874.
- [57] J. O'Callahan, "A procedure for an improved reduced system (IRS) model," *Proceedings of 7th International Modal Analysis Conference (IMAC VII)*. 1989.
- [58] D. Kammer, "Test-Analysis-Model Development Using an Exact Modal Reduction," *The International Journal of Analytical and Experimental Modal Analysis*, vol. 2. 1987.
- [59] Y. W. Luk and L. D. Mitchell, "Implementation of Dual Modal Space Structural Modification Method," in *Proceedings of the Second International Modal Analysis Conference*, Feb. 1984, pp. 930–936.
- [60] M. Moradi, M. H. Sadeghi, and E. H. Dowell, "Engineering notes experimental and theoretical flutter investigation for a range of wing wind-tunnel models," in *Journal of Aircraft*, 2018, vol. 55, no. 2. doi: 10.2514/1.C034311.